A BROADSIDE AND END-ON SEISMIC EXPERIMENT ON THE CRUSTAL STRUCTURE OF THE NEWFOUNDLAND APPALACHIANS

BRIAN J. ROBERTS

INFORMATION TO USERS

This manuscript has been reproduced from the microfilm master. UMI films the text directly from the original or copy submitted. Thus, some thesis and dissertation copies are in typewriter face, while others may be from any type of computer printer.

The quality of this reproduction is dependent upon the quality of the copy submitted. Broken or indistinct print, colored or poor quality illustrations and photographs, print bleedthrough, substandard margins, and improper alignment can adversely affect reproduction.

In the unlikely event that the author did not send UMI a complete manuscript and there are missing pages, these will be noted. Also, if unauthorized copyright material had to be removed, a note will indicate the deletion.

Oversize materials (e.g., maps, drawings, charts) are reproduced by sectioning the original, beginning at the upper left-hand corner and continuing from left to right in equal sections with small overlaps. Each original is also photographed in one exposure and is included in reduced form at the back of the book.

Photographs included in the original manuscript have been reproduced xerographically in this copy. Higher quality 6" x 9" black and white photographic prints are available for any photographs or illustrations appearing in this copy for an additional charge. Contact UMI directly to order.

UMI

A Bell & Howell Information Company
300 North Zeeb Road, Ann Arbor MI 48106-1346 USA
313/761-4700 800/521-0600

A BROADSIDE AND END-ON SEISMIC EXPERIMENT ON THE CRUSTAL STRUCTURE OF THE NEWFOUNDLAND APPALACHIANS

by

Brian J. Roberts

A thesis submitted to the

School of Graduate Studies

in partial fulfilment of the

requirements for the degree of

Master of Science

Department of Earth Sciences
Memorial University of Newfoundland

1998

St. Johns's Newfoundland

National Library
of Canada

Acquisitions and
Bibliographic Services

395 Wellington Street
Ottawa ON K1A 0N4
Canada

Bibliothèque nationale
du Canada

Acquisitions et
services bibliographiques

395, rue Wellington
Ottawa ON K1A 0N4
Canada

Your file Votre référence

Our file Notre référence

0-612-34222-0

Canada

ABSTRACT

A special broadside and wide-angle seismic experiment was conducted in central Newfoundland in order to test the feasibility of obtaining meaningful information on the true dip of reflectors and amplitude-offset relationships in a small area of psuedo-3D coverage.

The analysis of the data from this experiment involved producing 2D and 3D seismic images from the broadside shots, and producing a 2D section from the end-on-south shots. Also, an amplitude versus offset analysis (AVO) was completed on deep crustal reflections using the end-on-south shots. The seismic images have been interpreted in terms of the regional geological structures and correlated with the results from regional seismic reflection and refraction surveys.

It is determined that the quality of the low fold 2D sections produced using the wide-angle shots compares favourably with that of the high fold regional lines. The interpretation of the 3D volume was problematical, leading to recommendations for better 3D survey design: however, three horizons have been mapped and time structure maps display their 3D orientation. It is determined that information on the true dip of reflectors along the regional lines can be provided using the relatively inexpensive broadside shots. The AVO results fail to provide conclusive results for changes in Poisson's ratio across any of the major reflecting interfaces in the area of the broadside experiment in central Newfoundland. If the statisical

trends can be trusted, a decrease in Poisson's ratio at the top of the lower crust is indicated, however a firm value cannot be placed on this decrease. The AVO results are ambiguous probably because of seismic scattering due to a high degree of lateral inhomogeneity in the crystalline crust.

TABLE OF CONTENTS

LIST OF TABLES

LIST OF FIGURES

ACKNOWLEDGEMENTS

The author wishes to acknowledge the Department of Earth Sciences at Memorial University of Newfoundland and the Seismology and Electromagnetism Section of the Geological Survey of Canada for providing computer resources and technical support for the data processing. Jeremy Hall provided a great deal of support and advice, with many thoughtful recommendations, and the author is particularly thankful for the patience that Dr. Hall gave in the preparation of this thesis. Tony Kocurko (MUN) was instrumental in allowing the author to work remotely at the seismic processing facility at the Department of Earth Sciences while he was at the Geological Survey in Ottawa. Bernd Milkereit (GSC) has provided many insightful comments over the years which were much appreciated. The Canadian LITHOPROBE program financed the acquisition of the data. Comments from the two examiners were very beneficial in improving this document. Finally, the author would like to thank his family for their great support and patience.

Dedicated to the Memory

of

Hubert J. Hookey

1.0 INTRODUCTION

In 1989 a regional deep crustal seismic reflection survey was conducted in Newfoundland as part of the LITHOPROBE East transect of the national LITHOPROBE program, which integrates the various Earth science disciplines into a study of the lithosphere beneath the Canadian landmass and the surrounding continental margin. LITHOPROBE East is primarily concerned with the evolution of the Appalachian orogen and the tectonic framework of the surface geology of Newfoundland and adjacent regions. One of the objectives of the LITHOPROBE program is to test innovative techniques in the acquisition and processing of various data sets. During the regional seismic survey in Newfoundland, a special broadside and wide-angle seismic experiment was conducted on the Meelpaeg transect at the junction of lines 6 and 7, near Lake Ambrose in central Newfoundland (Roberts, 1990) (Figure 1.1). The processing and interpretation of the data from this special experiment is the subject of this thesis.

Three seismic reflection profiles were shot across the strike of the orogen in Newfoundland (Quinlan et al., 1992) to provide images of the crustal structure for LITHOPROBE East. The Meelpaeg transect crosses the whole of the central mobile belt of the orogen from the Bay of Islands in the northwest to Fortune Bay in the southeast and is approximately 340 km in length (Figure 1.1). In interpreting the crustal reflectivity patterns in such data the correlation with surface structure is important. However, isolated reflection profiles lack information on the strike of reflections, unless occasional cross lines are added. In the planning of LITHOPROBE East, cross lines were added at a few locations to add such strike information.

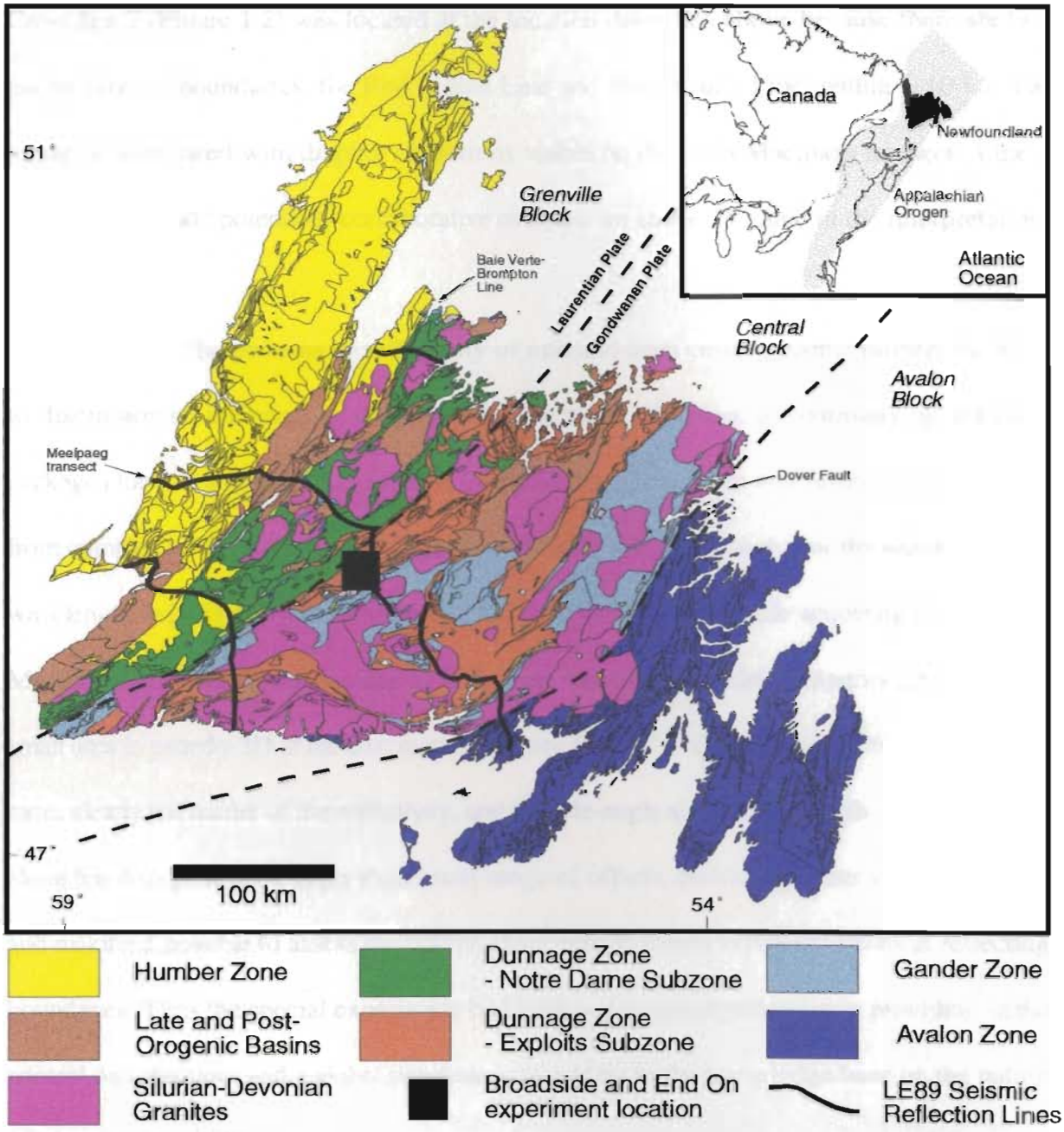

Figure 1.1 Geological map of Newfoundland

Geological map of Newfoundland with individual geological units grouped by colour into the main lithotectonic subdivisions (Colman-Sadd et al., 1990). Also shown are the crustal block boundaries of Marillier et al. (1989) with the alternative terminology proposed by Quinlan et al. (1992) (Laurentian and Gondwanan plates). The approximate location of the broadside seismic experiment and the LE89 seismic reflection transects are also indicated.

Cross line 7 (Figure 1.2) was located at the location described above because there are two major terrane boundaries, the Red Indian Line and Noel Paul's Line, within 5-10 km that might be associated with dipping reflections visible on the main Maelpaeg transect. Line 7 was located to add potentially corroborative evidence on strike, of value in the interpretation.

Further to this, the patterns of reflectivity of mid and deep crustal seismic profiles have led to discussion on the origin of deep crustal reflections. The lack of continuity of reflection packages has been used to indicate that the reflections arise from interference of reflections from complex geological structures with wavelengths smaller than that of the seismic source wavelength (e.g. Hurich and Smithson, 1987). In view of this, while acquiring line 7 of the Maelpaeg transect it was decided to add: i) an additional broadside experiment to study a small area in psuedo-3D at the intersection of lines 6 and 7 from the main profile, to establish more clearly the nature of the reflectivity, and ii) wide-angle shots in the north-south direction along line 6 to generate a larger than usual range of offsets, providing better velocity control and making it possible to assess the nature of amplitude versus offset variations at reflecting boundaries Thus the special experiment had both a regional significance in providing strike control on reflections and a global significance by adding to the knowledge base on the nature of crustal reflectivity.

A summary of the regional and local geology, and the tectonic framework are provided in Chapter 2. The geological location of the experiment is within the Exploits Subzone of the Dunnage Zone in central Newfoundland with the end-on shots to the south straddling the

boundary between the Gander and Dunnage Zones (Figure 1.2). The Dunnage Zone is a geologically complex region thought to represent the vestiges of Ordovician island arc sequences which were destroyed with the closure of the Iapetus ocean in Silurian time. The Gander Zone is interpreted to represent the remnants of an old continental margin on the south side of the Iapetus ocean (Williams et al., 1972). Noel Paul's Line is the linear, northeast-southwest trending fault zone which separates the Exploits Subzone of the Dunnage from the Gander Zone (Williams et al., 1988). North of Lake Ambrose, the Red Indian Line is interpreted as the boundary between Exploits and Notre Dame subzones of the Dunnage Zone and thus, oceanic assembleges from opposite sides of Iapetus. The uncertain tectonic relationship between the Gander and Dunnage Zones, i.e. the significance of Noel Paul's Line is one of the problems that the deep seismic data may help to resolve.

Chapter 3 describes the acquisition of the seismic data during the broadside experiment. A 12 km receiver spread from the regional survey was positioned along line 6, straddling line 7, and the vibrator trucks moved away from the spread in both the in-line directions along line 6 and in a roughly perpendicular direction along line 7. A total of 145 shot gathers of good quality data were collected in about one and a half days of work. The broadside data provide reflector coverage over a roughly 6 km^2 area and are used to generate a 3-D crustal image of this area. The end-on shots generate wide-angle reflection/refraction data up to a maximum offset of approximately 30 km, and these data were used for amplitude versus offset (AVO) studies. Strategies for data processing involved effective noise removal, deconvolution, coherency filtering and gain application. The data processing varied for the 2D, 3D and AVO

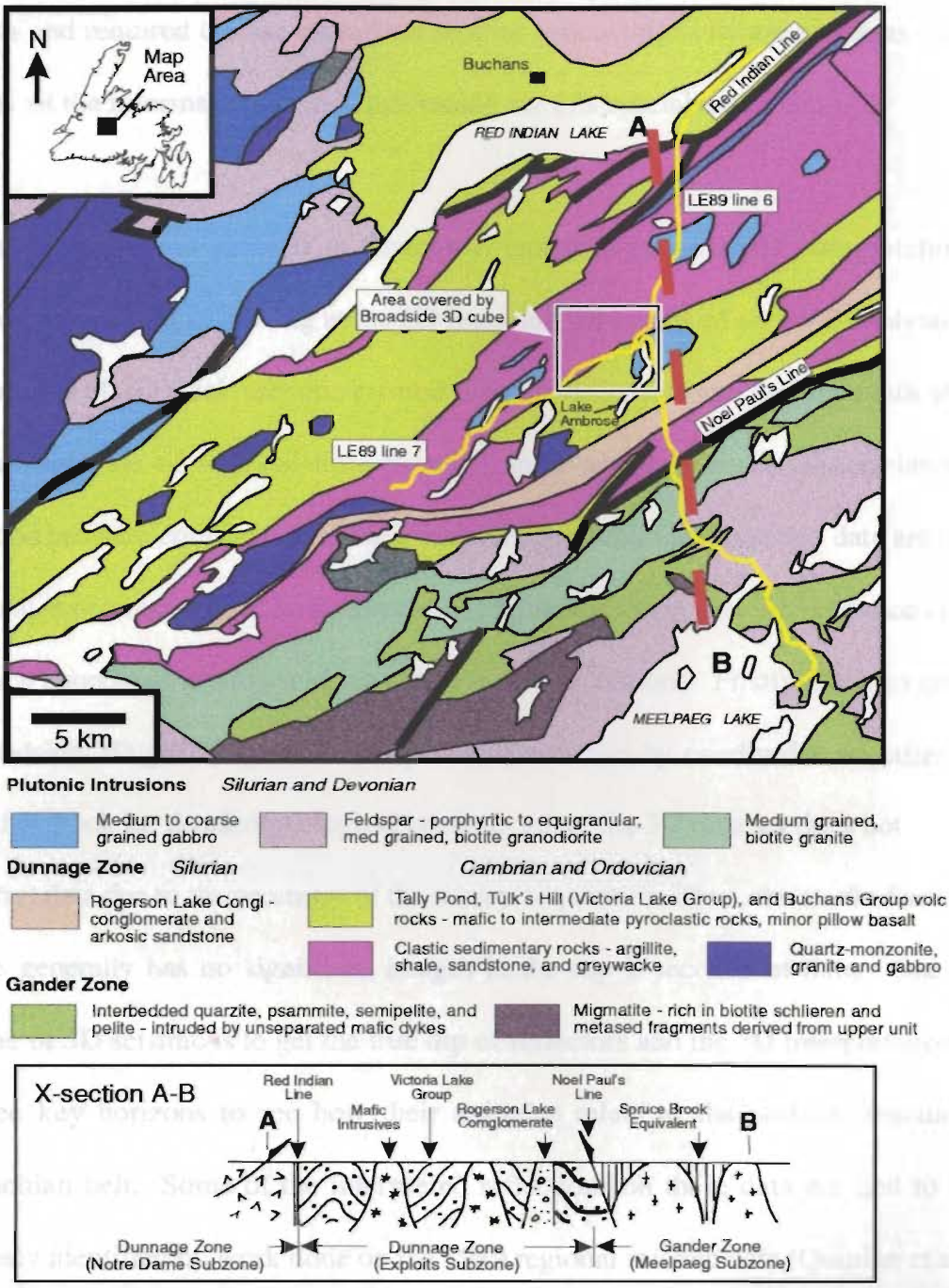

Figure 1.2 Detailed geological map for broadside and end-on survey area

Geological map of central Newfoundland near location of broadside experiment. The legend briefly describes the individual geological units (Kean and Jayasinghe, 1980, Colman-Sadd, 1987) . The broadside 3D grid is shown by a box, and lines 6 & 7 from the Meelpaeg transect of the LE89 seismic reflection survey are in yellow. Cross section A-B shows the relationships of the major geological units and fault zones along line 6 (Piasecki et al, 1990).

data sets and required the use of various seismic processing software packages. Chapter 4 contains all the information on data processing for this special experiment.

Data interpretation is outlined in Chapter 5 and focuses on a 3D interpretation of the broadside data as well as looking at the 2D lines and the results of an AVO analysis. In-line comparisons of 2D stack sections created with the broadside and end-on-south shots with collinear sections of regional lines 6 and 7 show a good degree of correlation. This correlation provides confidence that the events imaged with the broadside data are related to geological structures in the Lake Ambrose area. However, tying specific reflections to known geological boundaries at surface is not possible for two reasons. Firstly, the area covered by the broadside 3D grid (Figure 1.2) is primarily overlain by overburden and there is little exposed bedrock for detailed geological control. Also, the 3D data set does not contain any near offset data due to the geometry of the survey acquisition. Thus, the stacked seismic data volume generally has no significant images in the top 2 seconds of data. One valuable outcome of 3D seismic is to get the true dip of reflectors and the 3D interpretation focuses on three key horizons to see how their attitudes relate to the surface structure of the Appalachian belt. Some of the interpreted reflections on these data are tied to horizons previously identified by work done on the 1989 regional seismic data (Quinlan et al., 1992) and the 1991 seismic refraction data (Hughes et al., 1994). Quantitative amplitude vs. offset analysis (AVO) has been carried out using large-fold CDP gathers with the goal of making some inferences about rock properties at various depths in the crust. Results from these analyses are somewhat ambiguous because of the difficulty in following specific reflection

events over a wide range of offsets. This problem may be related to the high degree of scattering of the seismic energy in such a complex geological area.

Chapter 6 presents the conclusions from the analysis of this unique data set and provides some comments on the value of the experiment.

2.0 BACKGROUND GEOLOGY, GEOPHYSICS AND TECTONICS

2.1 Regional Geology

There is now widespread agreement that the Northern Appalachians evolved through an orogenic cycle that initiated in the late Precambrian and culminated in the Silurian. The cycle involved the opening and closing of an ancient ocean, named Iapetus, prior to the opening of the present day Atlantic ocean (Wilson, 1966). It is presumed that when the Iapetus ocean opened it split part of the Grenvillian continental crust that formed the eastern margin of North America (Williams and Hatcher, 1982). Estimates on the original width of the Iapetus ocean, based on palinspastic restoration of the widest segment of the Dunnage Zone, are in the order of 1000 km (Williams, 1980). As the Iapetus ocean closed, arc-continent collision (mid-Ordovician Taconic and Penobscot orogenies) followed by continent-continent collision (Silurian Salinic and Devonian Acadian orogenies) compressed remnants of oceanic seafloor, island arc sequences, and rocks forming the eastern passive margin of Iapetus onto the passive margin that formed the eastern seaboard of North America (Williams and Stevens, 1974; Dunning et al., 1990; Colman-Sadd et al., 1992).

The Canadian Appalachians are divided into tectonostratigraphic zones based upon surface geology (Figure 1.1): from west to east, these are the Humber, Dunnage, Gander, Avalon, and Meguma Zones (Williams, 1979). The interpreted origin of each tectonostratigraphic zone is briefly summarized below.

The Humber Zone represents the ancient margin of North America (Williams and Stevens, 1974), in which Cambro-Ordovician sedimentary rocks of the margin overlie Grenvillian crystalline basement. In the Dunnage Zone, the rocks represent what is left of the Iapetus ocean crust: calc-alkaline volcanic rocks from island arcs, and the sedimentary rocks that were deposited on the volcanics (Williams, 1979). In Newfoundland, the Dunnage Zone is a complex assemblage of these rocks, separated from the Humber Zone to the west by steeply dipping ophiolite complexes, found along the Baie Verte-Brompton Line (Williams et al., 1988). The Dunnage Zone has been further sub-divided into the Exploits and Notre Dame Subzones. The Notre Dame Subzone in the west is separated from the Exploits Subzone by the Red Indian Line (Figure 1.2), a faulted boundary that divides Ordovician volcanic-sedimentary rocks exhibiting contrasting geological features (Williams et al., 1988). The Gander Zone is interpreted to represent the eastern continental margin of Iapetus and the rocks of this Zone record the formation and destruction of a passive margin (Williams, 1979). Surface geology in the Gander Zone is dominated by metamorphosed Ordovician clastic sedimentary and volcanic rocks. The Gander-Dunnage boundary is best defined in Northeastern Newfoundland where the Gander Lake Subzone of the Gander Zone is faulted against adjacent rocks of the Dunnage Zone along the GRUB Line (Williams et al., 1988). Gander-Dunnage relationships are less straightforward to the southwest where inliers of Gander Zone material have been identified within the Dunnage Zone (Colman-Sadd and Swinden, 1984). A significant boundary for this study is that between the sedimentary and igneous rocks of the Exploits Subzone and the metaclastics of the Gander affiliated Meelpaeg

Subzone (Williams et al., 1988). This boundary occurs at Noel Pauls Line in central Newfoundland, an interpreted fault (Brown and Colman-Sadd, 1976) that is crossed by the wide-angle seismic data of this study. The most easterly part of Newfoundland is formed by the Avalon Zone. The Avalon Zone is mostly comprised of late Precambrian volcanic and sedimentary rocks that are relatively undeformed (Williams, 1979). The Avalon Zone appears to have evolved as a stable platform during the early Paleozoic and is presently separated from the Gander Zone by two major strike-slip fault zones, the Dover Fault to the Northeast and the Hermitage Bay Fault zone to the Southwest (Kennedy et al., 1982).

The Ordovician Taconian orogeny is interpreted to mark the closing of the Iapetus ocean followed by arc-continent collision, and accounts for many of the structures observed in the Humber Zone (Williams, 1979). Deformation in the Dunnage Zone is predominantly related to subsequent events, notably the Silurian Salinic and Devonian Acadian orogenies, although there is some Taconian deformation (Williams and Stevens, 1974; Dunning et al., 1990; Colman-Sadd et al., 1992). The rocks of the Gander zone appear to have been deformed primarily during the Acadian orogeny (Kennedy, 1976).

The Dunnage Zone volcanic and sedimentary rocks occupy the central mobile belt of the Appalachian orogen and they have complex relationships both internally and with rocks of the adjacent Zones. Exposure is limited in the heavily forested areas of central Newfoundland, but the following section describes the geological relationships that have been established in the region of this study.

2.2 Local Geology

The Geological Survey of Canada carried out regional mapping in central Newfoundland in 1965 and 1966 and produced a 1:125,000 map (Williams, 1970). Detailed mapping was done in the mid to late 70's by the Department of Mines and Energy of the Government of Newfoundland and Labrador with a comprehensive report covering the Lake Ambrose (12A/10) and Noel Paul's Brook (12A/9) map areas being produced in 1980 (Kean and Jayasinghe, 1980). The adjacent Snowshoe Pond map area (12A/7), which lies to the south of Lake Ambrose has also been described (Colman-Sadd, 1987).

Noel Paul's Line separates the Exploits Subzone of the Dunnage Zone from the Meelpaeg Subzone of the Gander Zone. South of Noel Paul's Line lie the Ordovician sedimentary and metasedimentary rocks of the Meelpaeg Subzone (Figure 1.2). These are monotonous sequences of interbedded shales and quartzites which have been intruded by pretectonic mafic dykes, and by biotite granites (Colman-Sadd, 1987), which are probably Silurian to Devonian in age (Kean and Jayasinghe, 1980).

North of Noel Paul's Line lies the Dunnage Exploits Subzone that include the Cambro-Ordovician sedimentary and volcanic rocks of the Victoria Lake Group (Figure 1.2). In the area of interest this Group has been subdivided into a unit of pyroclastic and epiclastic rocks, dominated by argillite, shale, sandstone, greywacke with minor pebble conglomerate; and the Tally Pond and Tulks Hill volcanics, which are mostly comprised of felsic tuff, porphyry,

breccia, and some mafic volcanic rocks (Kean and Jayasinghe, 1980). Mafic intrusive rocks within the Victoria Lake Group include diabase dykes and massive gabbro that are probably Ordovician in age. The dykes intrude the gabbro which is fine to medium grained. The Rogerson Lake Conglomerate is a late sequence of felsic sedimentary, metasedimentary and volcanic rocks that appears to be a local subaerial infill of a Silurian lineament at or near Noel Paul's Line, exhibiting the fabric of northwesterly directed overthrusting (Piasecki et al., 1990). Noel Paul's Line is better exposed to the southwest near Victoria Lake, where it is a layer-parallel (i.e. parallel and concordant to local layering), southeast-dipping ductile shear zone, approximately 1 km wide, along which Meelpaeg granite-mylonites are thrust northwest over Victoria Lake Group rocks (Williams et al., 1988).

The Gander Zone in this part of Newfoundland has been interpreted as windows, with Dunnage Zone thrust over them (Colman-Sadd and Swinden, 1984). Thus the observation of Noel Paul's Line as a southeast dipping shear zone indicates a more complex history, with a possible late northwest directed thrusting cutting over an assumed earlier southeast directed thrusting. The broadside survey could provide valuable evidence on the orientation of any structures imaged along the transect associated with Noel Paul's Line and dipping northwest.

North of Lake Ambrose the Red Indian Line separates the Notre Dame and Exploits subzones of the Dunnage Zone. In most places the Red Indian Line is a late rectilinear fault and when exposed it is observed to be a steep, brittle fault, downthrown on its southern side (Williams et al., 1988). The data that forms this study cannot shed much light on the nature of the Red

Indian Line and its subsurface expression, however the regional seismic data does cross this boundary and there is no clear image of the fault. This result would not be unexpected if the fault is a subvertical feature at depth as well as at surface.

2.3 Geophysical and Tectonic Framework

The tectonic model for the formation of the Appalachian orogen generally involves a collision of the North American passive margin with an island arc, above an east-dipping subduction zone during the Taconian orogeny (Jacobi, 1981). This event was followed by continent-continent collision during the Salinic and Acadian orogenies (Dunning et al., 1990). Although the direction of subduction has been a point of some contention, current models invoke eastward subduction (e.g. Stockmal et al., 1987; Quinlan et al., 1992). A further complication in the orogenic history of this region is the geometry of the eastern seaboard of the North American craton. This irregular margin may have resulted in continent-continent collision taking place in the northeast while the subduction of oceanic crust was still occurring to the southwest (Stockmal et al., 1987). Since indications are that there was almost complete subduction of oceanic seafloor in the southwest, models explaining how the subduction of buoyant continental crust in the northeast continued at the same time have been required. It has been proposed that upon continent-continent collision in the northeast, crustal scale delamination occurred at or near the base of the crust, enabling the crustal

thickening of the colliding continental lithosphere, as the crustal plates butted against each other (blind subduction) (Stockmal et al., 1987; Stockmal et al., 1990). This model has been reconciled with crustal fabrics observed in the recent LE89 deep seismic data (Quinlan et al., 1992). However, direct seismic evidence of a sub-crustal, eastward dipping shear zone that may represent the top of the subducting lithosphere has not been found (Figure 2.1).

The interpretation of marine deep seismic reflection data recorded in the period 1984 -1986 has indicated that the surface zones as described previously, may overly three distinct lower crustal blocks (LCBs) (Keen et al., 1986, Marillier et al., 1989). The LCBs were identified as Grenville, Central and Avalon from west to east (Figure 1.1) and are defined mostly by the character of the deep reflection data. The Grenville LCB, which has a weakly-defined deep Moho cut by northwest-dipping reflectors, is taken to represent the North American craton and has an eastern boundary that lies below the orogen. This boundary possibly extends as far as the surface expression of the Red Indian Line, which divides the Notre Dame and Exploits Subzones of the Dunnage Zone. The Avalon LCB has a deep, poorly-defined Moho and only modest lower crustal reflectivity. It lies beneath the Avalon Zone, and possibly the Meguma Zone, and has a western boundary that correlates with the surface boundary between the Avalon and Gander Zone. This implies that the Avalon Zone is autochthonous on the Avalon LCB and that the Central LCB is separated from the Avalon LCB by a major fault system represented at surface by the Dover and Hermitage Bay Fault zones (Marillier et al., 1989). The Central LCB lies between the Grenville and Avalon blocks and has a well-defined Moho reflection at modest depth overlain by a moderately reflective lower crust with

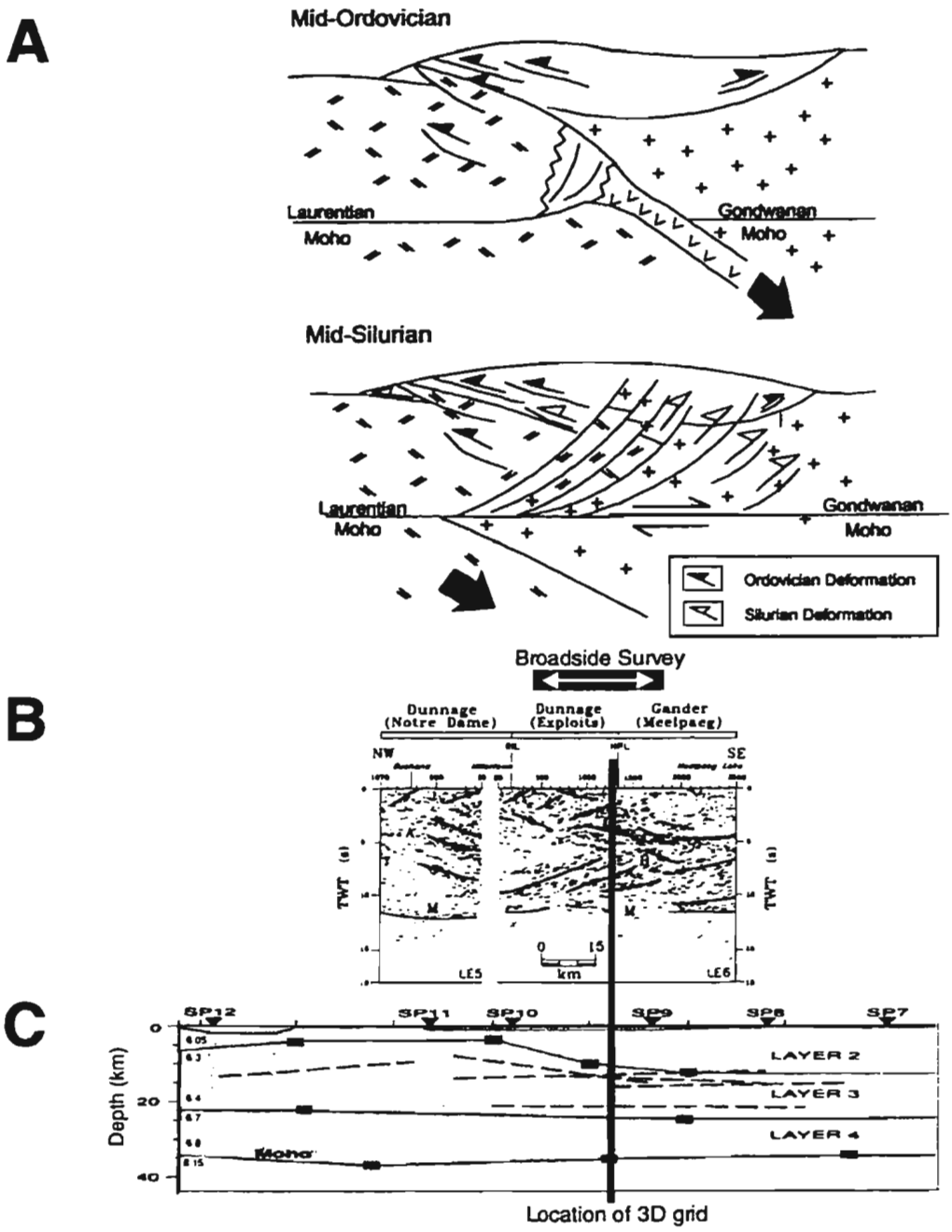

Figure 2.1 Tectonic relationships along the LE89 Meelpaeg transect

Results from the Meelpaeg transect of the LE89 reflection survey (Quinlan et al., 1992) (B) and the line 3 seismic velocity model from the LE91 refraction survey (Hughes et al., 1994) (C) are compared to a cartoon of Quinlan et al. (1992) (A) which shows how reflectivity patterns observed on the deep seismic data can be related to orogenic events occurring in the mid-Ordovician to mid-Silurian. The three sections are approximately aligned and similarly scaled. The position of the broadside experiment and 3D grid is indicated on (B) and (C).

predominantly northwest dipping reflections. The boundary between the Central and Avalon LCBs is suggested to be near vertical (Marillier et al., 1989). More recently however, high quality seismic data from the Meelpaeg transect of the LITHOPROBE East 1989 vibroseis survey (LE89), which crosses the proposed boundary between the Central and Avalon LCBs in southern Newfoundland, gives no indication of a near vertical boundary at that point (Quinlan et al., 1992). In fact northwest dipping zones of reflectivity seem to be continuous across areas of the crust identified as Avalon and Central LCBs. The recent seismic data from Newfoundland would seem to be more consistent with the idea that the Central and Avalon LCBs have the same Precambrian history and therefore, it would be more appropriate to think of this portion of crust as part of the Gondwanan plate (Quinlan et al., 1992). To be consistent with this terminology the Grenville LCB would be referred to as part of the Laurentian plate. Figure 2.1A shows a cartoon of the proposed crustal processes that produced the fabrics imaged by the 1989 seismic reflection data. A portion of interpreted seismic data from the Meelpaeg transect of the LE89 survey is positioned such that the observed fabrics can be approximately correlated with the model of Quinlan et al. (1992) (Figure 2.1B). The northwest dipping fabrics which characterize the Central LCB extend up to the middle crust where they are a significant target of the broadside experiment, which should establish how their strike compares with that of surface geology.

Refraction data collected in 1991 during the LITHOPROBE LE91 refraction program has further constrained tectonic processes that have produced the Appalachian orogen (Marillier et al., 1994; Hughes et al., 1994). The interpretations show normal lower crustal velocities

below most of the orogen indicating an intermediate composition for the lower crust (Hughes et al., 1994). It appears that a high velocity layer at the base of the crust at the western edge of the Humber Zone (Michel et al., 1991, Marillier et al., 1991) does not extend eastward below the central mobile belt. In other respects, lower crustal velocities are similar to that typically observed (6.7 - 6.8 km/s) and, as first seen by the 1989 reflection data and confirmed by 1991 refraction results, crustal thickness across the orogen is 35 +/- 3 km, consistent with normal continental crust. Notably, there is no crustal root beneath the Dunnage and Gander Zones, which when combined with the apparent intermediate composition of the lower crust has prompted investigators to suggest that the crust may have undergone significant re-equilibration since the early Paleozoic (Hughes et al., 1994). Figure 2.1C shows the interpreted line 3 from the LE91 refraction survey, which is collinear with the Meelpaeg transect in central Newfoundland, positioned in approximate alignment and at the same scale as the model and seismic reflection data for the same area. This section shows the broad crustal velocity structure in the vicinity of the broadside experiment, where the upper crustal velocity is 6.05 km/s, the middle crust is 6.3-6.4 km/s (10-22 km depth), and the lower crust is 6.7-6.8 km/s. The Moho marks the transition to the upper mantle (8.15 km/s) and is at approximately 35 km depth.

The tectonostratigraphic zonal divisions in Newfoundland also have distinct geopotential signatures (Miller, 1990). Important to this study is the fact that the Dunnage Zone is characterized by positive gravity anomalies, contrasting the negative gravity anomalies which are associated with the Gander Zone in northeast Newfoundland (Miller, 1990).

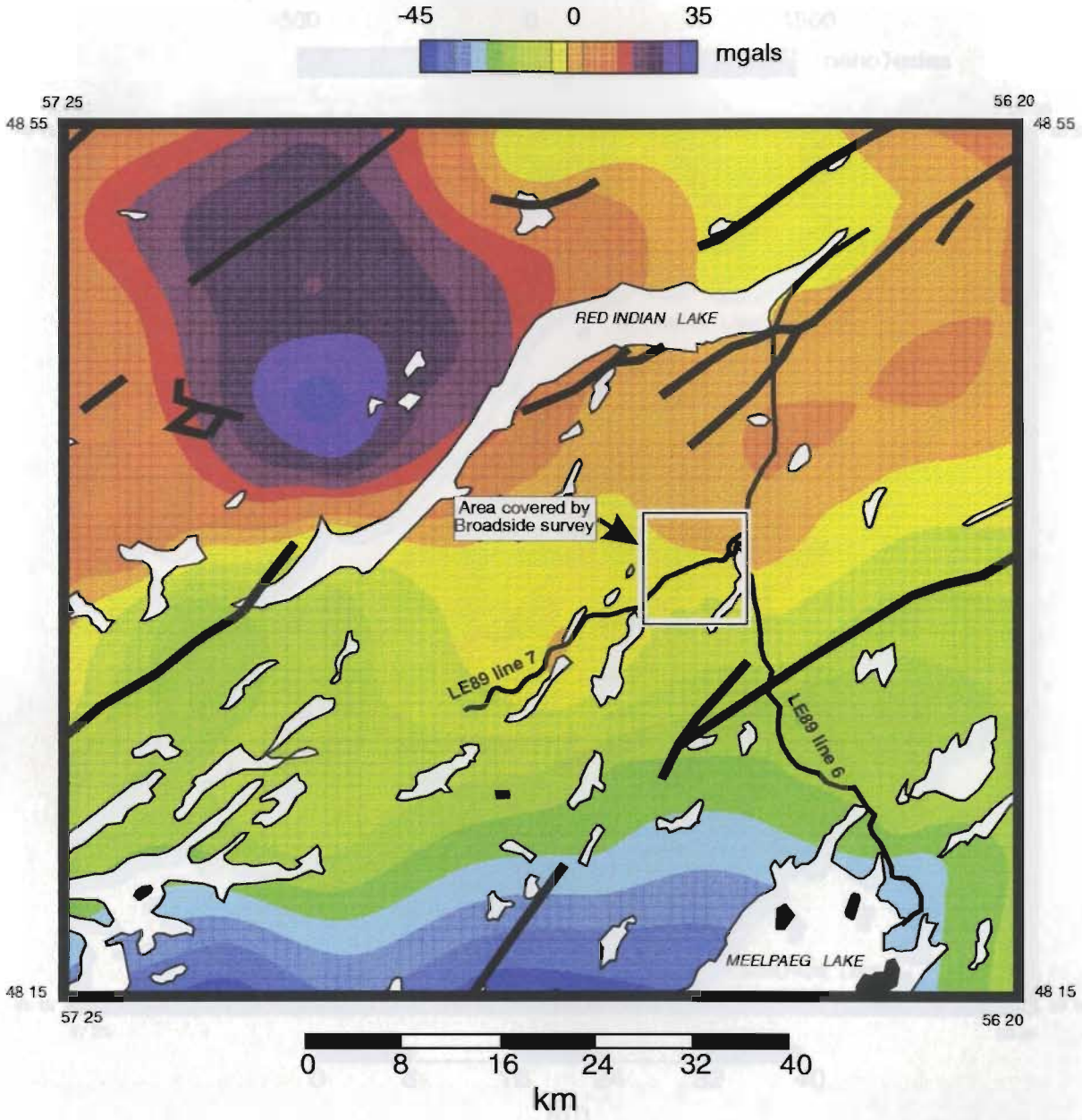

Figure 2.2 Contoured Bouguer gravity map

Contoured Bouguer gravity data overlain on same map section as Figure 2.2 with the same geographical features and major fault zones indicated. Gravity data courtesy of the Geophysical Data Centre, Geological Survey of Canada, Ottawa.

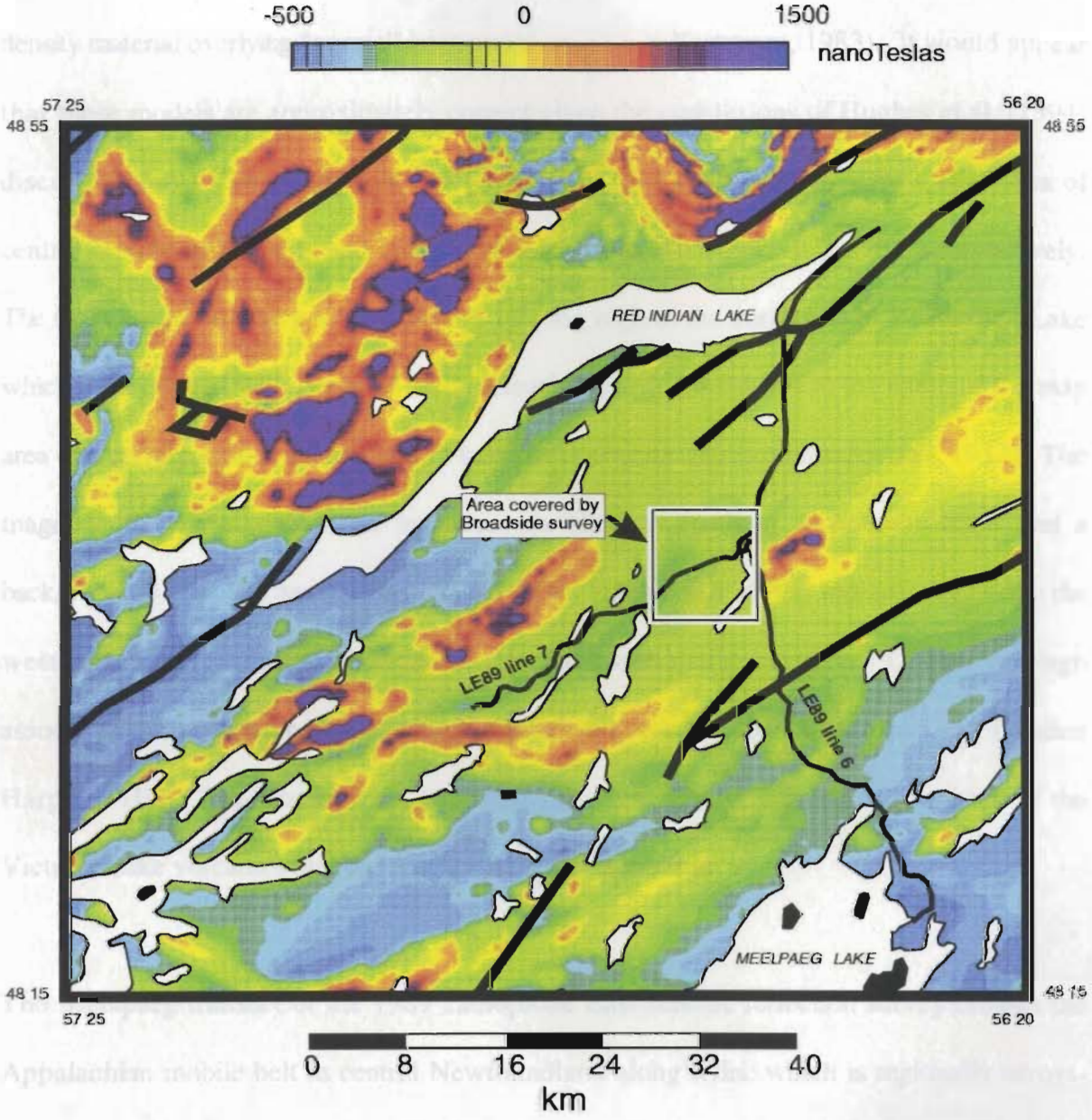

Figure 2.3 Contoured magnetic field data.

Contoured Magnetic field data overlain on same map section as Figure 2.2 with the same geographical features and major fault zones indicated. Aeromagnetic data courtesy of the Geophysical Data Centre, Geological Survey of Canada, Ottawa.

Conventional gravity models of the Dunnage Zone show a 10-15 km thick zone of higher density material overlying "normal" continental crust (e.g. Karlstrom, 1983). It would appear that these models are approximately correct given the conclusions of Hughes et al. (1994) discussed above. The contoured Bouguer gravity and magnetic field data for the area of central Newfoundland covered in Figure 1.2 are shown in Figures 2.2 and 2.3 respectively. The main features of the gravity field are a strong high to the northwest of Red Indian Lake which is associated with zones of mafic intrusives, and a broad low to the south of the map area that corresponds to a major belt of large, late-orogenic plutons (Blackwood, 1982). The magnetic map is characterized by numerous short to medium wavelength highs and a background of broader negative anomalies. The highs north of Red Indian Lake and to the west of the 3D grid area can again be associated with mafic intrusives. Of note is a high associated with a small gabbroic pluton immediately east of the join of lines 6 and 7, called Harpoon Hill. The broader lows to the southwest of Red Indian Lake are related to the Victoria Lake volcanics and the Annieopsquotch ophiolites.

The Meelpaeg transect of the 1989 Lithoprobe East seismic reflection survey crosses the Appalachian mobile belt in central Newfoundland along a line which is regionally across-strike. However, rather than assume that reflections on the profiles are dipping in the plane of the section, the opportunity was taken to run short cross-lines at a small number of locations where it was geologically worthwhile and logistically feasible, in order to provide information on the true dip direction of reflectors. Line 6 is part of the main transect; line 7 is a 20 km cross-line, close to several prominent structures (such as Noel Paul's Line) where

the tie to reflections was thought to be particularly useful. It was at this locality that the experiment described here was mounted (Figure 1.2).

3.0 DATA ACQUISITION

3.1 Seismic Method

The basic technique of seismic exploration consists of generating seismic waves and measuring the time required for the waves to travel from the sources to the receivers, or geophones. The geophones are typically arranged in a straight line going away from the source in one or two directions. A seismic record is a gather of the recordings from all the geophones for one shot. On a shot record numerous waves are observed with the important ones being the reflected and refracted waves. Figure 3.1 shows some of the typical signals seen on a seismic record. For both reflected and refracted waves the travel time from source to receiver depends upon the physical rock properties and the structural orientation of the lithological units. Thus, in seismic exploration the goal is to deduce information about the rocks and their structural orientation from the seismic data, primarily the observed travel times.

The sources for all the data recorded during the LITHOPROBE East 1989 reflection survey were large, truck mounted mechanical vibrators, using a method called vibroseis. The vibroseis technique is schematically shown in Figure 3.2 and briefly described below. The vibrator trucks, once in position, are remotely triggered by the recording truck. A frequency modulated sine wave (sometimes called a chirp) is sent to the vibrator from the recording truck, causing the vibrators to exert a quasi-sinusoidal force of many tons on the ground,

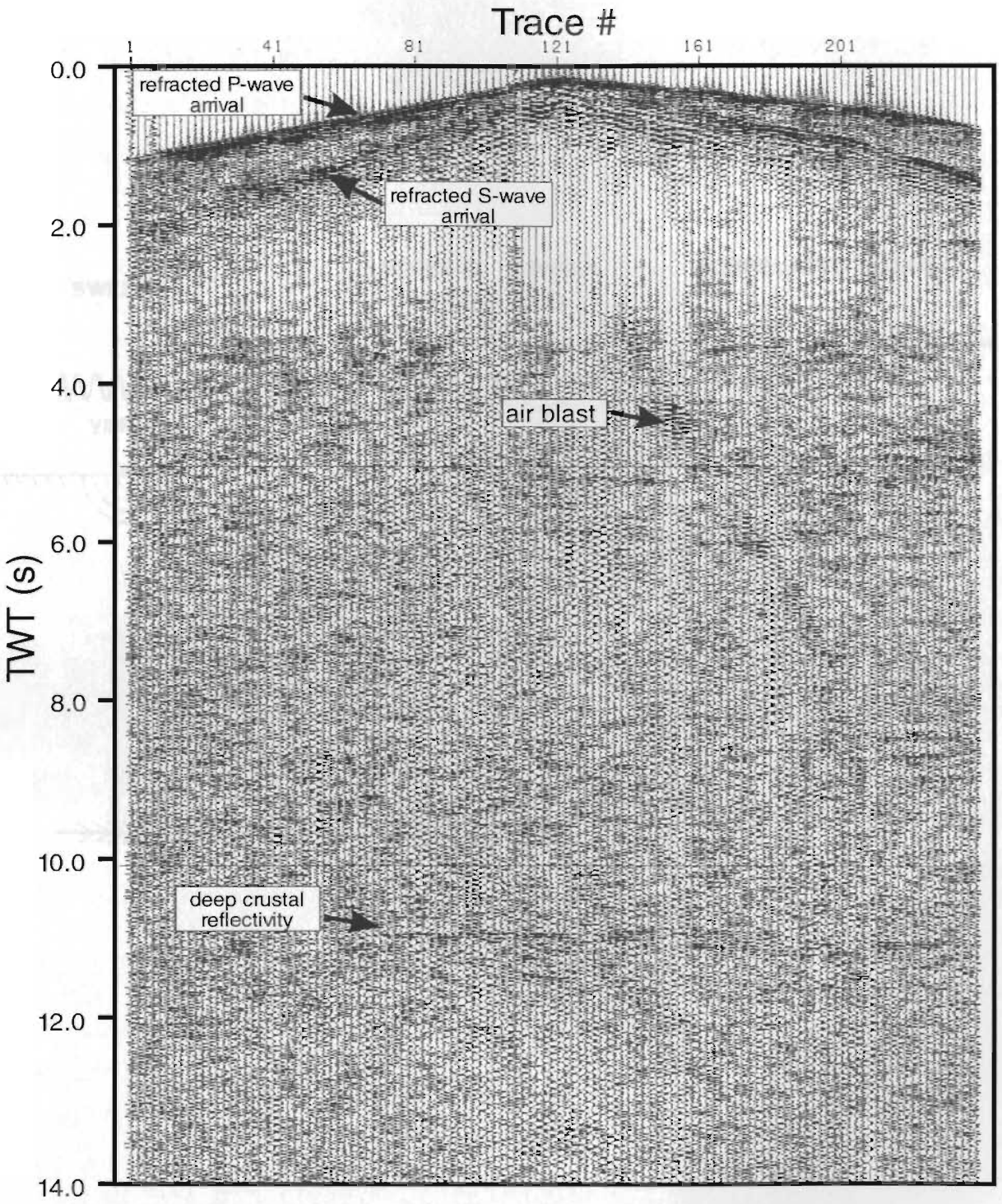

Figure 3.1 Broadside shot gather 1042.

Sample correlated shot record from the broadside seismic experiment (shot number 1042) with some of the observed wavefields labelled.

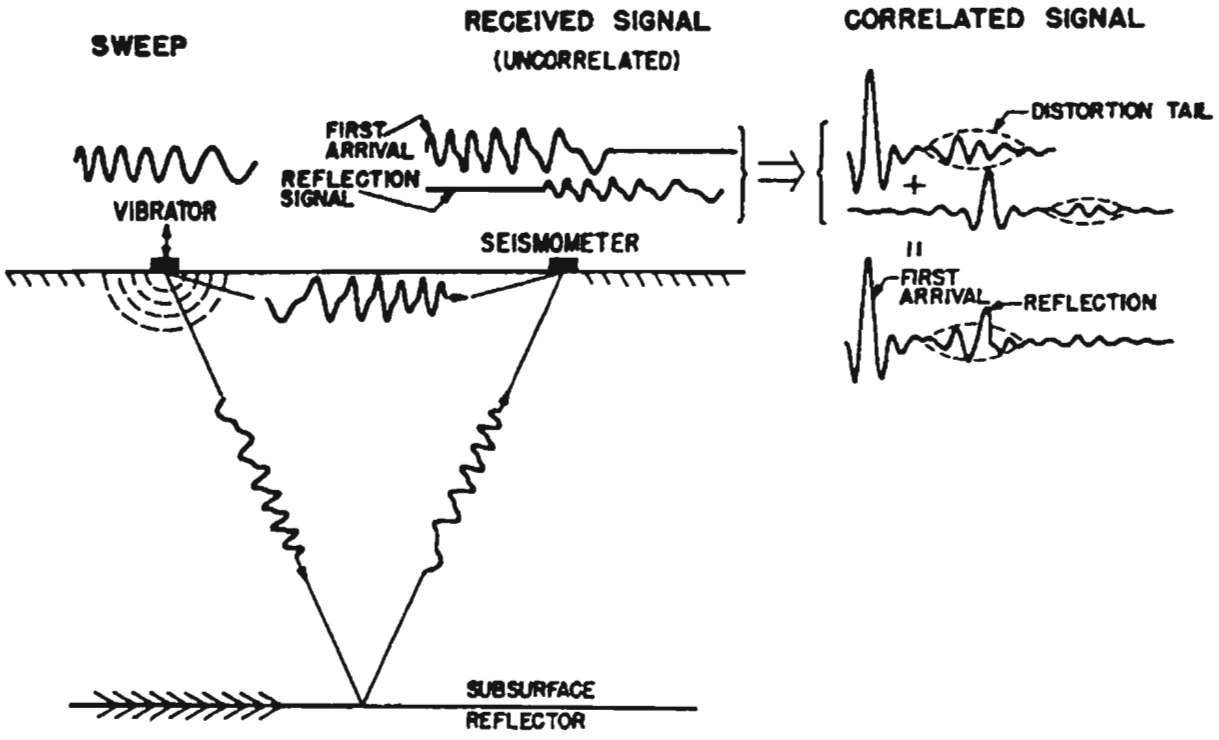

Figure 3.2 The vibroseis method

A schematic displaying the vibroseis method (Sheriff and Kim, 1970).

generating seismic waves. The recorded signals are a superposition of long wave trains arriving at different times and thus are not readily interpretable at this stage. The seismogram must be cross correlated with the sweep signal generated by the vibrator truck to produce a shot record like that shown in Figure 3.1. The benefits of using the vibroseis method are many; the source is very strong and can be scaled up by adding more trucks to the group, there is very little environmental risk with the vibrators, a crew can easily work around the clock if necessary without worrying about the safety precautions inherent with using dynamite, and the correlation process produces higher peak signal with respect to noise sources which are not simple combinations of sweep signals (Sheriff and Kim, 1970). On the negative side, harmonic distortion on the outgoing signal can produce tails or forerunners on fundamental pulses.

3.2 Geometry of the Survey

The broadside and wide-angle seismic experiment was performed as an add-on to the main LITHOPROBE East regional reflection survey in 1989. At the junction of lines 6 and 7 from the regional work (Lake Ambrose) it was decided to leave the 240 channel receiver spread on the ground and vibrate away from the spread in three directions; north along line 6 towards Red Indian Lake, south along line 6 towards Meelpaeg Lake, and west (broadside) along line 7 (Figure 3.3). The shotpoints were spaced at 300 m in all three directions. Shooting continued down each of the lines until radio communication between the recording truck and the vibrators was lost. Thus, the offsets reached by the end-on and broadside shots were

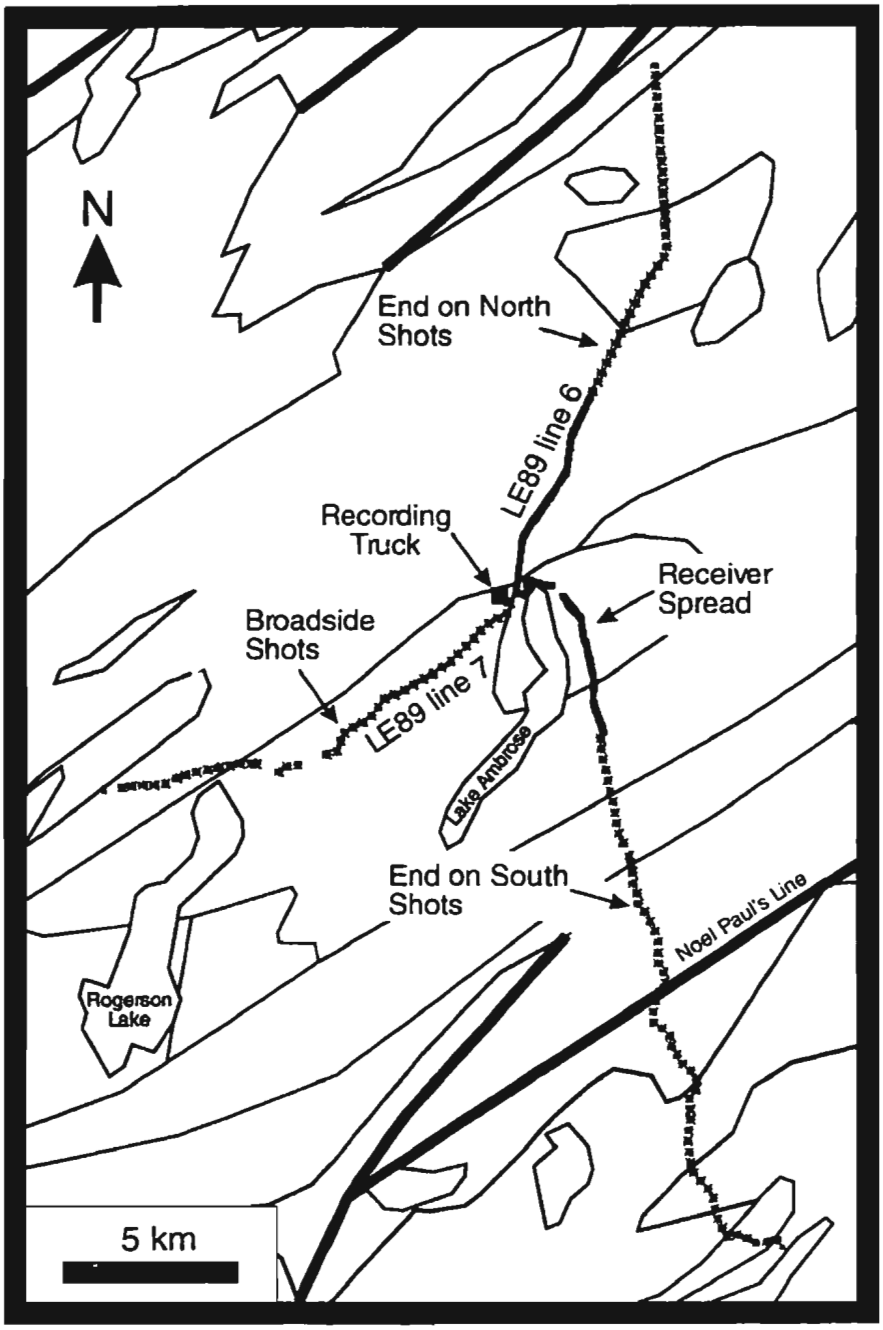

Figure 3.3 Geometry of the broadside experiment.

The geometry of the broadside experiment. The geological contacts (thin black lines), major fault traces (thick black lines), and lakes (grey) are the same as those in Figure 2.2, but at a reduced scale.

primarily controlled by the topography of the area. The maximum offsets from the recording truck, which was positioned at the junction of lines 6 and 7, were: broadside - 12.5 km, end-on-south - 18 km, end-on-north - 14 km.

3.3 Acquisition Parameters

The table below summarizes all the recording parameters for the experiment:

Table 3.1. Acquisition parameters: broadside and wide-angle seismic experiment

Recording

Contractor:	Capilano Geophysical Ltd.
Instrument:	CFSS/DFSV
High Cut Filter:	64 Hz/72 dB
Low Cut Filter:	out
Notch Filter:	out
Sample Rate:	4 ms
Tape Format:	SEGY
Density:	6250

Receivers

Number of Channels:	240
Geophone Frequency:	14 Hz
Make/Model:	Mark L-28
Geophones/group:	12
Groups/station:	1
Group Interval:	50 metres

Source

Source Type:	Vibrator (HEVIQUIP 44's)
Peak Force:	44,000 lb
Source Array:	4 over 30 m, move up 20 m
Number of Sums:	8

Sweep Length:	14000 ms
Record Length:	32000 ms
Listen Time:	18000 ms
Sweep Frequency:	8 Hz start / 40 Hz end
Taper:	500 ms start / 500 ms end

The source consisted of 4 Vibrators which generated their sweeps then moved up 20 metres and repeated the process. Two techniques were used to reduce noise levels during data acquisition: i) phase shifting the sweeps sent to the vibrators to reduce 60 Hz noise, and ii) diversity stacking. A pair of electrodes was placed in the ground near the recording truck and the background 60 Hz signal was constantly monitored. The first sweep signal sent to the vibrators was initiated on a peak of the background 60 Hz. The following sweep for the same shotpoint was triggered at a 1/2 wavelength shift for the same 60 Hz signal. Thus, of the 8 sweeps recorded, 4 would contain 60 Hz signal that is phase shifted by 1/2 a wavelength from the 60 Hz on the second 4 traces. In theory, any time-invariant background 60 Hz noise picked up by the geophones should be eliminated by the stacking process. In practice this method worked quite well as the amplitude levels for 60 Hz signal are extremely low relative to signal levels in the desired frequency range (Figure 3.4). Once the 8 traces at each shotpoint were recorded, they were diversity stacked to produce the raw uncorrelated traces. Diversity stacking involves calculating a rms value over small windows, which are centred on a given sample, on each input trace and then weighting the samples contribution to the stack by a factor of 1/rms. Thus a trace with an abnormally high amplitude over a given time window will not affect the overall quality of the stack. The uncorrelated traces are then correlated with the sweep trace to produce the correlated data. For this experiment both

uncorrelated and correlated data were recorded to tape in the field. This turned out to be important for reasons that will be discussed in coming sections.

An example of a raw shot gather from the broadside experiment is displayed in Figure 3.1. It can be seen that the data shows clear refracted compressional wave (P wave), refracted shear wave (S wave), and air blast arrivals. The refracted arrivals are head waves which propagate along the bedrock-overburden interface at a velocity equal to that of the bedrock material. In general, the signal to noise ratio is high and by looking at the levels of mid-crustal reflectivity it is apparent that the source is providing enough signal strength. Strong, coherent reflections at 11 sec which may be associated with the Mohorovic discontinuity (Moho) are also apparent on the shot gathers.

The recording parameters for the broadside and wide-angle experiment are identical to those used during the acquisition of the LE89 regional lines, with one exception; the sweep frequencies used during the regional work were 8-56 Hz compared to the 8-40 Hz sweep used for the broadside experiment (Figure 3.4). Other than testing the effect of removing the higher frequencies on data quality it is uncertain why the 8-40 Hz sweep was used. In retrospect the high frequencies would have been desirable for the broadside and wide-angle data. This is because it was found that the higher frequencies contained most of the useful signal and by limiting ourselves to 40 Hz we were left with only 20-25 Hz of "useful" bandwidth. In addition, it has been shown that the reflective properties of crystalline terranes are fundamentally different from a sedimentary basin environment. The reflection coefficients

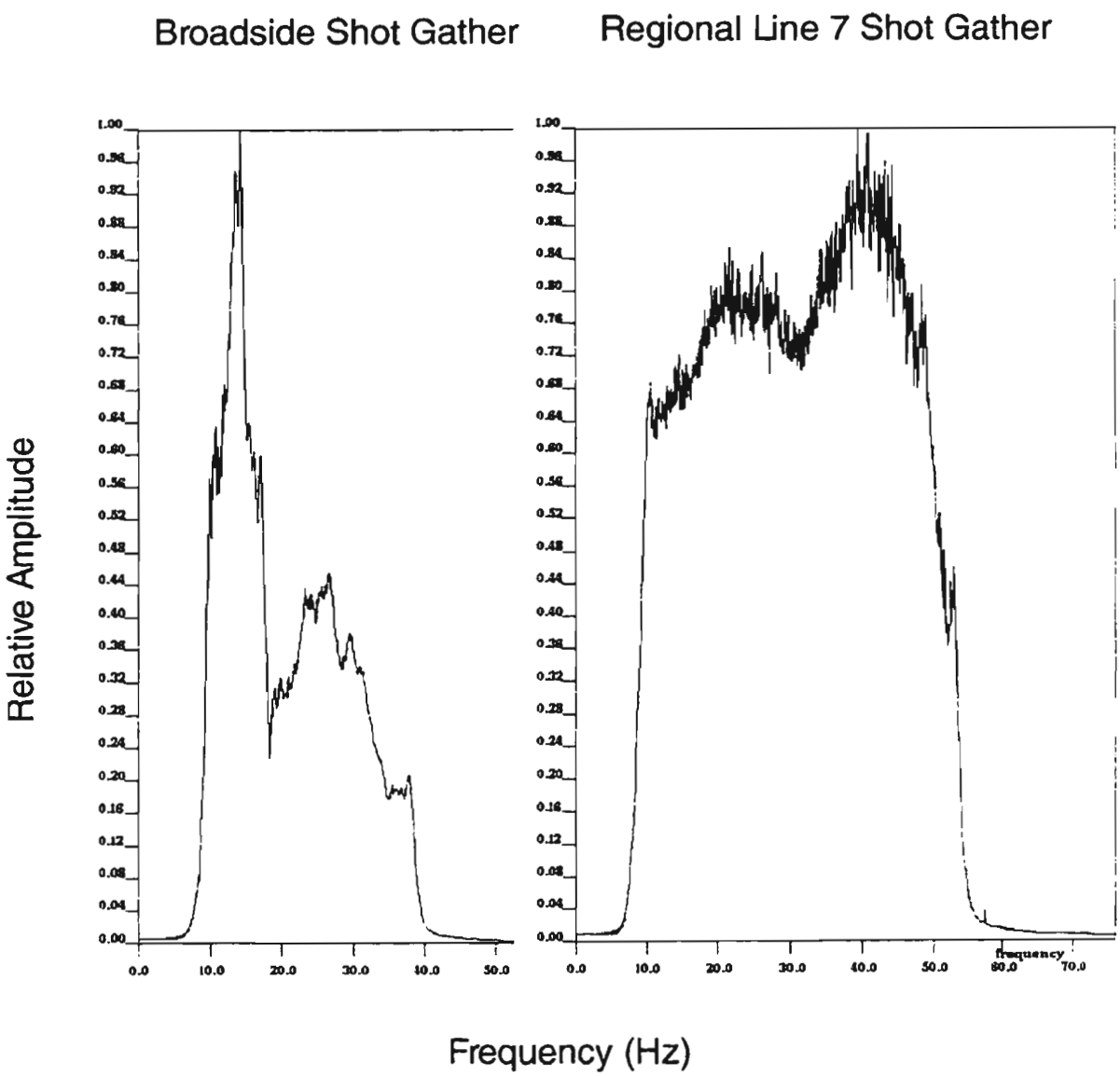

Figure 3.4 Frequency spectrum from Broadside survey and LE89 line 7.

A comparison of the frequency spectrum of a sample shot gather (240 traces, 14 s) from line 7 of the LE89 reflection survey (A) and shot gather 1042 (240 traces, 14 s) from the Broadside experiment (B). The vertical axis shows normalized amplitude and the horizontal axis is frequency (Hz).

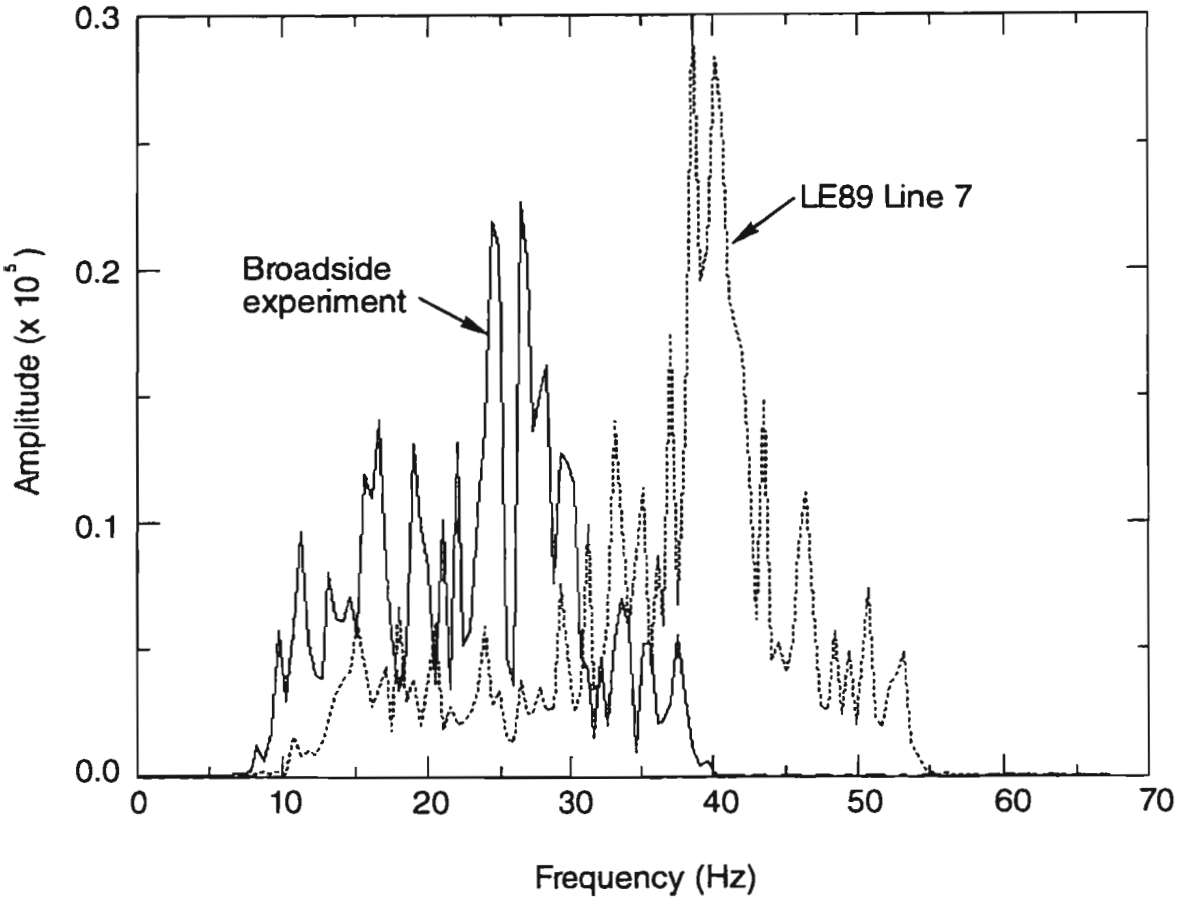

Figure 3.5 Frequency spectrum at 2 km offset for broadside and line 7 shots.

A comparison of the frequency spectrum for a trace from shot 1 of the Broadside experiment (solid line) and a trace from shot 1 of LE89 line 7 (dashed line). Both traces have an offset of 2 km. The vertical axis shows absolute amplitude and the horizontal axis is frequency (Hz).

in the crystalline crust are usually low relative to those found in sedimentary basins, especially in the 10-50 Hz bandwidth (Milkereit and Eaton, 1997). Comparing the frequency spectra from the broadside data with that of LE89 line 7 at the same scale shows that the power levels are similar, but the broader sweep used for the regional survey generated higher peak amplitudes at a higher frequency (Figure 3.5). Chapter 4 contains further discussion of the frequency content of the data and how it affected the processing applied to this data set. The wider shot spacing and narrow frequency band used in these experimental surveys indicate that the special experiments were not given the same priority as the regional lines in Lithoprobe East data acquisition. This is understandable but regrettable, as the results will show.

One type of noise which can be identified upon close examination of the shot records is the common occurrence of "reverse sweeps", or inverted copies of the original vibroseis sweep, overriding the trace data. These reverse sweeps are readily seen on a close-up of a raw shot gather (Figure 4.2A). The processing strategies to eliminate this source of noise will be covered in the next chapter.

4.0 DATA PROCESSING

4.1 Removal of Reverse Sweeps

The reverse sweeps mentioned in the previous section were discovered after the 1989 regional survey was well underway and the problem was fixed near the halfway point in the completion of the regional lines. After some investigation it was discovered that the uncorrelated data was contaminated with very high amplitude, single sample spikes, generated by the diversity stacking algorithm used by Capilano Geophysical Ltd (Figure 4.1). When the records were correlated with the vibroseis sweep to produce the shot gathers, the spikes produced reverse sweeps in the correlated domain (Figure 4.2). For the regional data the fold was high enough (nominally 60-fold) that automatic gain control (AGC) scaling of the data pre-stack reduced the contribution of the traces containing the high amplitude reverse sweeps, leaving reflection energy that was still strong (Quinlan et al., 1992). However, for the broadside experiment we have limited data and the CDP fold of individual gathers in any 3D processing scheme will be relatively low (average of 10-15 fold). Therefore it was important that the reverse sweeps be removed so that the weaker reflection energy could be enhanced by the stacking process.

We were fortunate with the broadside experiment, in that the uncorrelated data was also collected and stored on 9-track tape. An algorithm was designed that effectively removed the high amplitude spikes from the uncorrelated data. In a given trace the rms amplitude is

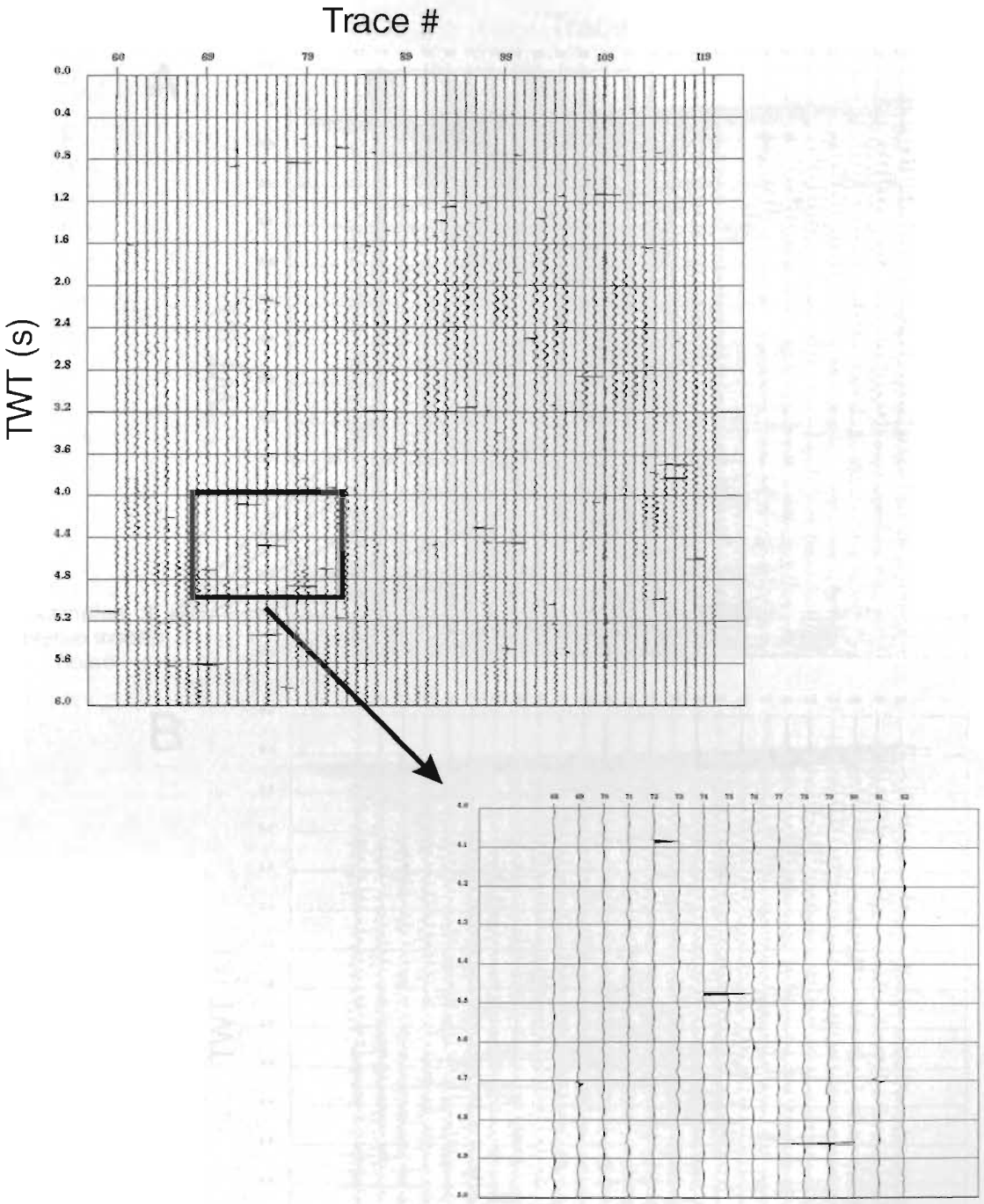

Figure 4.1 Reverse sweep noise

Close-up of a section from an uncorrelated shot gather from the broadside and end-on experiment with a further close-up displaying the exact nature of the high amplitude spikes that contaminated the raw shot gathers from this survey.

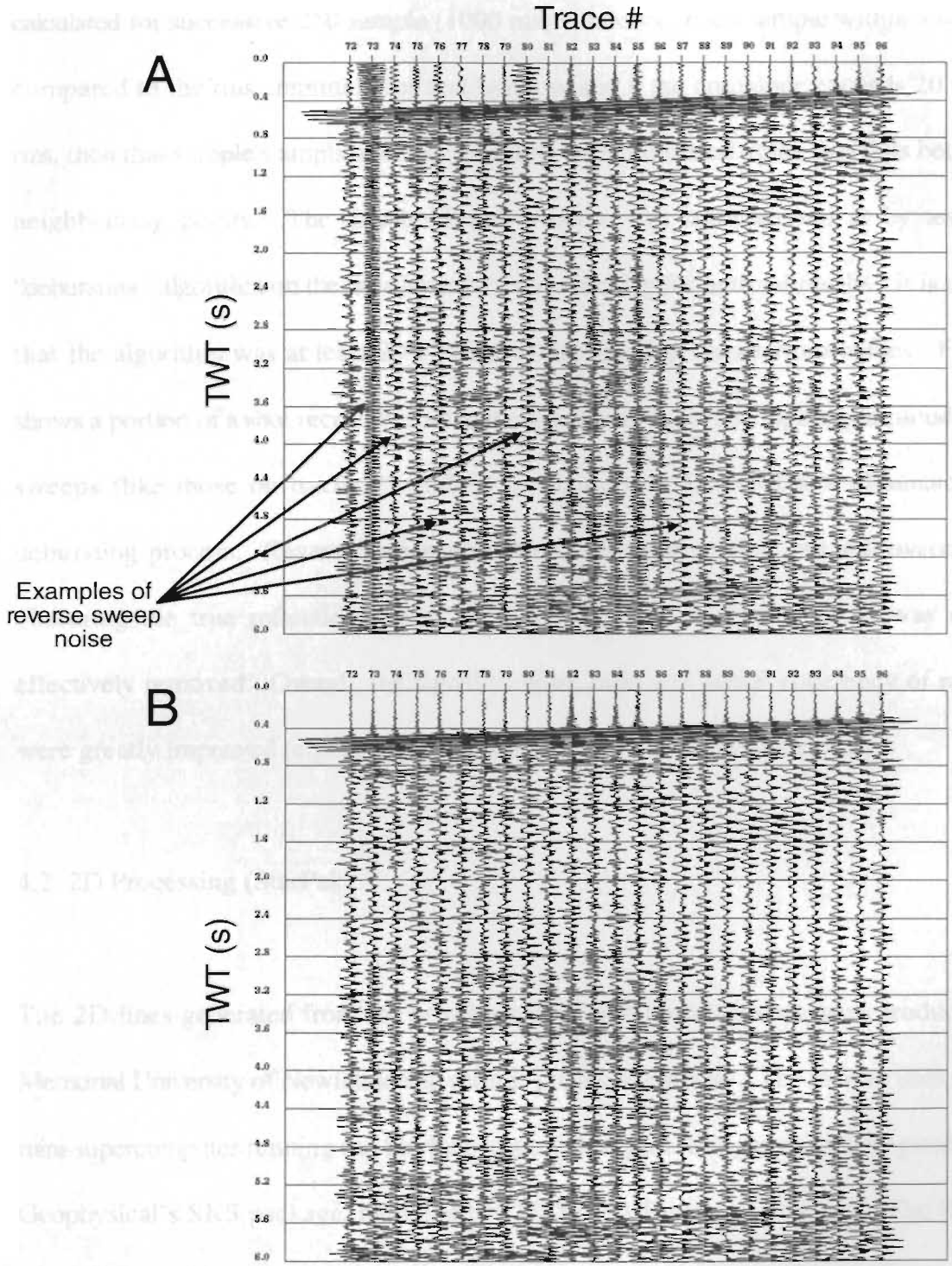

Figure 4.2 Removal of reverse sweep noise

A portion of a correlated broadside shot gather before (A) and after (B) application of debursting algorithm.

calculated for successive 250 sample (1000 ms) windows. Each sample within a window is compared to the rms amplitude for that window and if the amplitude exceeds 20 times the rms, then that sample's amplitude is replaced by an interpolated value that falls between the neighbouring points. The threshold and window size were arrived at by testing this "debursting" algorithm on the broadside data and checking for optimal results. It is estimated that the algorithm was at least 90% effective in removing the spurious spikes. Figure 4.2 shows a portion of a shot record before and after debursting. The highest amplitude reverse sweeps (like those on traces 73 and 80 in Figure 4.2A) were 100% eliminated by the debursting process. Reverse sweep noise that is not dominating, but still overriding and obscuring the true reflection energy (e.g. traces 82-87 in Figure 4.2A) was also very effectively removed. Overall, the signal to noise ratio and lateral coherency of reflections were greatly improved (e.g. at approximately 3.6 s and 5.6 s in Figure 4.2).

4.2 2D Processing (StarPak)

The 2D lines generated from the broadside and wide-angle data set were produced at the Memorial University of Newfoundland seismic processing facility. The facility uses a Convex mini-supercomputer running the StarPak seismic data processing package (originally Merlin Geophysical's SKS package, modified by GECO and Texaco as StarPak). The three parts of the data set that were processed with the StarPak software were in-line sections along both regional lines 6 (end-on-south line 1) and 7 (broadside line 13), and a series of high fold CDP gathers along line 6 using the end-on-south wide-angle shots.

4.2.1 In-line Sections

The processing sequence used for the two in-line sections was relatively straightforward and is detailed on the flow chart in Figure 4.3. Some parts of the processing do require further discussion; specifically the selection of velocities for normal moveout (NMO) corrections, bandpass filtering, and coherency filtering. A satisfactory refraction statics solution could not be produced using the StarPak processing package, perhaps due to the irregular geometry and unreversed travel times that the broadside and end-on survey presented. However, refraction statics was applied to the 3D cube with the INSIGHT package. Refraction statics have the greatest effect on high frequency, near-surface events, but for the lower frequency, deep crustal events that we focus on with this study the static corrections are not as important. The following points also apply to similar steps in the 3D processing sequence.

1) Velocity Control

The selection of velocities for the NMO correction of the broadside and wide-angle data would have been very difficult if this were an isolated data set. The generally low fold and patchy reflectivity encountered with the broadside data made the standard techniques for velocity analysis practically useless. However, velocity profiles obtained from the analysis of the high fold regional data in the same area as the broadside experiment were available. It is clear from looking at the first break information on the shot gathers that in the Lake Ambrose area there is a thin, low velocity overburden (not always present) with high velocity

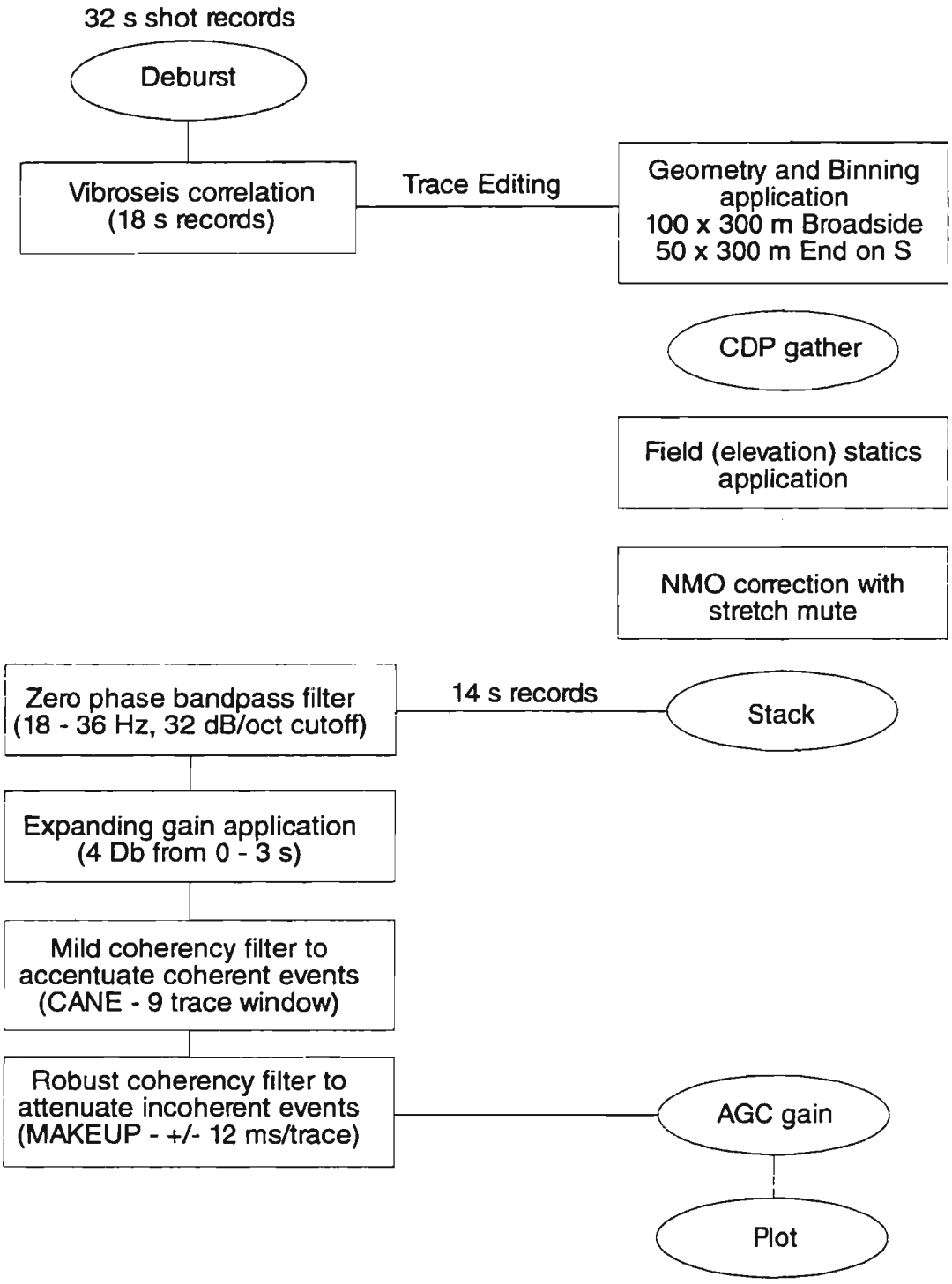

Figure 4.3 2D in line processing sequence.

Processing sequence used for the 2D in line sections generated from the broadside and end-on-south shots using the StarPak seismic data processing package.

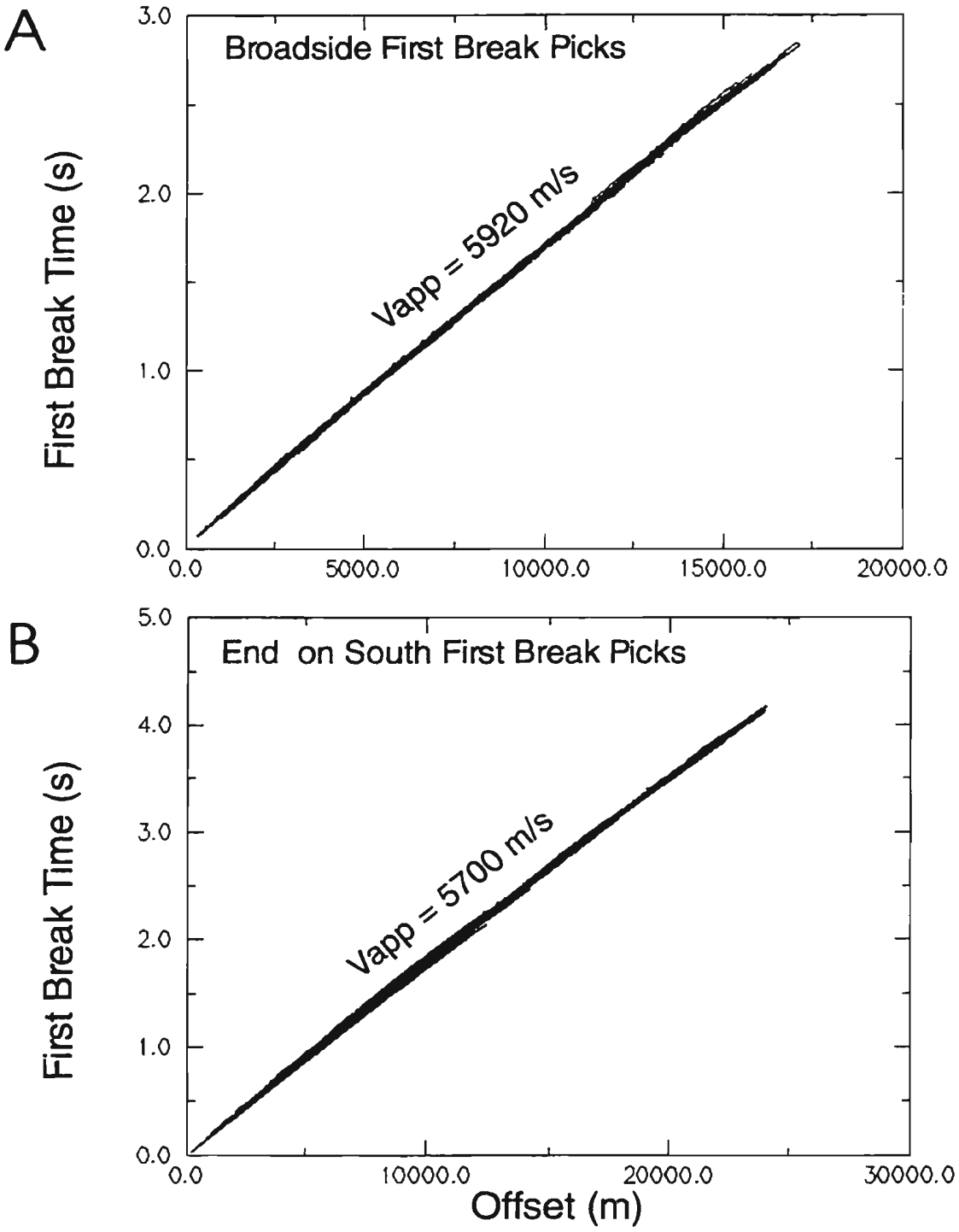

Figure 4.4 First break picks for the broadside and end-on-south shots.

A summary of all the first break picks for the broadside (A) and end-on-south (B) shots. Each first break pick time is plotted as a single point with each plot containing over 10,000 points.

metamorphic and volcanic rocks immediately below. The first break picks from the broadside and end-on-south shots (Figure 4.4) show that the apparent velocity of the basement rocks in this area is 5800 +/- 120 m/s. The somewhat lower average velocities seen from the end-on-south shots can likely be attributed to the presence of the lower velocity Rogerson's conglomerate which is positioned between the receiver spread and the shots. Some constant velocity stacks were made for the in-line section along regional line 7 and it was found that the focussing of the mid to lower crustal reflectivity was quite insensitive to velocity differences in the order of 5 to 10%. Thus, a single velocity function based on those from the processing of the regional lines, and adjusted slightly after analysing the constant velocity stacks, was used for both the broadside and end-on-south data. The velocities used are detailed in the table below.

Table 4.1, Velocity functions for NMO corrections

Broadside / End-on-South	
2 way Travel Time (ms)	Vstack (m/s)
150	5200
400	5500
1800	5800
2700	6000
3600	6400
6500	7000

2) Bandpass filtering

The earlier discussion on the recording parameters referred to the frequency spectrum of the data acquired in this experiment. Figure 4.5 shows the frequency spectrum of shot gather 1042 (Figure 3.1) from the broadside data. In addition to seismic reflection energy the top 6 s of the shot gather contains all the energy from the first arrival P and S waves as well as contributions from ground roll and air blast (Figure 4.5A). These various elements of seismic "noise" dominate the shot gathers in the 5 - 20 Hz range. Below 6 s we observe that the dominant energy is in the frequency range of 15 - 35 Hz with a peak at 25 Hz and we are only left with a small peak at 10 Hz which can be attributed to air blast energy (Figure 4.5B). The primary source of seismic energy in this frequency range can be attributed to reflected and scattered signal which is superimposed on the ambient background noise. It was decided to apply a bandpass filter of 18 - 36 Hz with a 32 dB/oct cutoff on each end in order to retain the desired seismic signal while removing the bulk of the unwanted noise. Filtering out the low frequencies from this data has left us with only one octave of effective bandwidth, however, this is an acceptable trade-off in order to remove as much noise as possible from the shot gathers.

3) Coherency filtering

Coherency filtering is very common with the processing of deep crustal data, in order to enhance relatively weak, but coherent, reflection signal and eliminate incoherent background

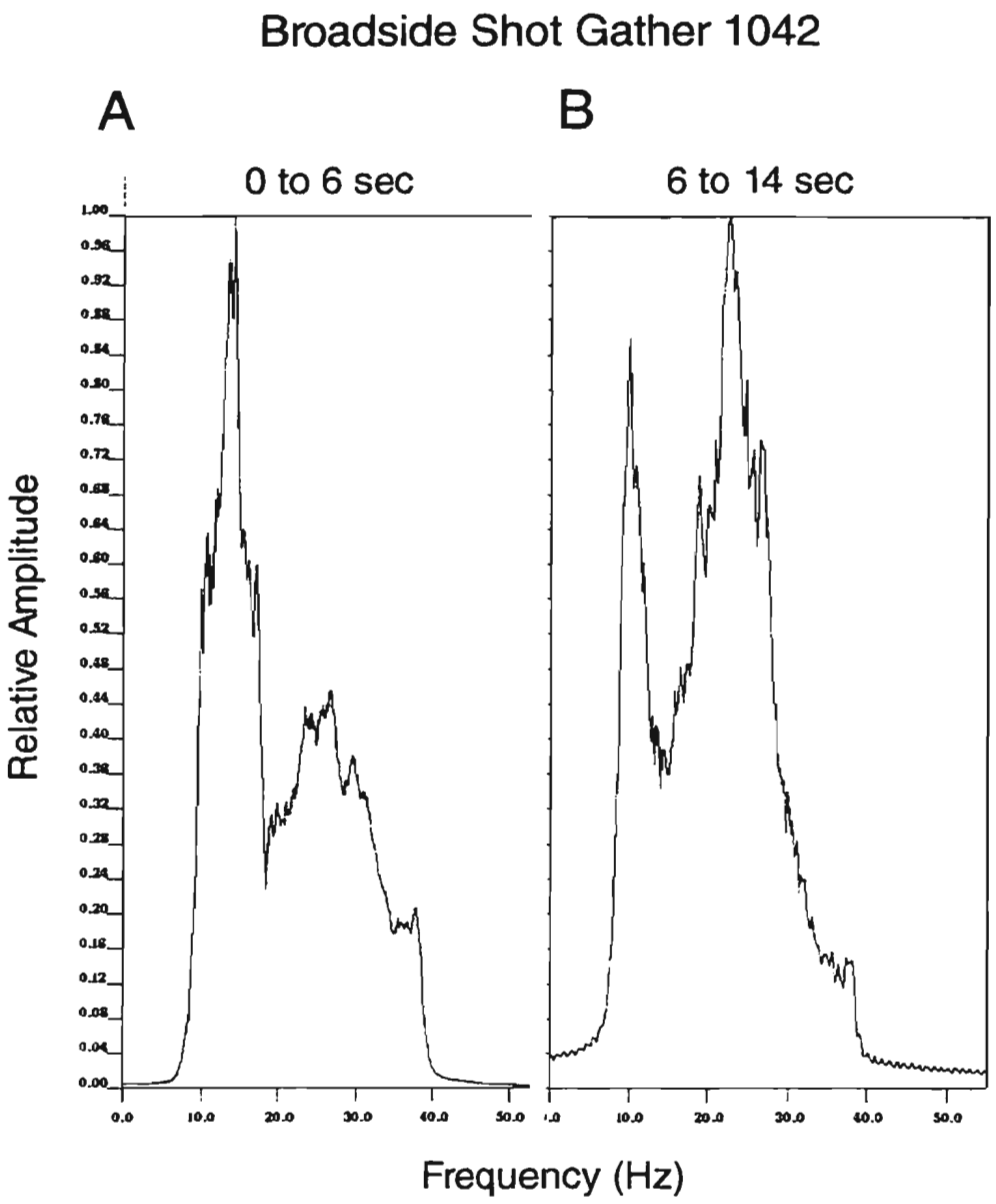

Figure 4.5 Frequency characteristics of broadside shot gather 1042.

The frequency spectrum of broadside shot gather 1042 (240 traces) for 0 to 14 seconds (A) and 6 to 14 seconds (B) (see figure 3.1). The vertical axis is normalized amplitude and the horizontal axis is frequency (Hz).

noise or steeply dipping coherent noise. With the StarPak software the coherency filtering of the data was a two step process (Figure 4.3). First a mild coherency filter (CANE) is applied that will improve the coherency of events by applying a process similar to non surface consistent residual statics. CANE crosscorrelates a user defined number of adjacent traces with the centre trace (pilot) in a small time window. The crosscorrelations are searched for the maximum peak and the corresponding trace sub-windows are shifted by the peak lag times, weighted, stacked, and tapered. The sub-stacks are then combined at the appropriate times to produce the output trace. This results in the improvement of the alignment and amplitudes of coherent events but has very little effect on the overall look of the section. Secondly, a spatial enhancement processor is applied that attenuates incoherent energy by performing stacks along dip planes at a sequence of dips within set time and trace windows (MAKEUP). For each input time sample MAKEUP checks the neighbouring traces for waveform alignments along several different slopes. Once all the coherences are found for a given point, data with low coherences are attenuated. Seismic events aligning with at least one of the slopes generate large coherences and are preserved, whereas noise, generally having no coherence, will be attenuated. Coherent noise can also be attenuated as long as the slope of the noise falls outside the user defined slope fan. MAKEUP will preserve relative amplitudes by doing a suite normalization after all the filtered traces are put back together, although alternative options exist for scaling the data that will not maintain the amplitude relationships of the data. In Chapter 5 the effects of using coherency filtering on the data used for an amplitude versus offset analysis will be discussed. This filter has to be carefully applied because a section can be easily over filtered, removing not only the background noise

but also the more subtle reflections.

Coherency filtering of the 3D data was performed using a routine called SLCW from the INSIGHT data processing software. This process accentuates coherent energy on given dip planes over a set trace window and is very effective at enhancing low signal reflectivity. The SLCW module applies a forward slant-stack transformation to a user-defined small trace subset of the section. The slant stacks are weighted according to their semblance after which an inverse transformation is done to create the middle trace of the subset. The slopes which display high semblance will dominate the centre trace of the trace subset and hence, coherent events are enhanced at the expense of the incoherent noise. The time-trace window slides along the section one trace at a time until the whole section is processed. As with MAKEUP, SLCW requires careful selection of parameters to ensure that the section is not over filtered or artifacts introduced into the data.

4.2.2 Large-fold CDP's

The end-on-south shots generated a midpoint coverage that enabled the creation of CDP bins containing traces with a wide range of offsets. With the good reflection energy seen in the shot gathers, this data produced an opportunity for an amplitude versus offset (AVO) analysis on some of the deep events that are observed. To perform an accurate AVO analysis it is critical to correct for amplitude variations that can be attributed to source and receiver differences, and the predictable loss of energy that occurs as the source-receiver distance increases (geometrical spreading). It is also important that no processing be applied that destroys the relative amplitude information of the reflections, e.g. automatic gain control (AGC). The processing sequence used to generate and prepare the CDP gathers for an AVO analysis is shown in Figure 4.6. The bin size used was 125 m long (in-line) x 1000 m wide (cross-line) giving a maximum fold of 189 and gathers that contained offsets ranging from 4 to 20 km (Figure 4.7). Scaling was applied twice: 1) traces falling into a common offset range (bin width of 100 m) were balanced within a sliding 2 s time window in order to correct for differences in coupling for both source and receivers (SWTGAIN), 2) a correction for loss of amplitude due to spherical divergence, based on a simplified velocity function (SPHRD). The SWTGAIN program stacks all traces falling into a common offset bin and calculates a gain function based on the stacked trace. The gain function is calculated by dividing a reference absolute amplitude value (constant) by the average absolute amplitude found in a 2 s sliding window and using that value for the sample at the centre of the window for all input traces in the bin. Figure 4.8 shows a CDP (CDP 46) which has been prepared for a

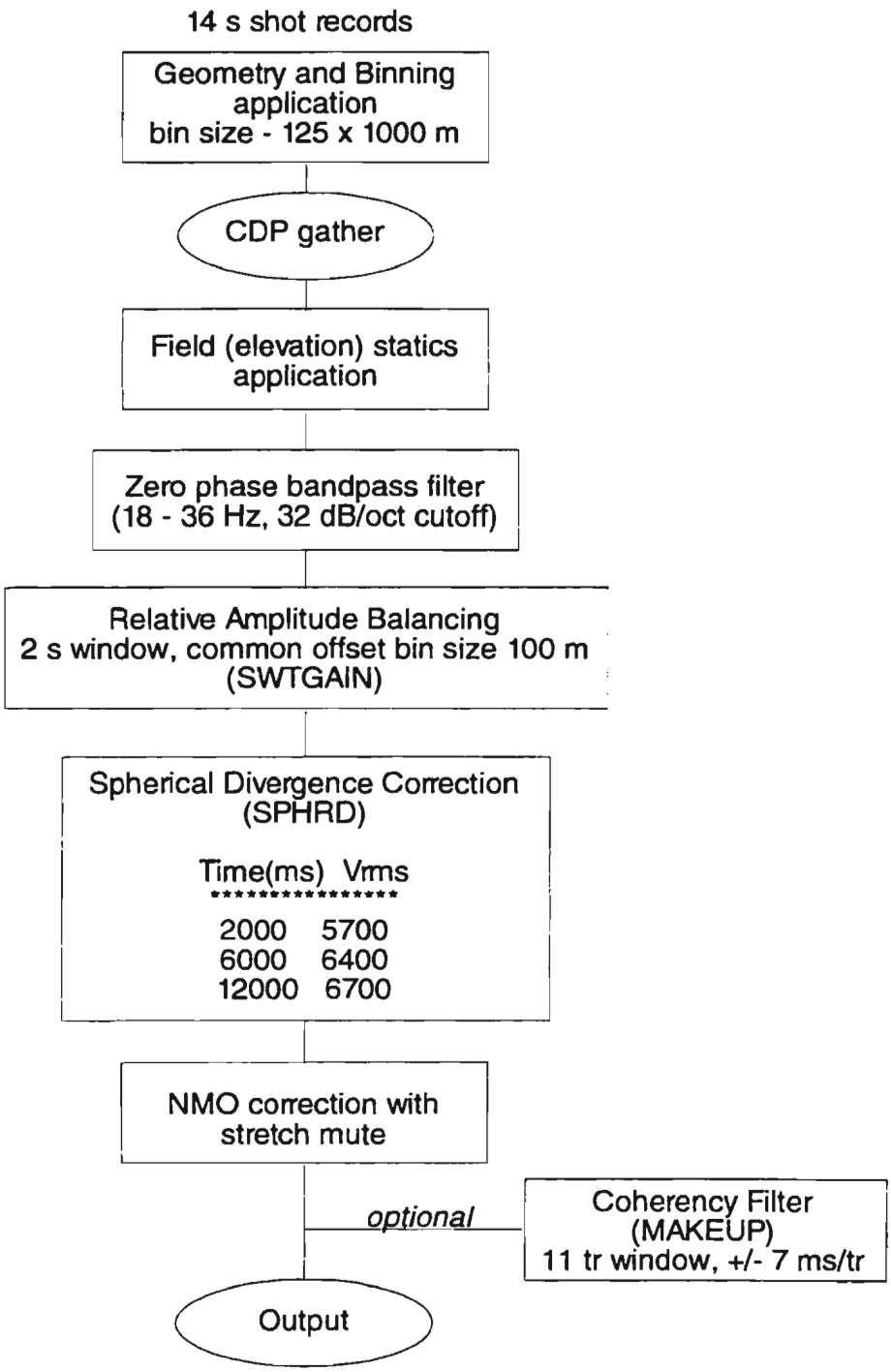

Figure 4.6 Relative amplitude processing (RAP) flow

Processing sequence used for generating the large fold cdps from the end-on-south data which are used for an amplitude versus offset analysis. Processors are all from the StarPak seismic data processing package.

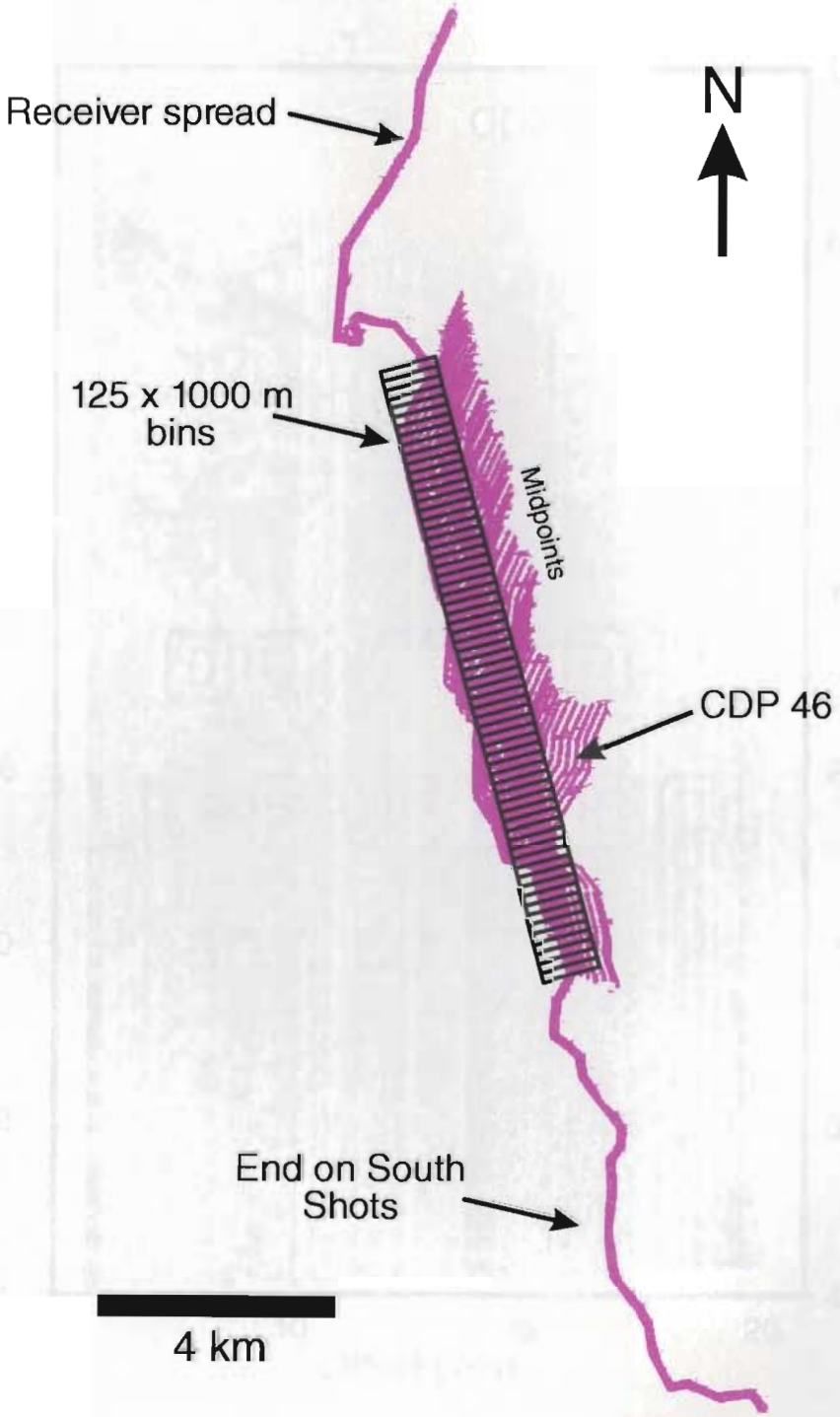

Figure 4.7 Processing line for generating large fold cdp gathers.

The midpoint distribution for the end-on-south shots with the processing line used for generating large fold cdp gathers overlain.

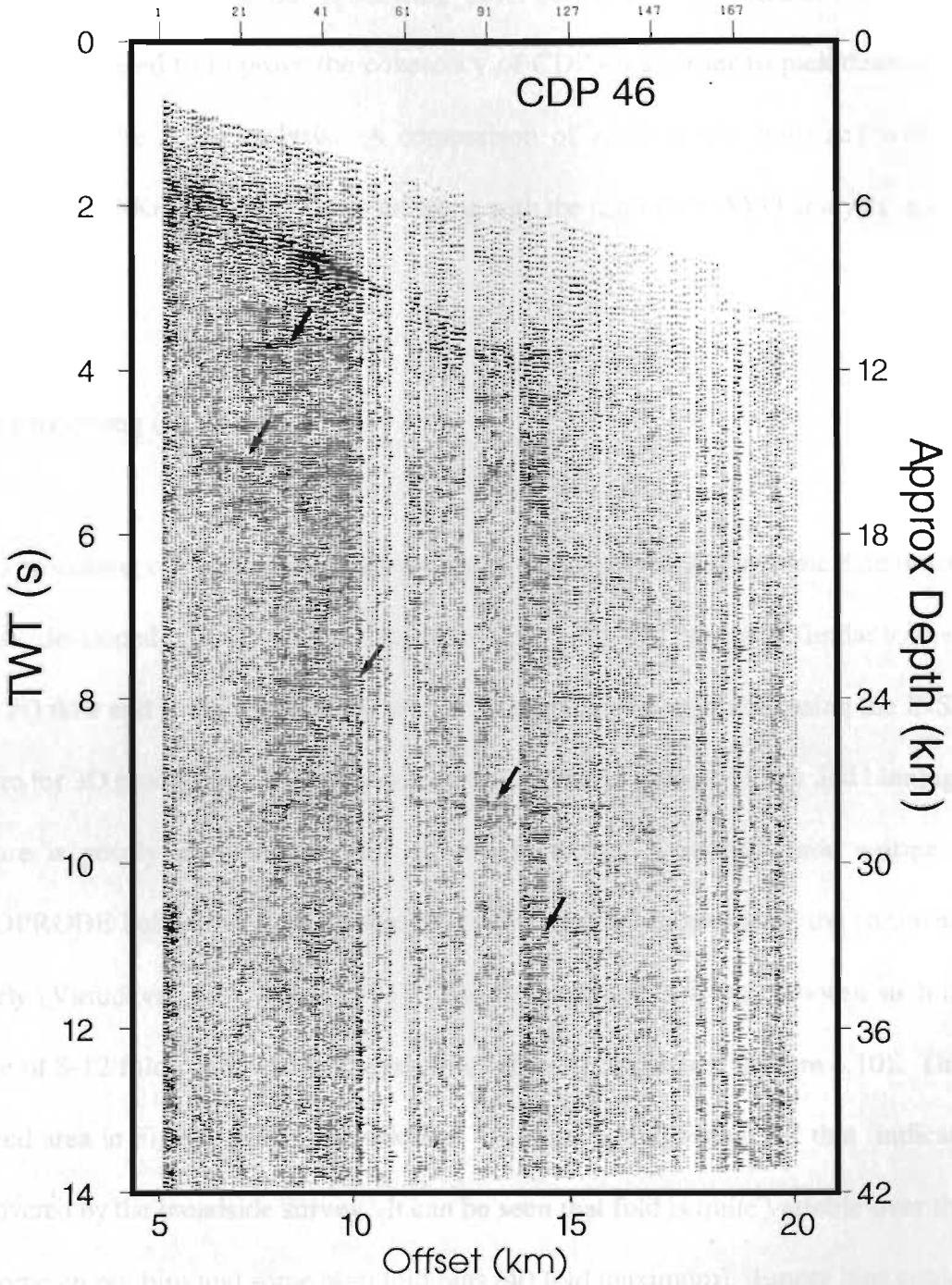

Figure 4.8 Large fold CDP 46.

Large fold CDP 46 as prepared for amplitude versus offset analysis by the processing flow shown graphically in Figure 4.6.

gross AVO analysis using the processing described above. MAKEUP, as previously described, was used to improve the coherency of CDP 46 in order to pick discrete events during part of the AVO analysis. A comparison of AVO results with and without the application of MAKEUP will be discussed along with the rest of the AVO analysis in Chapter 5.

4.3 3D Processing (INSIGHT)

The 3D processing of the broadside data was done with the INSIGHT seismic data processing software (developed by IT&A). The data processing sequence used was similar to that used for the 2D flow and is displayed in Figure 4.9. The main challenge with using the INSIGHT software for 3D processing is correctly defining and applying the geometry and binning. The software is poorly documented with numerous errors. A course guide written at the LITHOPROBE Seismic Processing Facility (LSPF) helped in getting all the parameters set properly (Vasudevan and Maier, 1994). The bin sizes selected were chosen such that an average of 8-12 fold could be maintained throughout the grid area (Figure 4.10). The total coloured area in Figure 4.10 is equivalent to the small box in Figure 1.2 that indicates the area covered by the broadside survey. It can be seen that fold is quite variable over the area with some empty bins and some high fold bins (40 fold maximum). Empty bins could have been avoided with a larger bin size, but it was important to keep enough bins in the both the in-line and cross-line direction to ensure that there were sufficient traces to follow reflectors across the area of 3D coverage. Also, larger bins would include traces that are sampling

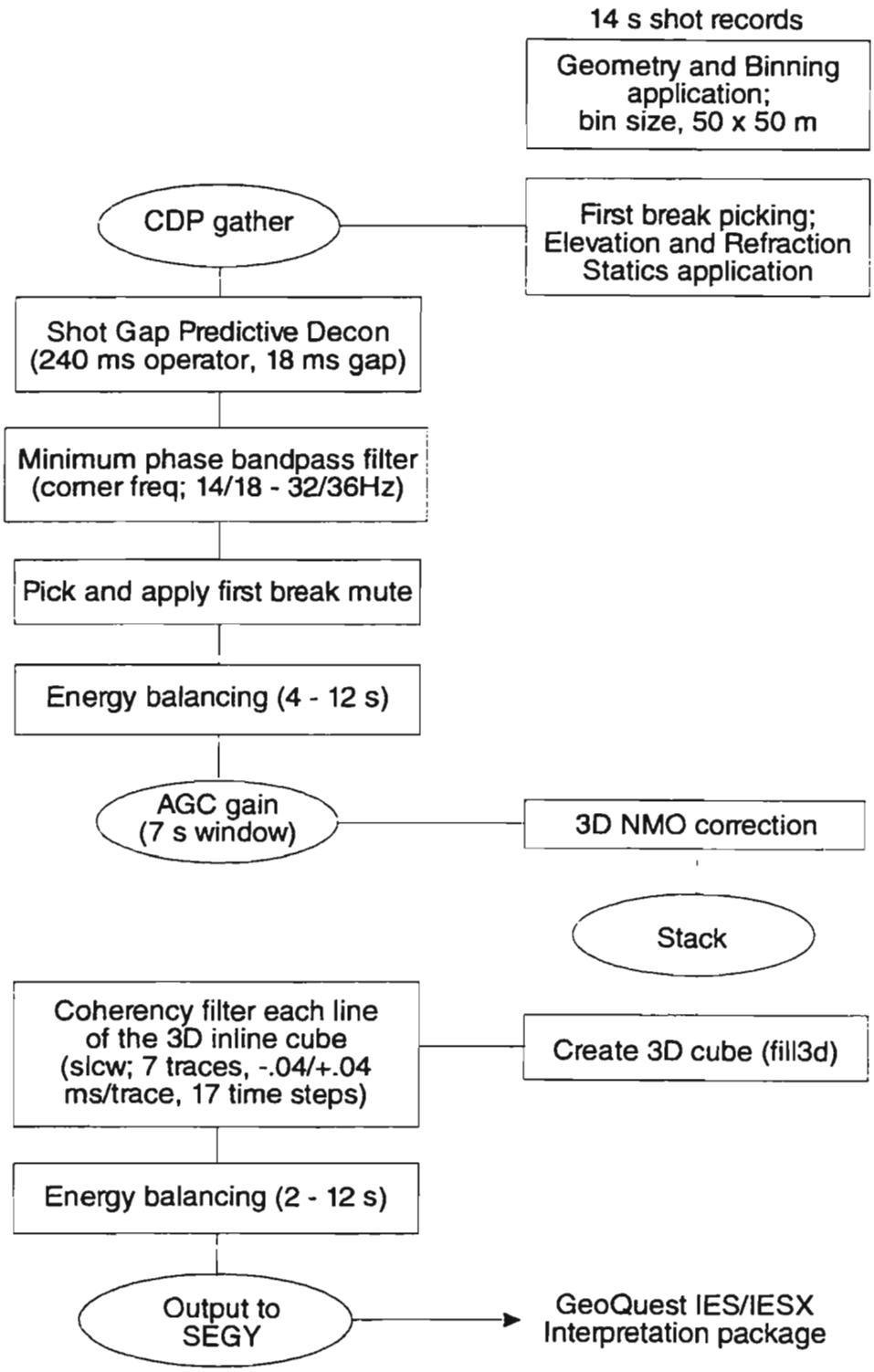

Figure 4.9 The INSIGHT processing flow used to produce a 3D cube from the broadside data.

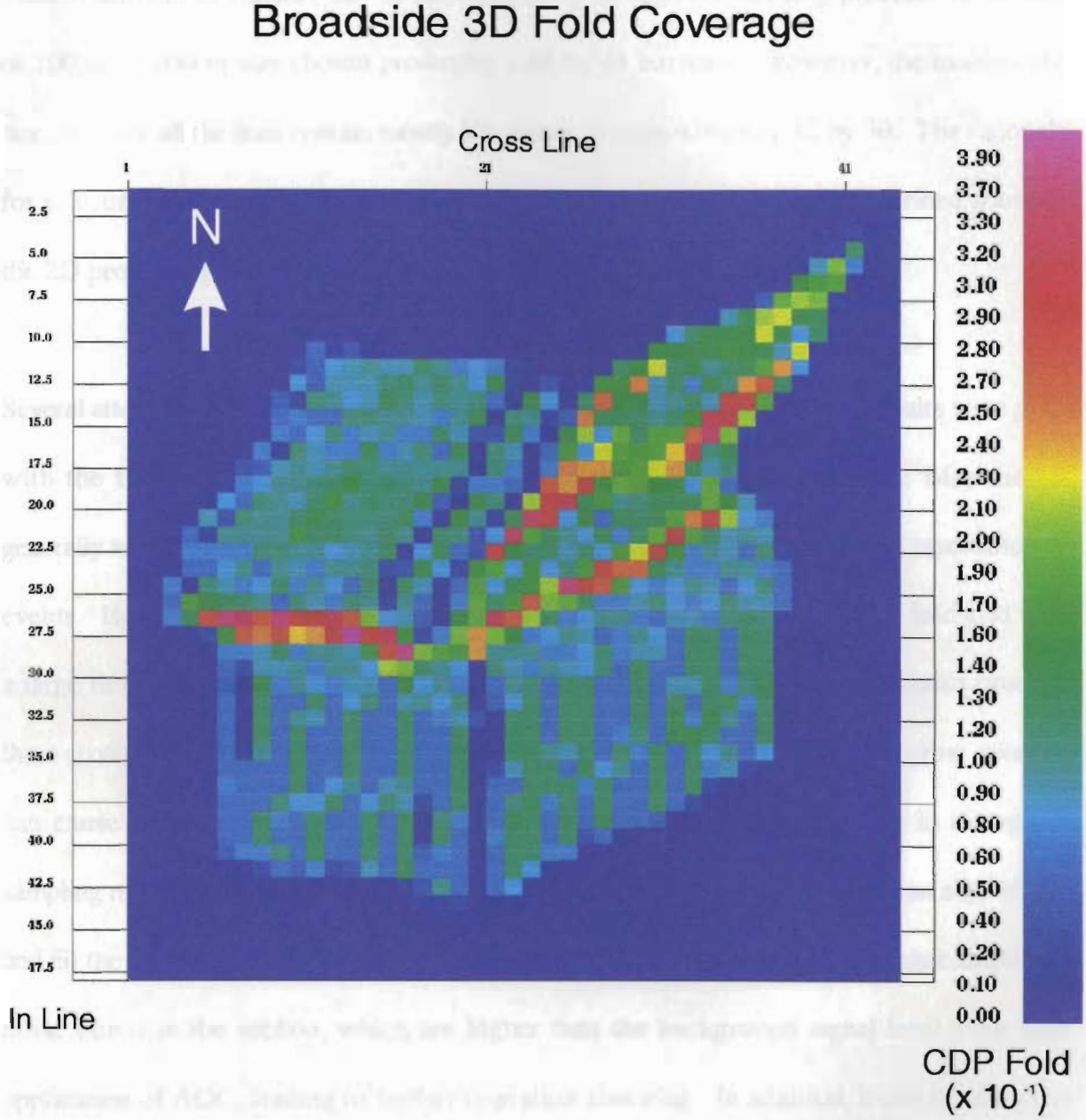

Figure 4.10 CDP fold coverage for the broadside 3D grid area.

CDP fold values for individual bins are colour-coded and the colour scale is indicated on the right hand side of the plot.

different parts of the subsurface, so any lateral differences in the geological structure could make it difficult to enhance any of the reflectivity through the stacking process. A bin size of 200 m by 200 m was chosen producing a 48 by 44 bin matrix, however, the usable cube size, in which all the lines contain mostly live traces, is approximately 32 by 30. The rationale for selecting the filter parameters and velocity function was the same as described above in the 2D processing section (4.2).

Several attempts were made at migrating the broadside 3D volume, but the results were poor with the final cube being dominated by artifacts and migration "smearing". Migration is generally very effective with 3D data since there is no ambiguity in the spatial orientation of events. However, in the broadside data set we have a sparsely sampled, low fold grid with a large time window and relatively low signal to noise ratio. These characteristics produce three problems for migration: i) the aperture size is small (30-40 traces) and a narrow aperture can cause strong smearing for many migration algorithms (Yilmaz, 1987); ii) the sparse sampling may result in spatial aliasing which is problematical for many migration algorithms; and iii) the combination of low fold and low signal to noise ratio leaves some higher amplitude noise bursts in the section, which are higher than the background signal level even after application of AGC, leading to further migration smearing. In addition, it can be observed that many events have sharp discontinuities and are not strongly coherent across the entire section (e.g. Figure 5.9). These discontinuities can be one further source of migration artifacts. It was decided to proceed with the interpretation on the stacked 3D volume.

5.0 INTERPRETATION

5.1 2D In-line Sections

Reflection profiles that follow regional lines 6 and 7 from the LE89 reflection survey were produced using the data acquired during the broadside experiment. The broadside data were used to create a line along line 7 (broadside line 13) and the end-on-south data was used to create a line along line 6 (end-on-south line 1) (Figure 5.1). The main reason in doing this is to demonstrate that relatively low fold data with a limited offset range can produce interpretable sections which show the major features seen in the high fold regional data. The regional data displayed in this section are from the RNA stacks (Random Noise Attenuated) provided by the processing contractor for the LE89 survey (Western Geophysical Ltd.).

Figures 5.2 and 5.3 show sections of data from line 7 and broadside line 13 respectively. It can be seen that the major features on this part of line 7 (events marked A to F) are also evident on broadside line 13. There are also smaller less continuous reflections that are indicated on Figures 5.2 and 5.3 (in yellow) which correlate very well between the two sections. The resolution on line 13 is certainly lower, due in part to the reduced sweep frequency range, but some events are focussed very well, including a strong event (F on Fig 5.3) that is not readily apparent on the line 7 stack. Line 7 provides clear evidence that the strong subhorizontal, mid-crustal reflections that are seen south of Noel Paul's Line on line 6 (Figure 2.1B) have significant dip to the east as seen by reflectors C and D (Figures 5.2 and

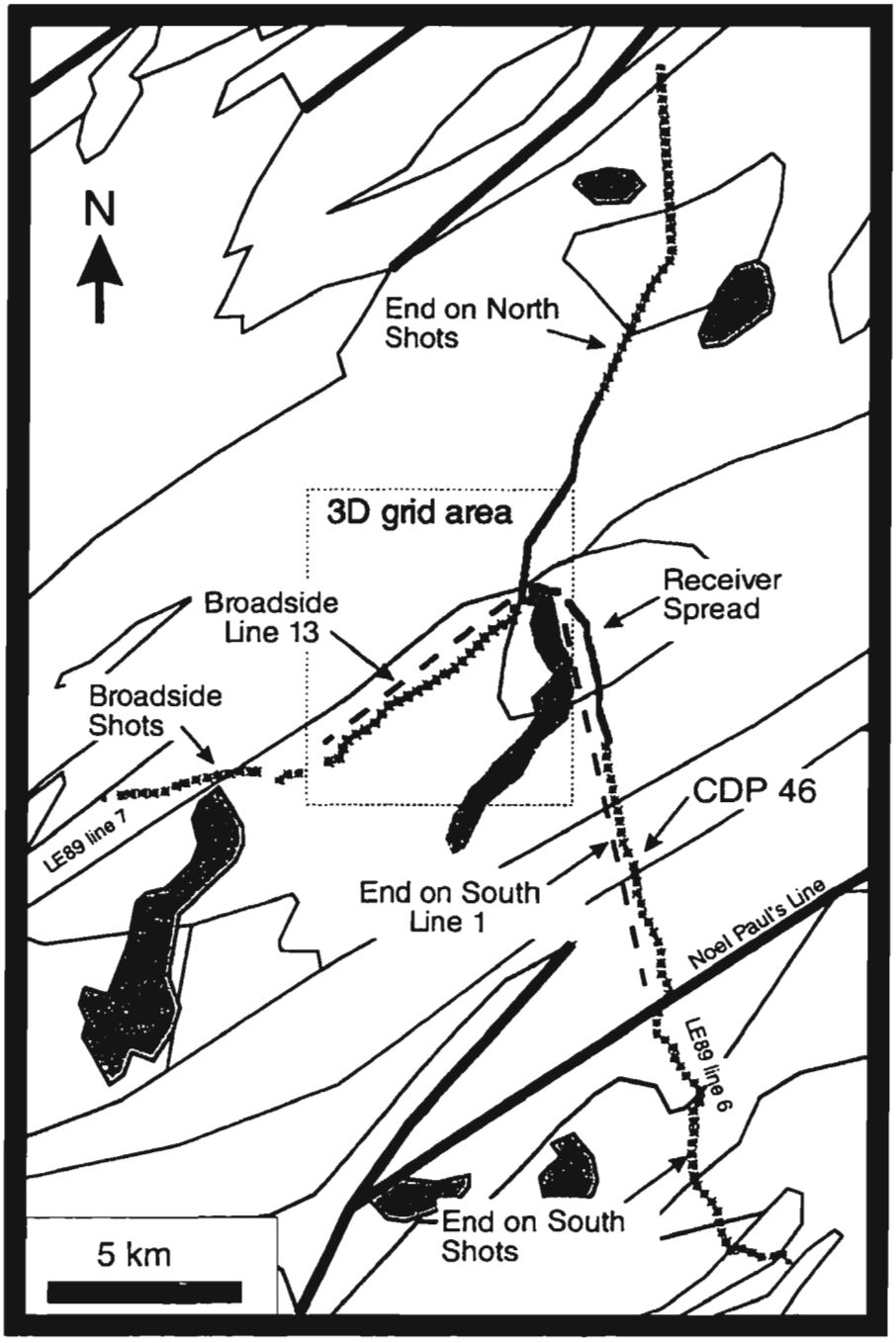

Figure 5.1 Location map for 2D and 3D processing areas.

Map showing location of broadside line 13, end-on-south line 1 and the 3D grid area relative to other regional lines and local geology. The geological contacts (thin black lines), major fault traces (thick black lines), and lakes (grey) are the same as those in Figure 2.2, but at a reduced scale.

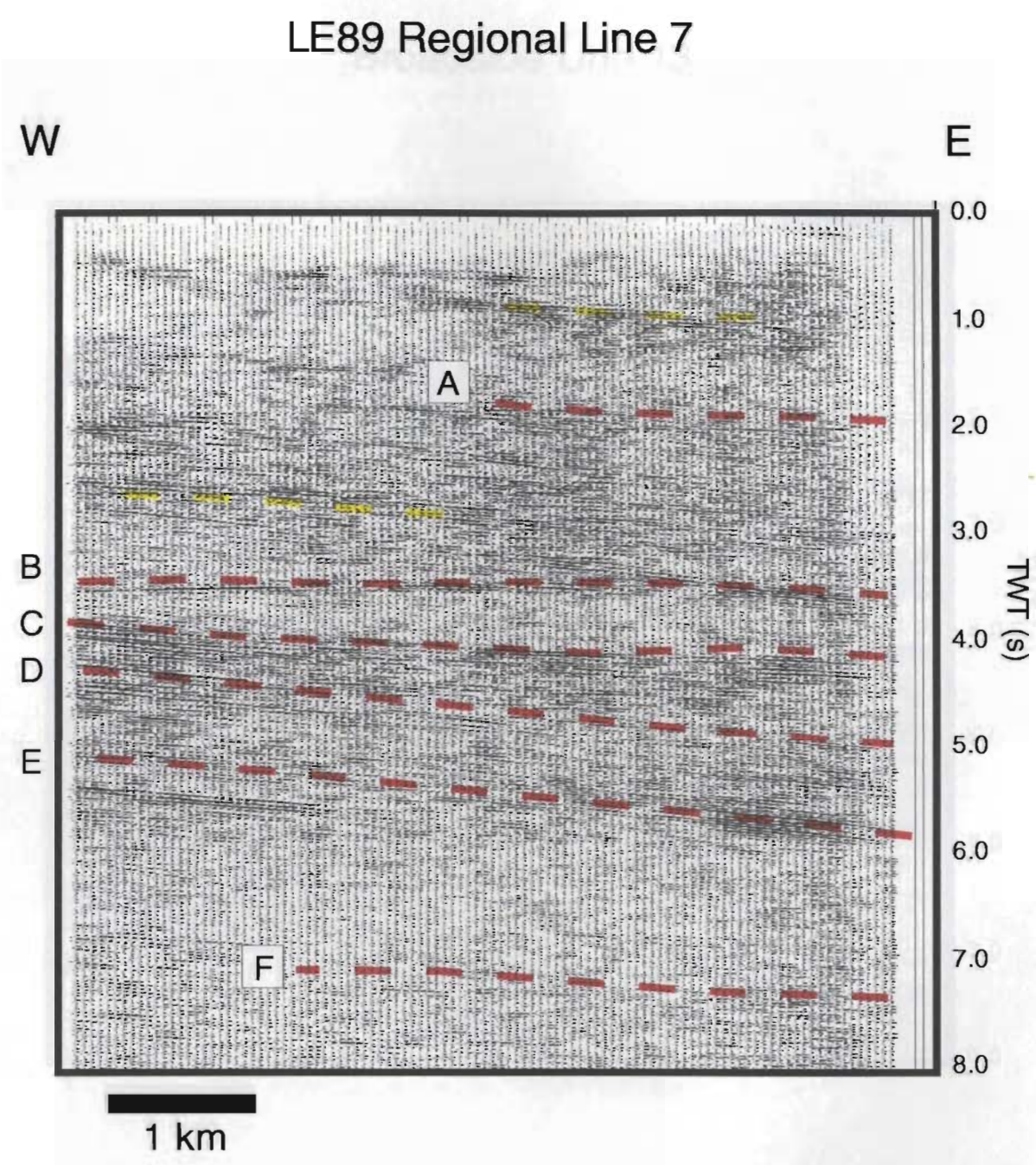

Figure 5.2 Stacked line 7 from LE89 reflection survey.

A section from stacked line 7 of the LE89 reflection survey with interpretation overlay showing major reflecting horizons with red dashed lines (labelled A to F) and other strong, but less continuous reflections, with yellow dashed lines.

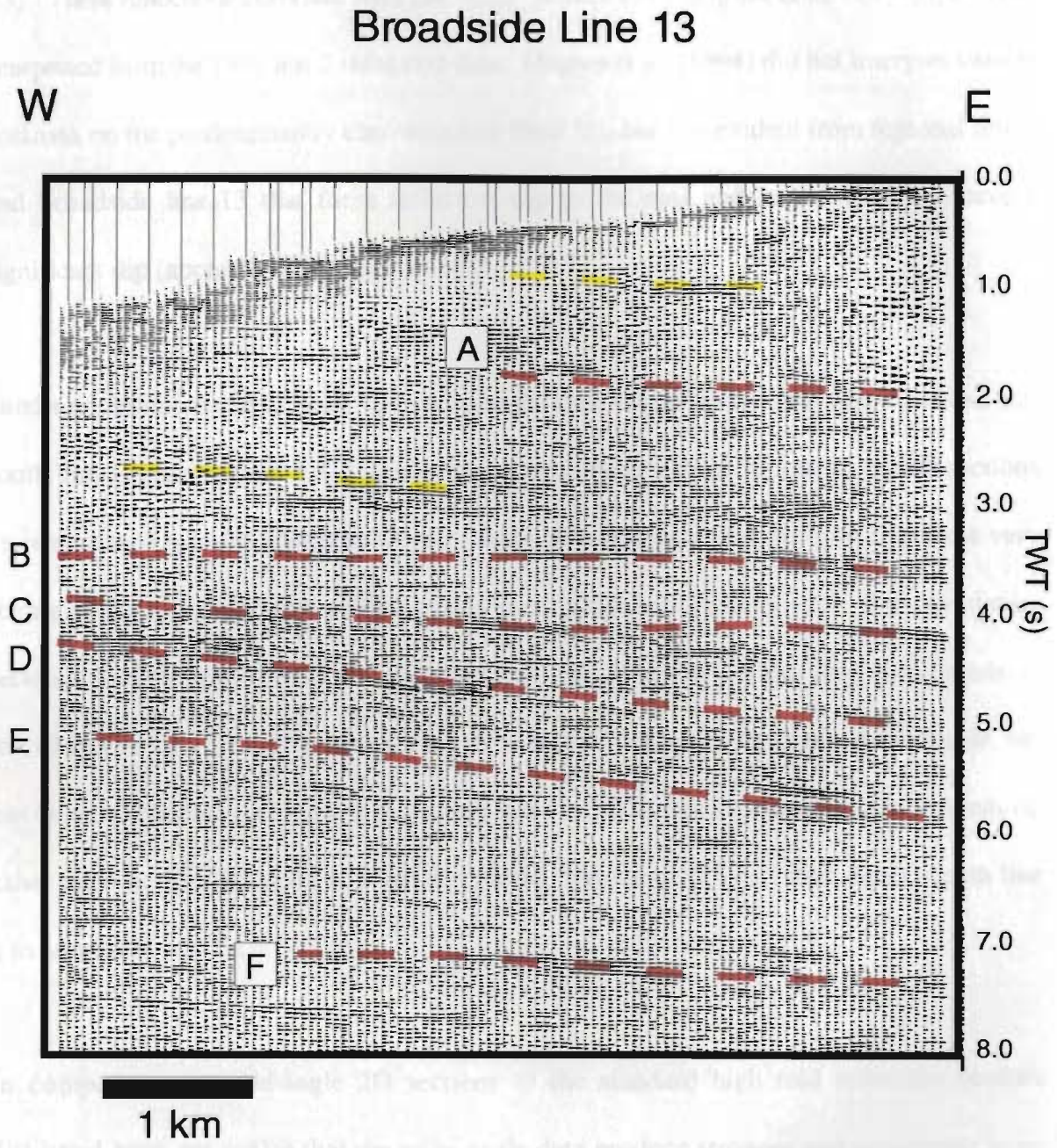

Figure 5.3 Stacked broadside line 13.

Broadside line 13 at the same scale as the section of LE89 line 7 from Figure 5.2, with interpretation overlay showing major reflecting horizons with red dashed lines (labelled A to F) and other strong, but less continuous reflections, with yellow dashed lines. The interpretation overlay is identical to that in Figure 5.2.

5.3). These reflections correlate with the "thin" reflectors of Hughes et al. (1994) that were interpreted from the 1991 line 3 refraction data. Hughes et al. (1994) did not interpret similar horizons on the predominantly east-west line (line 31), but it is evident from regional line 7 and broadside line 13 that these reflectors dip to the east and, at least locally, have a significant dip (apparent dip as high as 34°).

Similar comparisons can be made by looking at the matching sections from line 6 and end-on-south line 1 (Figs 5.4 and 5.5). Again the major features can be followed on both sections (events marked A to E). Primarily we see a series of subhorizontal reflections which are very strong in the mid-crust and weaker in the lower crust and Moho levels. The correlation between features seen on end-on-south line 1 and line 6 is less obvious than with broadside line 13 and line 7. This difference seems to be related to the fact that we have stronger, but less discrete reflectivity along line 6, making it more difficult to identify individual events on either section. This is apparent when comparing both line 6 to line 7 and end-on-south line 1 to broadside line 13.

In comparing the wide-angle 2D sections to the standard high fold reflection profiles displayed here, we notice that the wide-angle data produce stronger and sometimes more coherent events in the deep parts of the section (6-8 s for broadside line 13 and 8-12 s on end-on-south line 1). This discrepancy is due to variations in the processing sequence applied to the wide-angle and normal incidence sections. The regional lines had an AGC gain applied pre-stack, with scaling based on the RMS values in specific time windows post-stack. This

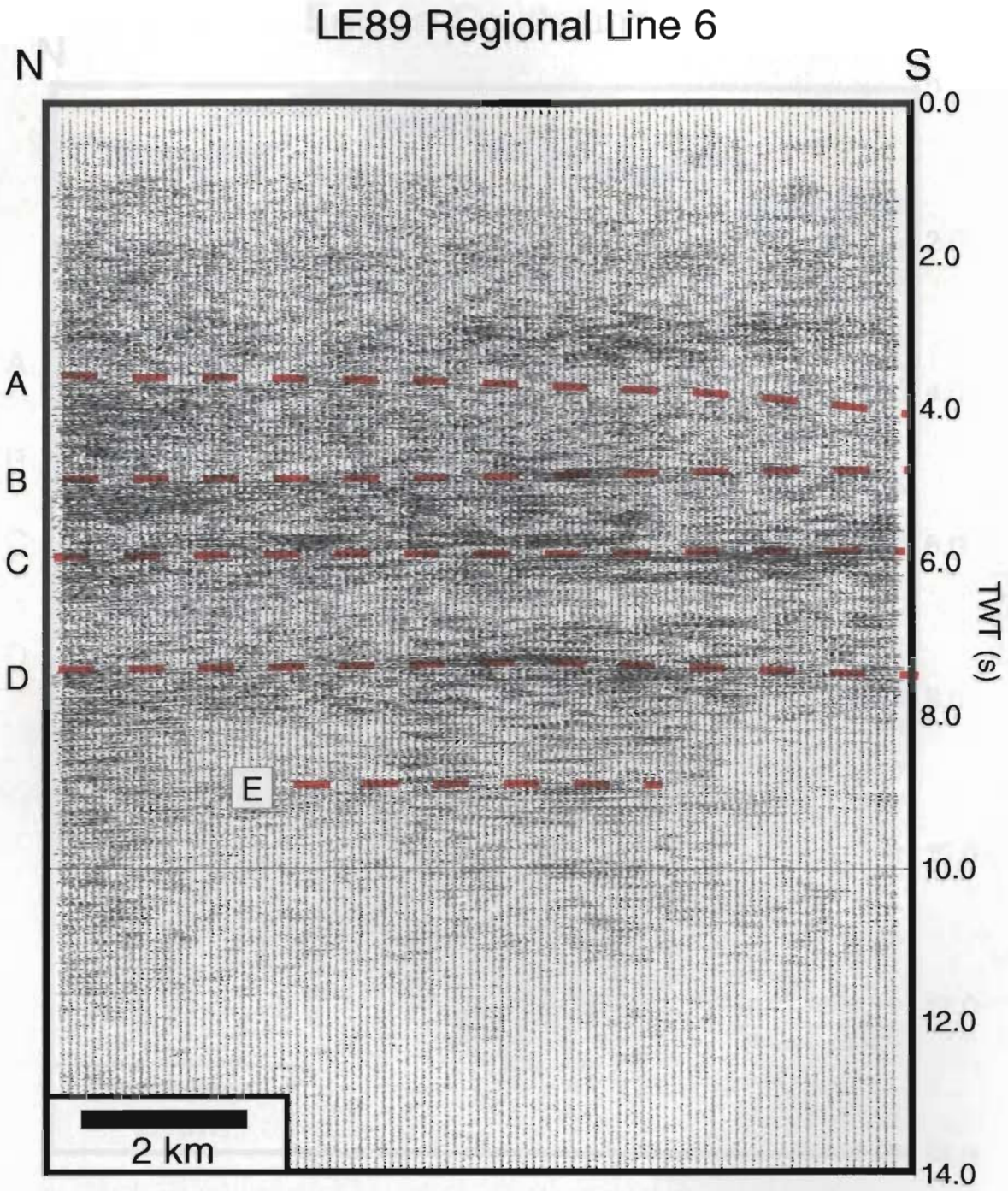

Figure 5.4 Stacked line 6 from the LE89 reflection survey.

A section from stacked line 6 of the LE89 reflection survey with interpretation overlay showing major reflecting horizons with red dashed lines (labelled A to E).

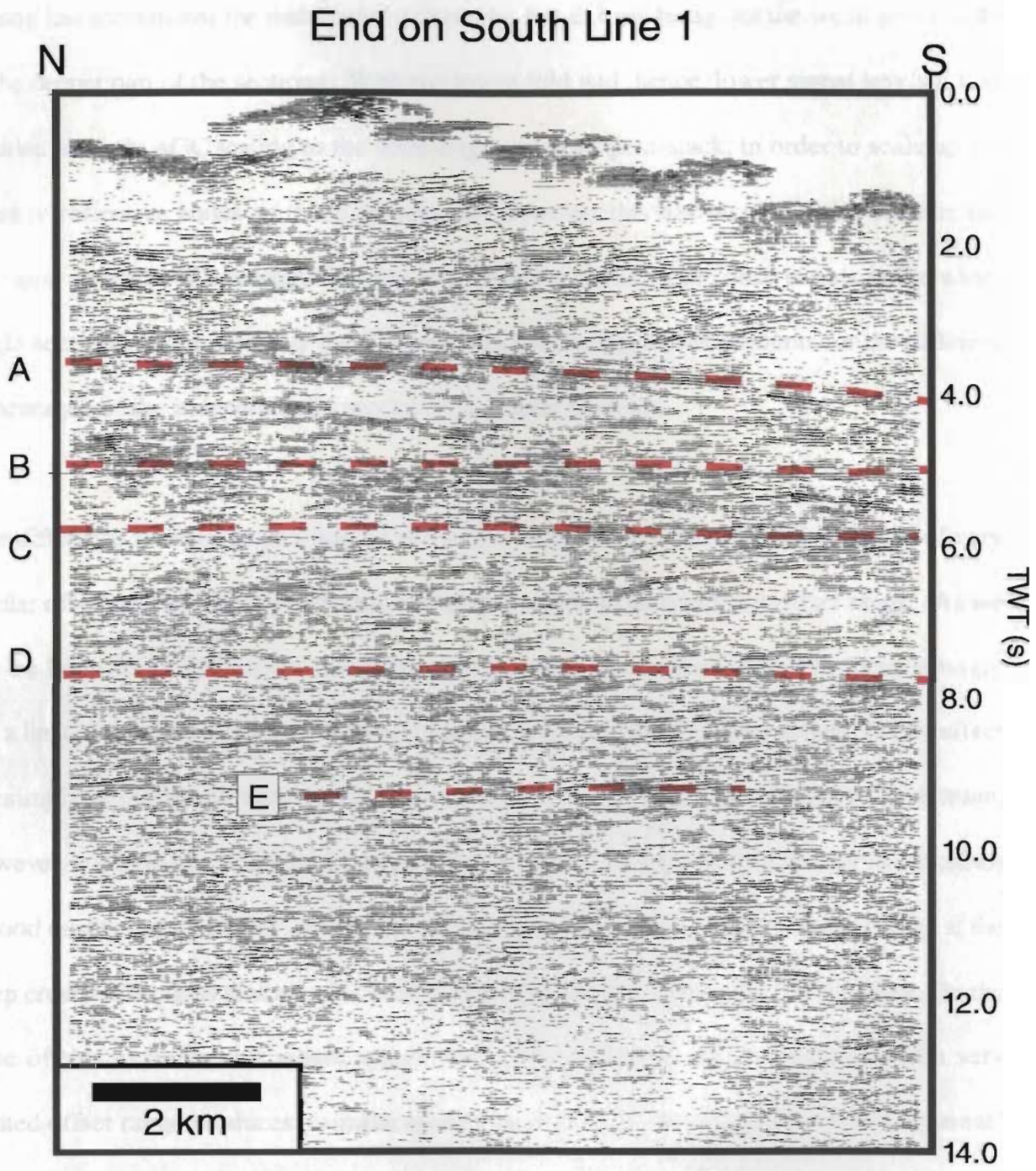

Figure 5.5 End-on-south Line 1.

End-on-south line 1 at the same scale as the section of LE89 line 6 from figure 5.4 with interpretation overlay showing major reflecting horizons with red dashed lines (labelled A to E). The interpretation overlay is identical to that in Figure 5.4.

scaling has accentuated the mid-crustal reflectivity, but did not bring out the weak reflectivity in the deeper part of the sections. With the lower fold and, hence, lower signal levels it was decided to apply AGC scaling to the wide-angle sections post-stack, in order to scale up the weakly reflective zones as much as possible, however this has increased the noise in the sections as well. Coherency filtering has tended to enhance the deep events in the wide-angle sections, but it is mainly the difference in the scaling which accounts for the different appearance of the independently produced, collinear sections.

One difference between lines 1 and 13 is that the CDP bins for line 13 contain traces of very similar offset whereas for line 1 we are stacking traces with a significant offset range. As we see on large-fold CDP 46 (Figure 4.8) individual reflection events appear to focus strongly for a limited range of offsets. Whether or not this is an amplitude versus offset (AVO) effect or simply a matter of varying source and receiver conditions is difficult to determine, however, stacking traces which only display intermittent strong reflectivity may not produce a good quality stack section. An AVO analysis is made in a later section to determine if the deep crustal reflections that are observed in this area display significant AVO effects. In the case of this experiment it would appear that a low fold stack which bins traces of a very limited offset range produces a similar quality section to a low fold section with a "normal" range of offsets. With the strong but patchy reflectivity seen in the shot gathers it would appear that using a smaller offset range may be successful for stacking some events, but not all events as seen on figures 5.2 and 5.3. For example, just below reflector 'E' a strong reflector shows up on the regional line (Fig. 5.2) but it is not seen at all on broadside line 13

(Fig. 5.3). Thus, CDP's that contain offsets where reflections are strong will show a clear event when stacked, however in other parts of the line where offsets are not favourable there will be no signal to stack. Generally, one requires a range of offsets to image all structures properly and the advantages of using high fold data are clear when comparing the sections from line 7 and broadside line 13 (Figs. 5.2 and 5.3).

5.2 3D volume

Since the acquisition of the broadside data in 1989 there have been a number of special experiments, conducted by different LITHOPROBE transects and by others, which have generated 3D volumes (e.g. Cook and Coflin, 1990, Kanasewich et al., 1995, and Vasudevan et al., 1995). The success of these experiments appears to be strongly dependent on the source/receiver geometry and the target(s) available for the survey to image. The LE89 broadside survey has three main disadvantages with regard to the above points: i) the area of midpoint coverage is small (6 x 6 km) for the interpretation of crustal scale events which may be traceable for 100 km or more, ii) the shot spacing was 300 m, producing low 3D fold coverage, iii) the shots are all on one side of the receiver spread so that we have no reversed raypaths for the calculation of statics. In spite of the negative points above, a 3D volume was generated, as detailed in the previous section on data processing, and an interpretation attempted. The main goal of the interpretation is measuring the true dip of some key horizons in order to see if they follow the surface structure of the Appalachian belt, as is assumed in other interpretations (e.g. Quinlan et al., 1992).

The 3D cube produced using the broadside data was loaded into the GeoQuest IES/IESX 2D/3D interpretation package at the Geological Survey of Canada in order to identify and map horizons and visualize the 3D volume. It is often difficult to follow single events throughout the cube, but an attempt has been made to do so, and some observations can be made about the attitudes of some key horizons. Reflections centred at approximately 4.5, 8.2 and 11.0 seconds have been selected for interpretation because of their relatively high signal level, lateral continuity, and relevance to previous studies published for this area (e.g. Hughes et al., 1994).

As stated above, picking discrete events in the 3D data is difficult. The approach taken was to scan through the in-line and cross-line sections sequentially and try to sort out what energy is being observed consistently from section to section. Once this is done, the best coherent phase is picked across a series of sections and the perpendicular sections are then examined to ensure that the picks also align with coherent phases in the other direction. This is an iterative process which eventually leads to the picking of the best coherent horizon over the 3D area. There is a relatively low degree of confidence in the picks on individual traces, but overall, the picked horizons appear to be real and traceable between adjacent lines in the 3D volume. The travel time maps produced have had no smoothing or interpolation performed so that there is a certain degree of confidence that the trends observed through the 3D area are real, although the displays do not have the smooth appearance of a contoured grid.

The 4.5 s event was traceable throughout most of the grid area and a time structure map for that horizon has been produced (Figure 5.6). The horizon interpretation maps created for the broadside data cube (see also those for 8.2 and 11.0 s, Figures 5.8 and 5.10) display the actual time picks from the data using a consistent colourmap. The area covered by the time structure maps is approximately equivalent to the grey shaded area on Figure 5.1 and the area indicated by the square outline in Figure 1.2. We observe from Figure 5.6 that the 4.5 s horizon has a clear and consistent dip of 27° to the northeast (assuming a velocity of 6.0 km/s). This trend can also be seen on the data from two traverses (A-A' and B-B') that have been defined through the cube to follow the event at this time interval (Figure 5.7). On these traverses we see that the horizon is dipping to the east in the in-line direction (A-A') and to the north along the cross-line direction (B-B'). The 4.5 s horizon from the cube correlates with the highly reflective zone bounded by events C and D from the 2D interpretation of broadside line 13 and LE89 line 7 (Figs 5.2 and 5.3) and what we had observed as a strong, apparent easterly dipping trend actually appears to be a complex structure with 27° dip to the northeast, striking N50°W. This series of reflections corresponds to an area of conflicting dips along the Meelpaeg transect (Figure 2.1B) and to the top of layer 3 from the LE91 line 3 interpretation, where Hughes et al. (1994) have modelled a number of floating reflectors (Figure 2.1C). The LE89 reflection data strongly image fabrics produced by wedging that is attributed by Quinlan et al. (1992) to continent-continent collision in the Mid-Silurian (Figure 2.1A). In the mid-crust these fabrics would appear not to be perpendicular to the approximate regional strike for the surface structures of the Appalachian belt (~N40°E) and, in fact, the interpretation above indicates that the fabrics are dipping in the regional strike

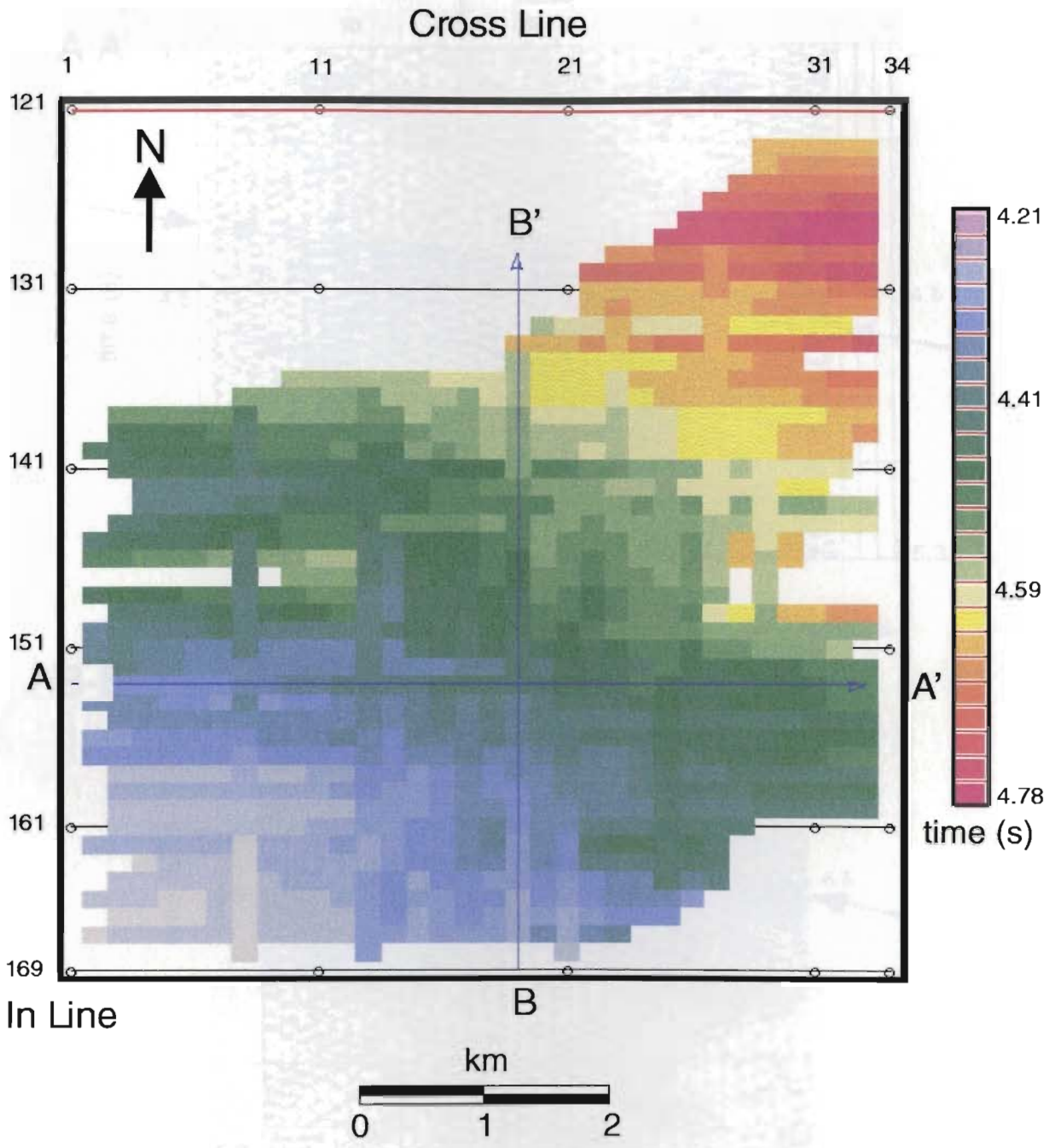

Figure 5.6 Time structure map for a horizon centred at 4.5 s in the 3D volume.

The bar on the right side of the plot shows the relationship between the colourmap and reflection time in seconds. Traverses A-A' and B-B' show the orientation and location of the sections in figure 5.7.

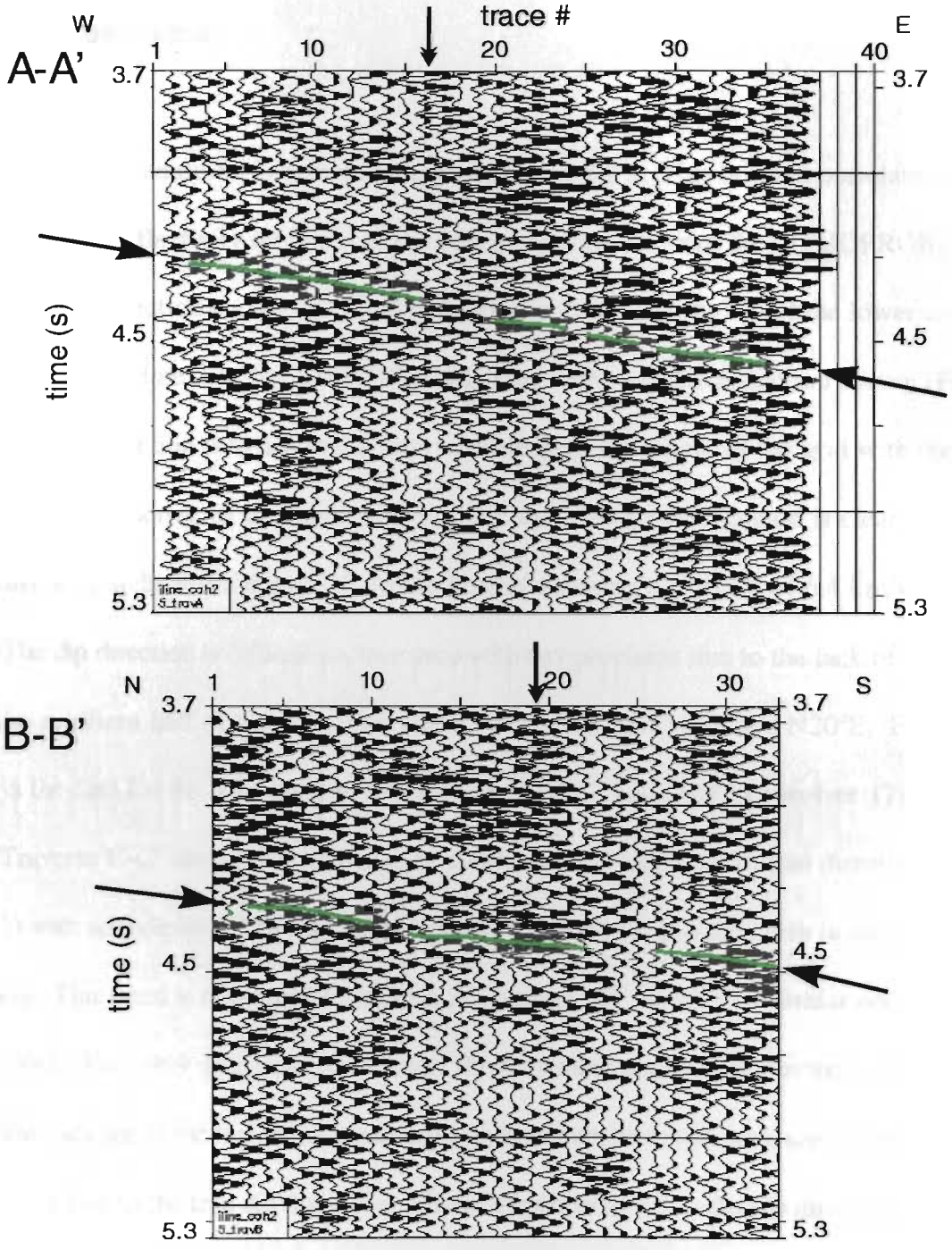

Figure 5.7 Traverses A-A' and B-B' from figure 5.6.

The coloured line indicates the interpreted horizon. Small arrows above the sections show the intersection point of the two traverses.

direction of the orogen.

The next horizon analysed is centred at approximately 8.2 s. This horizon correlates with a strong band of reflectivity on line 6 of the Meelpaeg transect from the LITHOPROBE East 1989 seismic reflection survey (labelled B on Figure 2.1B) and the top of the lower crust as interpreted from line 3 of the LITHOPROBE East 1991 seismic refraction survey (Figure 2.1C). This reflection was not easily interpretable over the whole of the grid with the data quality being superior to the south end of the cube. Where the horizon is clear, the time structure map indicates a dip of 21° to the north (assuming a velocity of 6.4 km/s) (Figure 5.8). The dip direction is difficult to determine with any precision due to the lack of coverage over the northern half of the cube, and could vary between N30°W and N20°E. Figure 5.9 displays the data for the 8.2 s horizon along traverses C-C' and D-D' (cross-line 17) (Figure 5.8). Traverse C-C' shows the horizon to be sub-horizontal along the in-line direction (traces 1 to 21) with an indication of a slight dip to the west, but dipping to the north in the cross-line direction. This trend is reinforced by looking at section D-D' in which a similar northerly dip is observed. The 1989 deep seismic data also shows a clear apparent dip to the north for this reflection package at the top of the lower crust and the interpretation presented here indicates that this is close to the true dip direction. Given the uncertainty in the dip direction from the 3D interpretation, we can only state that locally, the strike of the fabrics modelled by Quinlan et al. (1992) for the lower crust (Figure 2.1A) are more closely parallel to the regional strike of the surface structures of the Appalachian belt than the mid-crustal structures.

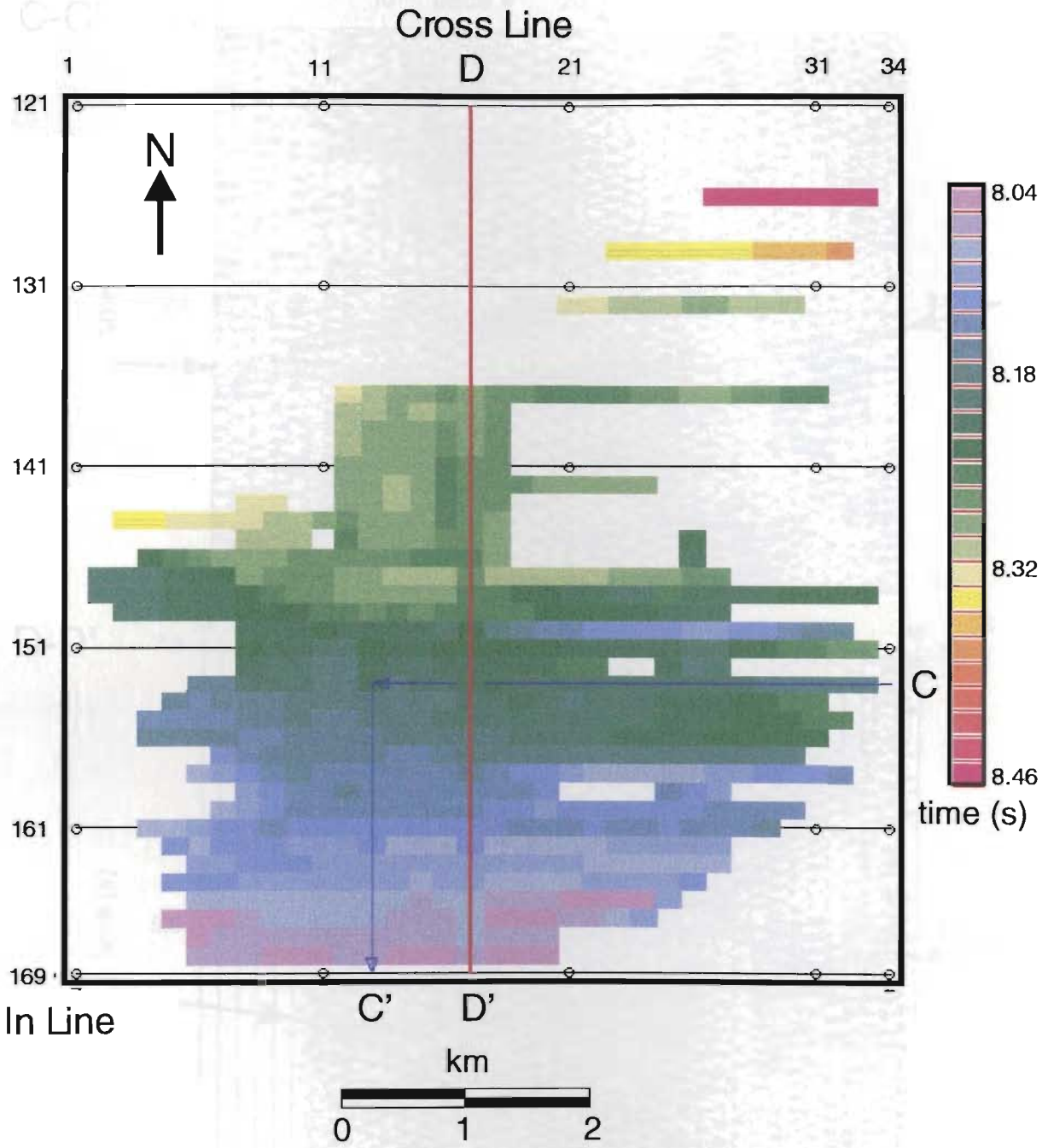

Figure 5.8 Time structure map for a horizon centred at 8.2 s in the 3D volume.

The bar on the right side of the plot shows the relationship between the colourmap and reflection time in seconds. Traverses C-C' and D-D' show the orientation and location of the sections in figure 5.9.

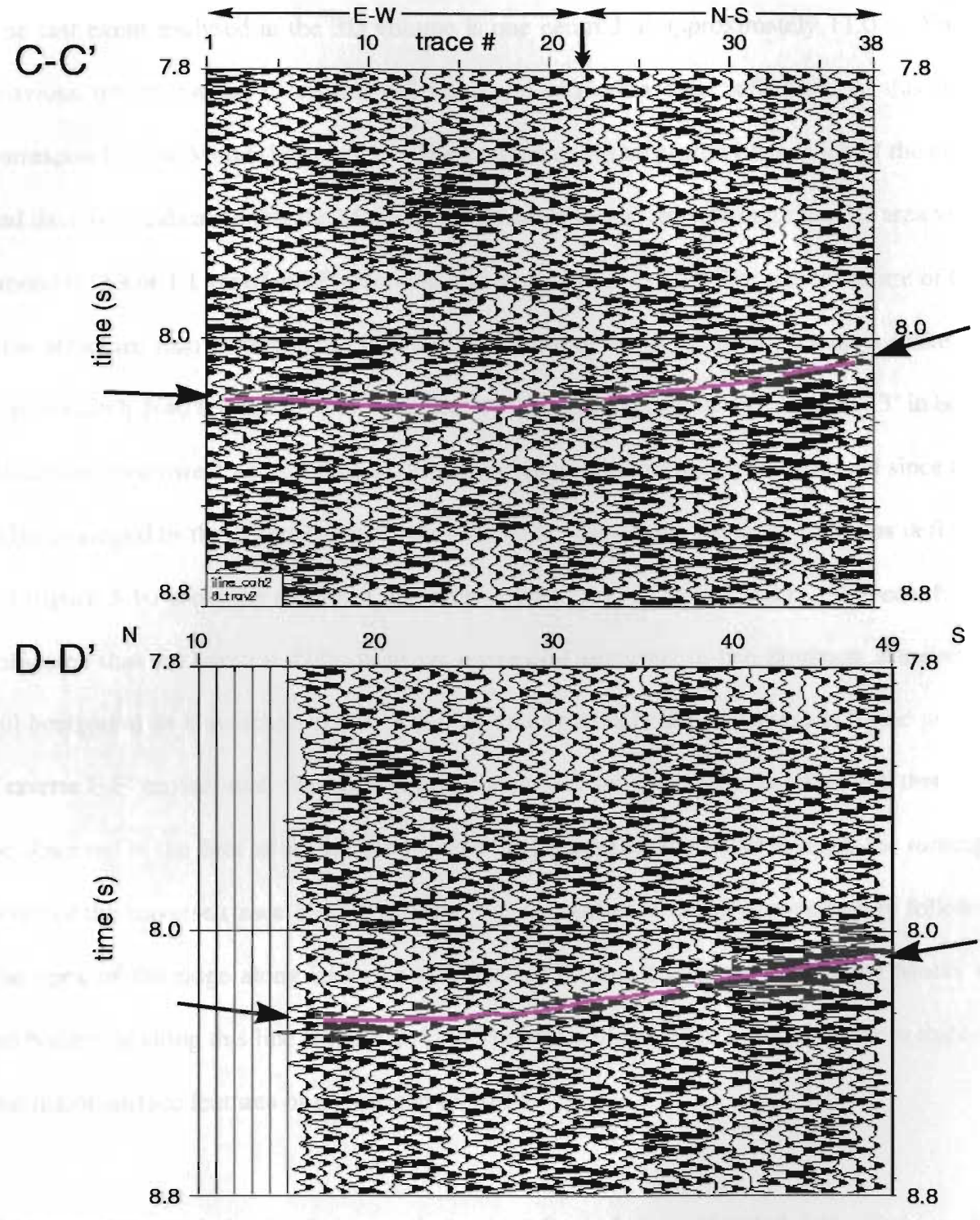

Figure 5.9 Traverses C-C' and D-D' from figure 5.8.

The coloured line indicates the interpreted horizon. The small arrow above section C-C' show the corner point of the traverse as it changes from in line to cross line.

The last event analysed in the 3D volume is one centred at approximately 11.0 s. From previous interpretations of crustal reflection and refraction data, reflections at this time correspond to the Moho (Figure 2.1). The horizon could be picked over much of the cube and there is an indication that the Moho has discernible topography through the 3D area with around 0.16 s or 1.1 km of relief (assuming a velocity of 6.8 km/s). The major feature of the time structure map at this depth is a northeast-southwest trending ridge with a strike of approximately N40°E (Figure 5.10). The flanks of the ridge appear to dip at about 33° in both directions (northwest and southeast), however, these dips are poorly constrained since the ridge as imaged by the 3D cube is less than 4 km wide. Data along the three traverses defined on Figure 5.10 show the nature of this ridge in more detail (Figure 5.11). Traverse E-E' indicates that the horizon shallows as we move east along the in-line direction, remaining subhorizontal as it switches to the cross-line and eventually deepening again to the north. Traverse F-F' crosses over the ridge in both the in-line and cross-line direction and that can be observed in the data as we see the two elevated areas dipping down towards the turning point of the traverse (trace 30). A traverse was also selected which approximately follows the apex of the ridge along its strike (section G-G') and it is apparent that the Moho is subhorizontal along this line (Figure 5.11). The strike of the ridge is very similar to that of the major surface features of the orogen (N40°E).

As was earlier noted, the data interpretation was performed on unmigrated data. Had the 3D volume been more suitable for migration and one had been applied, we would likely observe the reflections described above in a somewhat different orientation. Migration increases the

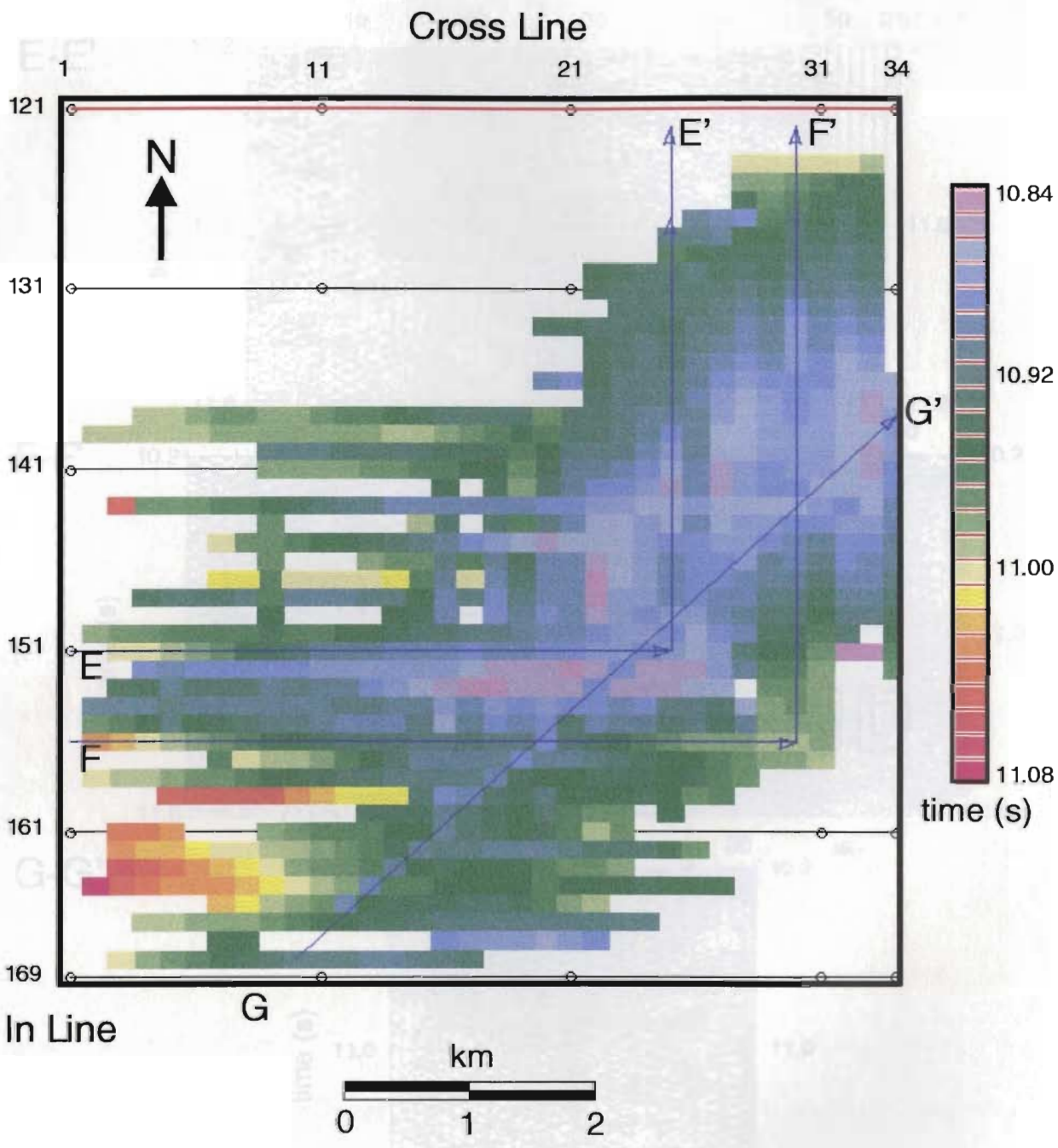

Figure 5.10 Time structure map for a horizon centred at 11.0 s in the 3D volume.

The bar on the right side of the plot shows the relationship between the colourmap and reflection time in seconds. Traverses E-E', F-F' and G-G' shows the orientation and location of the sections in figure 5.11.

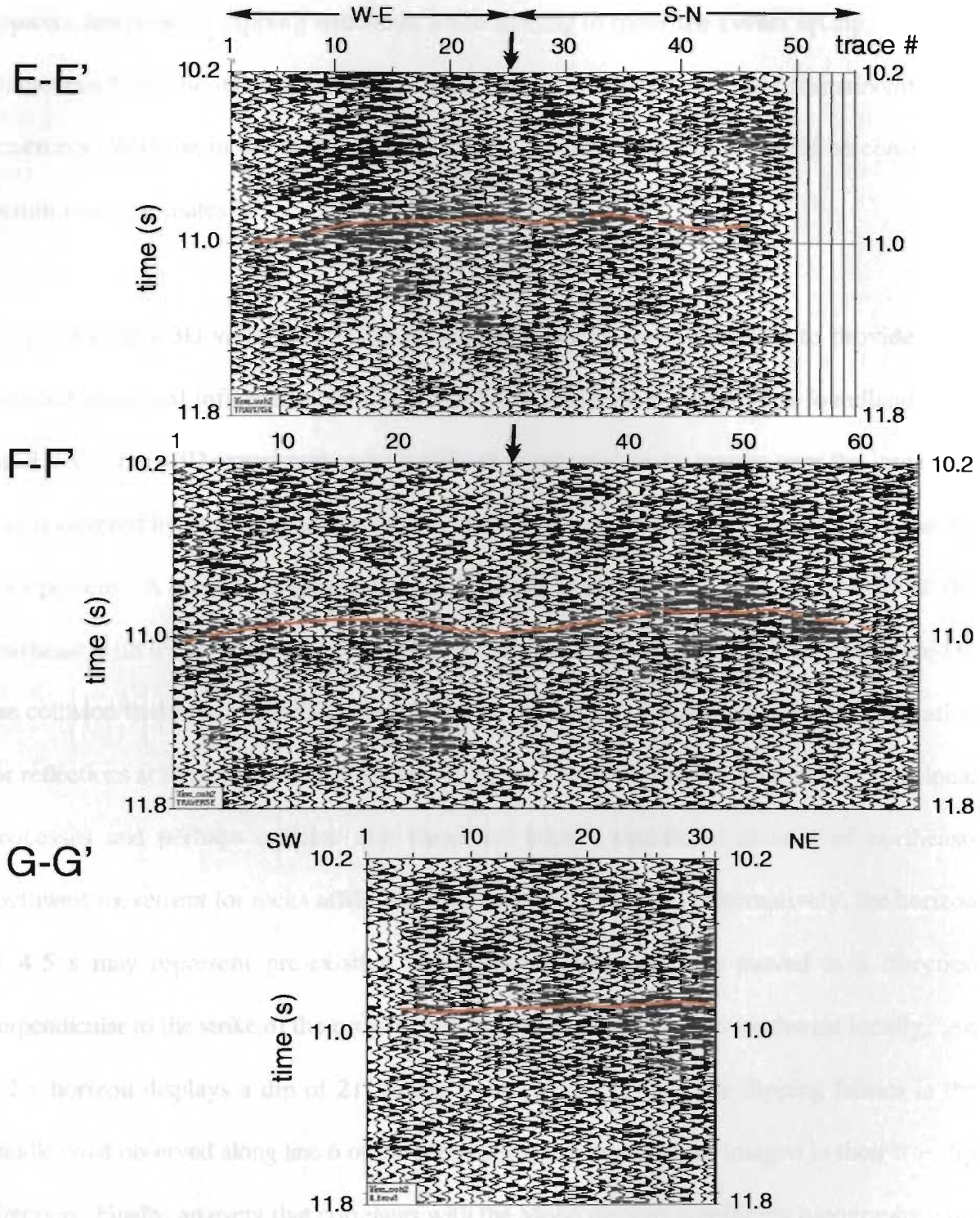

Figure 5.11 Traverses E-E', F-F' and G-G' from figure 5.10.

The coloured line indicates the interpreted horizon. Small arrows above sections E-E' and F-F' show the corner point of the traverses as they change from in line to cross line.

apparent steepness of dipping structures while tending to move the events up dip, collapses diffractions from discontinuities and point sources, and properly defines antiformal/synformal structures. With this in mind, the dips referred to in this interpretation should be considered as minimum estimates.

By producing a 3D volume from the broadside shots we have been able to provide more detailed structural information on three important horizons in central Newfoundland. The small scale of this 3D experiment make it difficult to extrapolate the results over the large area that is covered by the Appalachian orogen, but we can still explore the possibilities that the data present. A horizon at approximately 4.5 s has been shown to be dipping at 27° to the northeast with a overall strike of N50°W. If the fabrics imaged at this depth are related to the collision that affected the Dunnage Zone in central Newfoundland, then the orientation for reflections at the top of the middle crust suggests a high degree of obliquity for collisional processes and perhaps indicate that there has been a significant amount of northeast-southwest movement for rocks affiliated with the Dunnage Zone. Alternatively, the horizon at 4.5 s may represent pre-existing structures which have been moved in a direction perpendicular to the strike of the orogen, but happen to dip northeast-southwest locally. An 8.2 s horizon displays a dip of 21° to the north, indicating that the dipping fabrics in the middle crust observed along line 6 of the Meelpaeg transect are being imaged in their true dip direction. Finally, an event that correlates with the Moho displays significant topography over the 36 km^2 area, and has a ridge-like appearance with a strike direction approximately equivalent to that of the major surface structures of the Appalachian belt. As stated above,

if the orogenic activity associated with the collision of Laurentia and Gondwana is responsible for the structures we observe today in the deep crust, then this result suggests that for the lower crust, and possibly the upper mantle, compressional forces from continent-continent collision were roughly perpendicular to the regional strike of the orogen. Perhaps structures in the lower crust have not been overprinted by late orogenic activity which has affected the middle and upper crust, and in many orogens appears to favour strike slip motions (e.g. Beck, 1986). This may be because the lower crust has responded ductilely during the margin-parallel translation of mid to upper crustal material, possibly accounting for some of the strong reflectivity we observe in the lower crust (Beaudoin, 1994).

Given the limitations that existed due to the survey geometry, the fact that we can still satisfactorily image some events and provide some structural details is encouraging. There would appear to be significant potential for a superior 3D image with a better designed survey. In terms of acquiring data that is suitable for 3D interpretation, one would prefer as broad an areal extent as possible with midpoint coverage that enables a grid of CDP bins to achieve sufficient fold over much of the area (> 15 fold). This primarily involves using as dense a shot spacing as is feasible and positioning shots on as many sides of the receiver spread as is possible. The broadside survey used a shot spacing of 300 m and was only recorded from one side of the receiver spread (only road available). A geometry similar to the experiment reported on by Vasudevan et al. (1995), where an "X" in the road network enabled the vibrators to move away from both sides of the spread generating a larger, denser grid of midpoints, would be preferable.

5.3 Amplitude versus offset (AVO) analysis

One of the principles that conventional common depth point (CDP) reflection seismology relies on is that the angle of incidence has only minor effects on P-wave reflection coefficients over propagation angles commonly used (Ostrander, 1984). It has been found, however, that most reflecting interfaces can generate systematic changes in the P-wave reflection coefficient with angle of incidence (Koefoed, 1955). In the petroleum industry the identification of high intensity seismic reflections or "bright spots" has become a standard exploration tool, particularly in the search for commercial accumulations of gas. The inherent concepts of relating amplitude variations to physical rock properties has been extended to deep-crustal structures (e.g. Louie, 1990) and it appears that gross scale AVO trends may help constrain physical parameters arrived at by the analysis of seismic reflection data (e.g. P-wave velocity (V_p), S-wave velocity (V_s), density (ρ), Poisson's ratio (σ)). With the end-on-south data set we have offsets which provide a wide spread of incidence angles (up to 39°) for the whole crustal section, and strong, relatively coherent reflectivity which can be analysed in the CDP domain (pre-stack). The following analysis of the gross AVO trends seen in the end-on-south data can be compared to work already completed with the regional seismic data in central Newfoundland that has produced estimates of bulk Poisson's ratio (σ) and the lithological composition of the crust (Hughes et al., 1994).

5.3.1 Theory

The compressional wave reflection coefficient as given by the Zoeppritz equations has been simplified to a form which is amenable to a generalized interpretation of reflection data for amplitude versus offset variations (Shuey, 1984). The following equation summarizes Shuey's results for the computation of the absolute reflection coefficient R(θ) as a function of incidence angle (θ):

$$R(\theta) = R_0 + [A_0 R_0 + \frac{\Delta\sigma}{(1-\sigma)^2}]\sin^2\theta + \frac{1}{2}\frac{\Delta V_p}{V_p}(\tan^2\theta - \sin^2\theta) \qquad (1)$$

where

$$A_0 = B - 2(1+B)\frac{1-2\sigma}{1-\sigma} \qquad (2)$$

and

$$B = \frac{\Delta V_p / V_p}{\Delta V_p / V_p + \Delta\rho/\rho} \qquad (3)$$

Note that in the above equations (1 to 3), $\Delta V_p/V_p$ is the fractional downward change of the P-wave velocity (V_p) across the reflecting interface, $\Delta\rho/\rho$ is the downward fractional change in density across the reflecting interface, R_0 is the reflection coefficient at normal incidence, and σ is Poisson's ratio. To further generalize, the 4th term in (1) can be dropped for

incidence angles less than 30° as the contribution is minimal. For wide-angle data, i.e. beyond the critical angle, the velocities become the overriding factors in determining reflection amplitudes. The maximum incidence angle in the analysis of the end-on-south data is 39°, but most of the events analysed are recorded at incidence angles less than 30°. Thus Shuey's simplified equation (1) predicts (as Koefoed (1955) had earlier observed) that an increase in Poisson's ratio for an underlying medium produces an increase in the reflection coefficient at larger angles of incidence, and that the same corresponding relationship is true for a decrease in Poisson's ratio (Shuey, 1985).

For crustal scale investigations, where we are primarily dealing with high velocity, high density metamorphic and igneous rocks in which velocity and density increase with depth, we can make a reasonable estimate of the dimensionless parameter B, which is the velocity/impedance ratio. Then with an estimate of the bulk Poisson's ratio (σ) we can approximate A_0. For reasonable density and velocity changes within the crust in central Newfoundland (5-10%increase at an interface), B is in the range 0.4 to 0.6 (3). Using the values from Hughes et al. (1994) for the interface between the mid and lower crust (mid: Vp=6.3 and ρ=2.7; lower; Vp=6.7 and ρ=2.9) B is 0.46. Using a bulk crustal Poisson's ratio of 0.23 (Hughes et al., 1994), a value of -1.6 for A_0 can be calculated (2). Thus for reasonable values of B and σ, A_0 is small and negative. This means that in the absence of a change in σ at a reflecting interface in our study area, the trend of reflection amplitude as a function of offset will be steadily decreasing (1). For the data of this study we will attempt

to provide a quantitative estimate of changes in σ by examining the relative change in reflection strength or reflection coefficient using the following relationship from Shuey (1985);

$$R(\theta)/R_0 \cong 1 + A\sin^2\theta \tag{4}$$

This is simplified from (1) by dropping the third term as discussed above and dividing through by R_0 so that we have an expression for the relative change in the reflection coefficient. The values R_0 (reflection coefficient at normal incidence) and A are defined as follows,

$$R_0 \cong \frac{1}{2}\left(\frac{\Delta V_p}{V_p} + \frac{\Delta\rho}{\rho}\right) \tag{5}$$

$$A = A_0 + \frac{1}{(1-\sigma^2)}\frac{\Delta\sigma}{R_0} \tag{6}$$

We can now perform an analysis to see if some of the horizons where strong reflectivity is observed display convincing AVO trends, and if these trends could possibly be attributed to changes in Poisson's ratio. If $R(\theta)/R_0$ can be defined with any accuracy on the AVO plots, we may be able to state that the AVO trend differs from that expected in the case of no change in Poisson's ratio and place a value on $\Delta\sigma$.

5.3.2 Analysis

The rationale and methodology used in preparing the data for an AVO analysis has already been discussed in Chapter 4 and a flow chart of the data processing steps was displayed (Figure 4.6). For one of the chosen horizons (8.15 s on Figure 5.12) the AVO results have been plotted for both raw data and data processed for amplitude recovery (relative amplitude processing - RAP) (Figure 5.13). The RAP processing has increased the amplitudes and flattened the expected negative slope seen on the raw data, though a small negative trend is still seen in the amplitudes. This is as predicted above for "typical" continental crust with a constant Poisson's ratio. This provides confidence in the processing sequence used for the AVO analysis. In addition to the 8.15 s horizon an AVO analysis was made for five other events at times where we observe coherent reflectivity on CDP 46: 3.64 s, 5.05 s, 7.89 s, 9.64 s, and 10.7 s.

The analysis was conducted using two different methods on the best CDP gather from the large-fold CDP's generated for this study (CDP 46). Initially the StarPak processor LITHO was used for the AVO analysis (method 1). LITHO analyses events on NMO corrected gathers and for each event defined, incident angles (θ) are calculated at constant offset intervals using an estimate of the true velocity function. A maximum amplitude is selected in a 100 ms window centred around the event and results are plotted as amplitude versus $\sin^2(\theta)$ (Figures 5.14 - 5.16). The best fit linear function through the data points on this plot

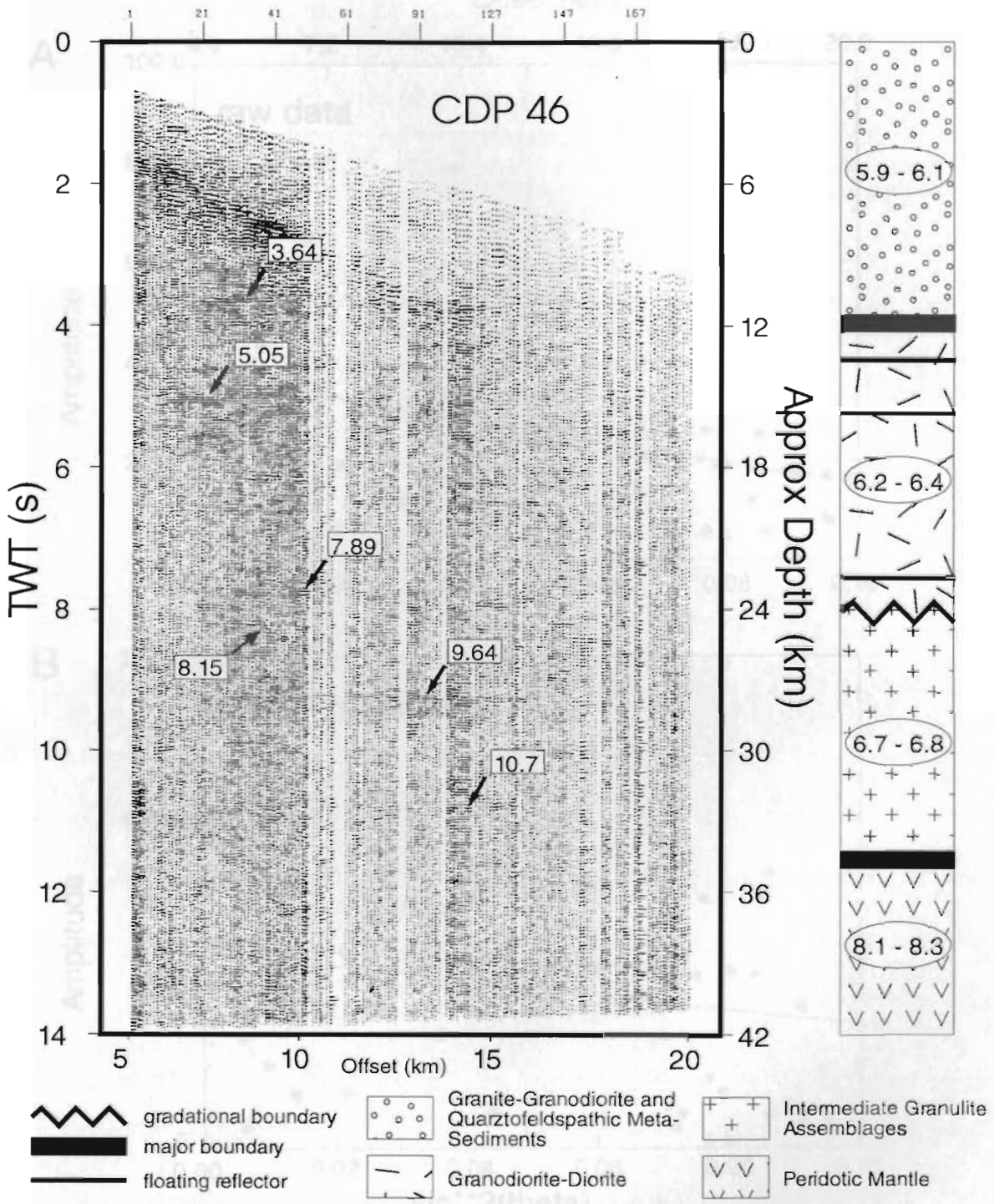

Figure 5.12 Large fold CDP 46 with geological interpretation.

Large fold CDP 46 with the times indicated where AVO analyses have been performed. Alongside CDP 46 is a bar which summarizes the line 3 interpretation of Hughes et al. (1994) for the Lake Ambrose area of central Newfoundland, with the suggested compositions indicated in the legend below.

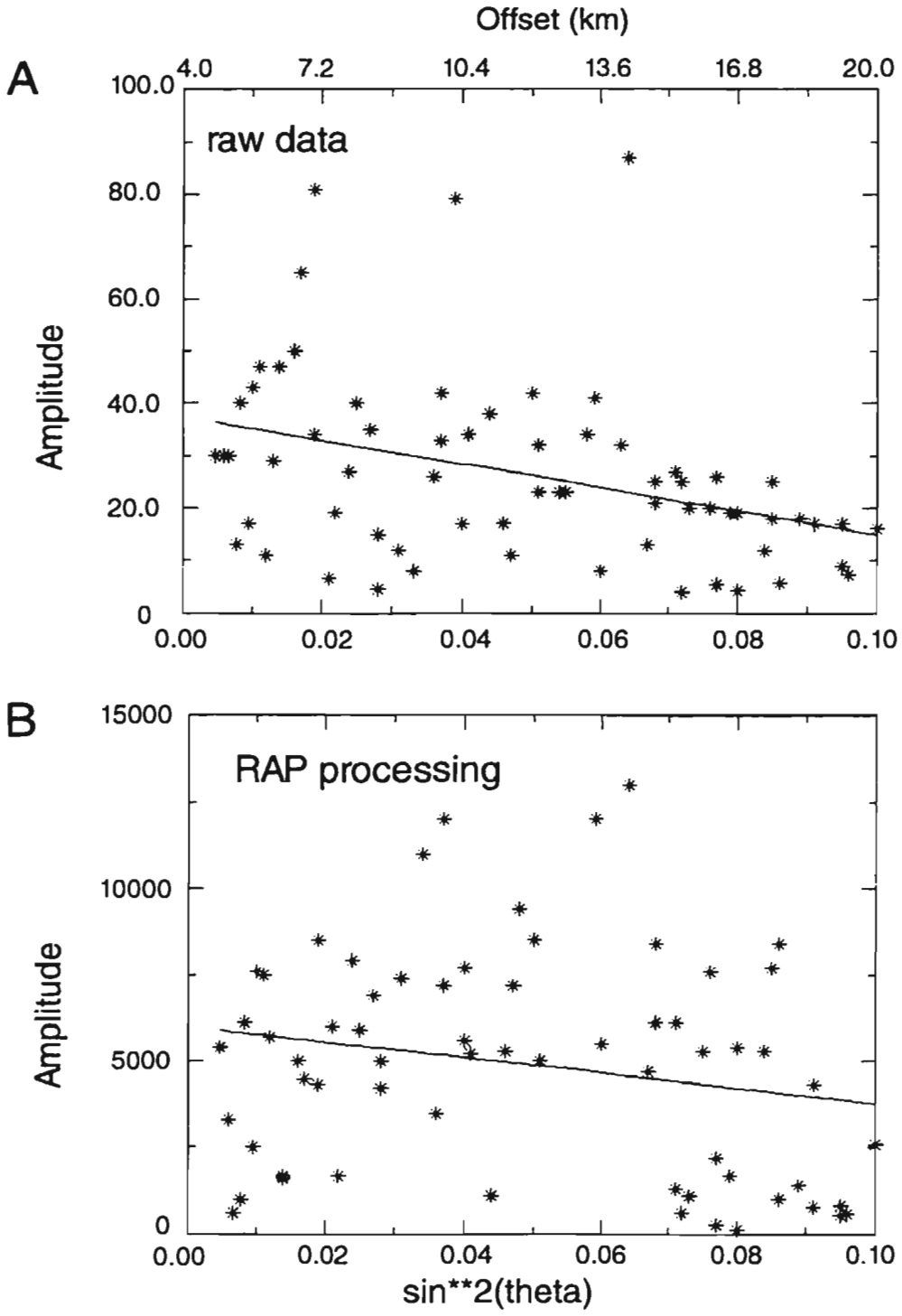

Figure 5.13 AVO results at 8.15 s; raw vs. relative amplitude processing (RAP).

Comparison of the AVO results for an event centred at 8.15 s on CDP 46 before (A) and after (B) RAP. The vertical axis is amplitude and the horizontal axis is sin**2(theta), where (theta) is the incidence angle of the reflecting waves. Sin**2(theta) relates to offset as indicated by the scale across the top of A.

can be expressed as $R(\theta) = X + Y\sin^2(\theta)$. The slope (Y) of this line has lithological significance in that it may be possible to estimate $\Delta\sigma$ if we can provide reliable approximations for density and P-wave velocity at a given depth. The second method (method 2) used for AVO analysis of these data was closer to the typical technique that is commonly utilized in the oil industry. An event (peak or trough) is picked across the seismic section, or in this case the CDP gather, and the amplitude at the picked time for each trace is plotted versus offset (Figures 5.17 - 5.20). In method 2 only traces in which a clear event could be picked were used for the analysis. Linear trends in these plots can be analysed exactly as in the initial method described above.

Method 1 was used in an attempt to extract AVO information out of the patchy, sometimes incoherent, reflectivity that we observe in this data set. Where singular reflection events cannot be followed from near to far offset it was hoped that finding the maximum amplitude within a window might still target a single interface. For this to be a valid approach we are assuming that the event should be visible at all offsets and the lack of coherency in the reflecting horizon is caused by a low signal to noise ratio on many traces, due to poor receiver coupling and/or high noise levels, or perhaps there are unresolved statics problems. In such a scenario a statistical look at the data may do a better job than visually picking an event. Alternatively, the main cause for the patchy reflectivity may be the structural complexity of the reflecting horizon, making it very difficult to characterize the AVO behaviour. In the presence of a dipping or curved horizon a full prestack migration is required in order to

retrieve AVO information (Resnick et al., 1987), but where the subsurface is highly complex, the processing problems may be insurmountable and an AVO analysis may prove to be ambiguous. This appears likely in the case of this experiment and, in fact, we may be primarily observing scattered energy. A further discussion of the nature of deep crustal reflectivity follows in section 5.4.

As previously pointed out, it is difficult to trace individual reflections across a wide range of offsets with these data, but three events were chosen for analysis with method 2: a relatively coherent event at 7.9 s that is one of a series of reflections at that depth, an event at 9.6 s that can be convincingly traced from the nearest offsets (4 km) to approximately 16 km, and a Moho level reflection that is strong and coherent, but only traceable for about 60 traces. In order to better pick the events using the INSIGHT module *vaquick2*, a coherency filter has been applied to nmo-corrected CDP 46. The StarPak processor MAKEUP was used for this task since MAKEUP retains all relative amplitude information as long as certain parameters are properly set (MAKEUP is described in section 4.2.1). The picked event at 9.64 s and the corresponding AVO plot are shown for both the standard (Figure 5.18) and coherency filtered data (Figure 5.19). It is apparent that there are subtle changes in the AVO plots of Figures 5.18 and 5.19, but the differences appear small enough that we can be confident MAKEUP is not significantly altering the relative amplitude information. An interpretation of the AVO results derived by both methods for CDP 46 is discussed below.

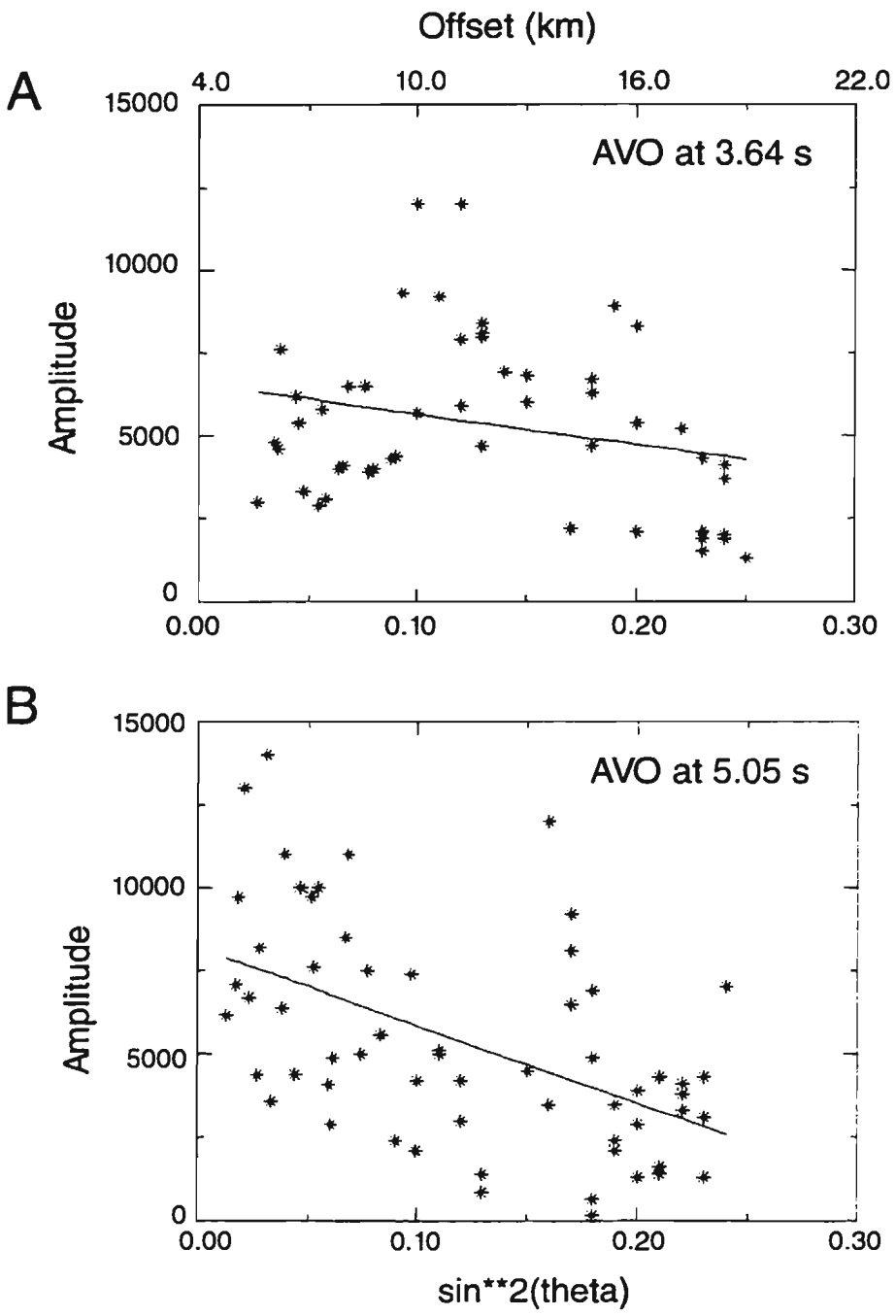

Figure 5.14 AVO results for events at 3.64 (A) and 5.05 s (B) on CDP 46.

The vertical axis on the plots is amplitude and the horizontal axis is sin**2(theta), where (theta) is the incidence angle of the reflecting waves. Sin**2(theta) relates to offset as indicated by the scale shown across the top of A.

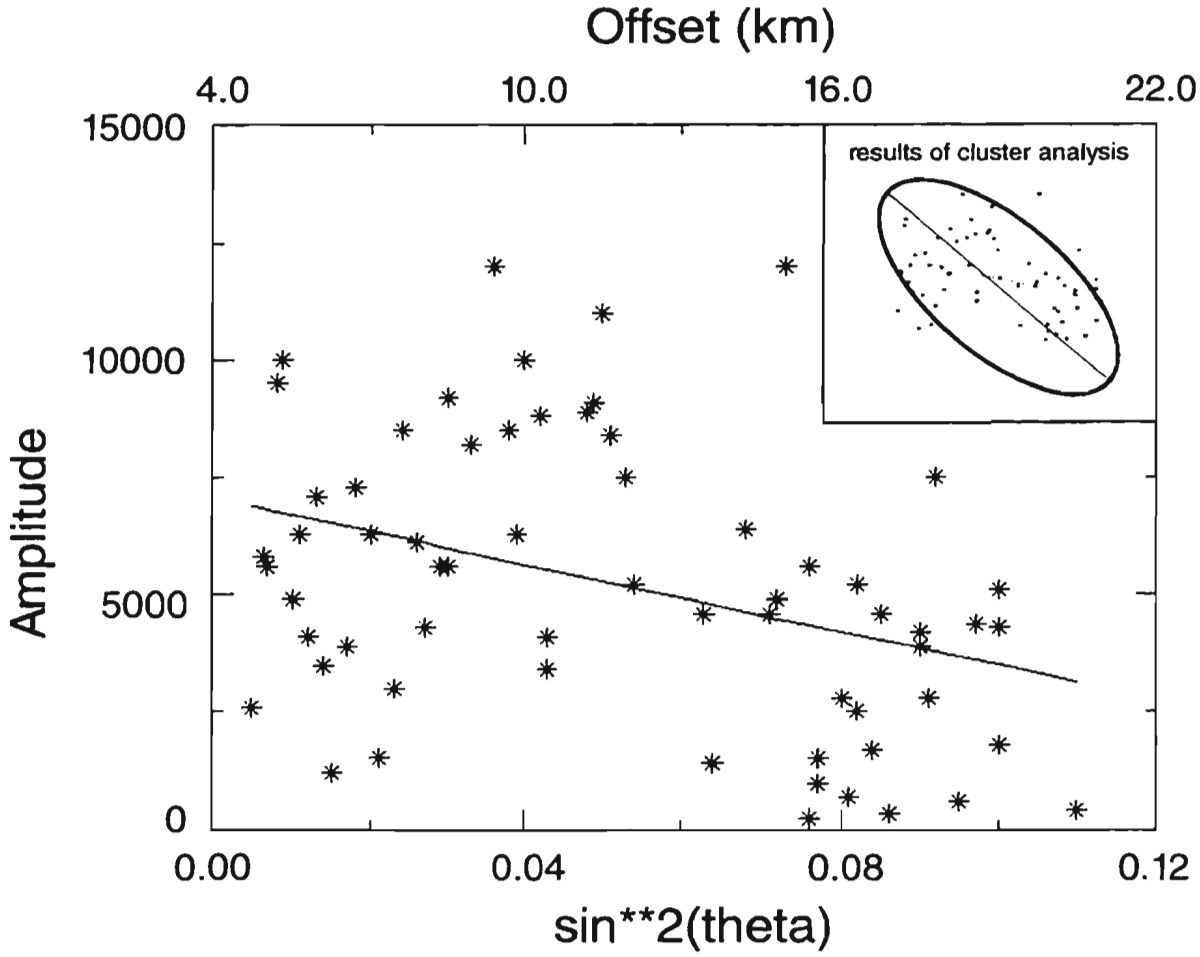

Figure 5.15 AVO results for an event centred at 7.89 s on CDP 46.

The vertical axis on the plots is amplitude and the horizontal axis is sin**2(theta), where (theta) is the incidence angle of the reflecting waves. Sin**2(theta) relates to offset as indicated by the scale shown across the top of the plot. The line through the data represents a linear regression (best fit) and has a correlation coefficient of 0.37. Also shown are the results of a cluster analysis with the best fit ellipse for points falling within one standard deviation of the mean (insert). The long axis of the ellipse provides another estimate for a linear trend in the points. The linear regression is also shown on the insert for comparison.

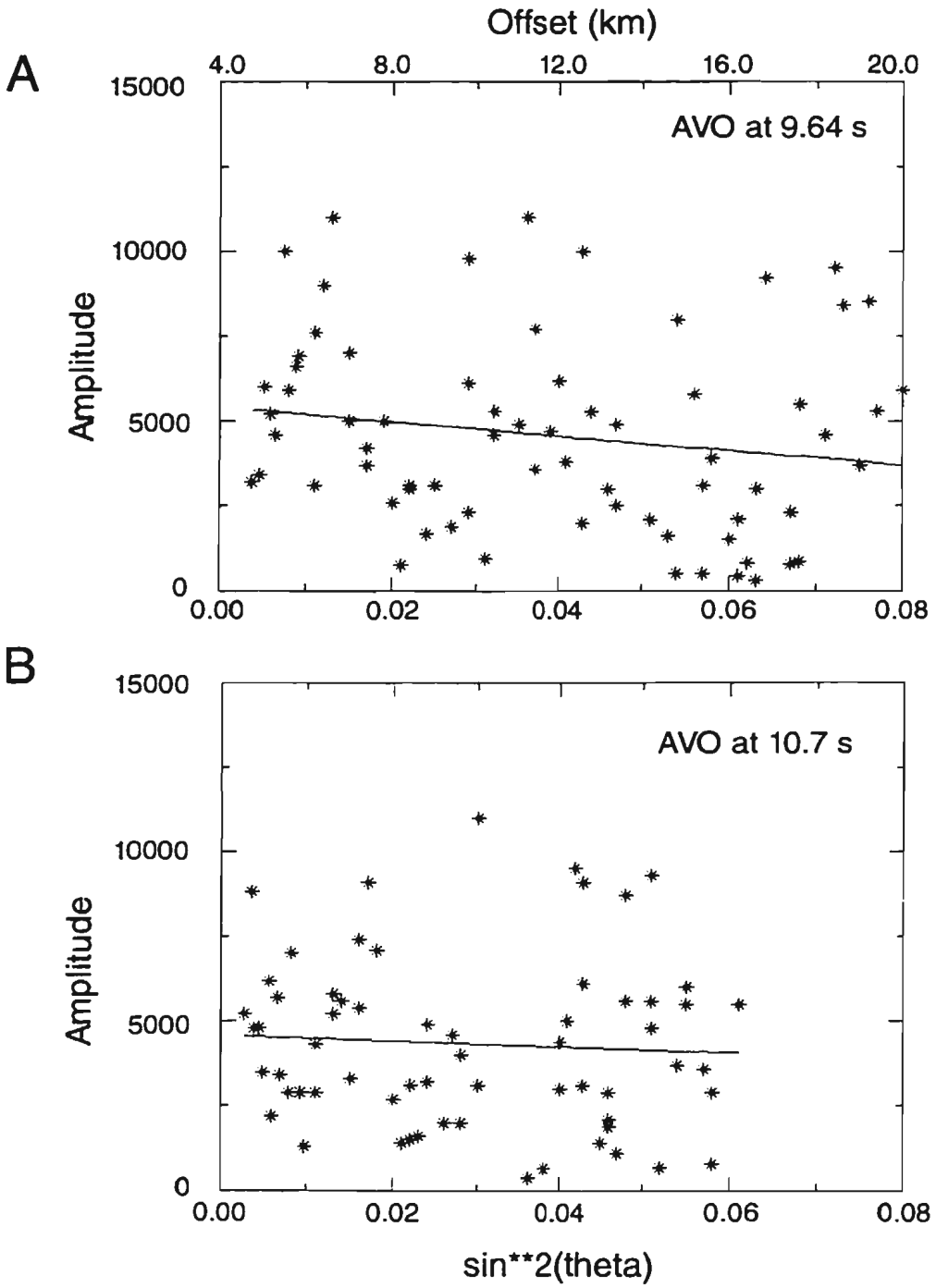

Figure 5.16 AVO results for events at 9.64 (A) and 10.7 s (B) on CDP 46.

The vertical axis on the plots is amplitude and the horizontal axis is sin**2(theta), where (theta) is the incidence angle of the reflecting waves. Sin**2(theta) relates to offset as indicated by the scale shown across the top of A.

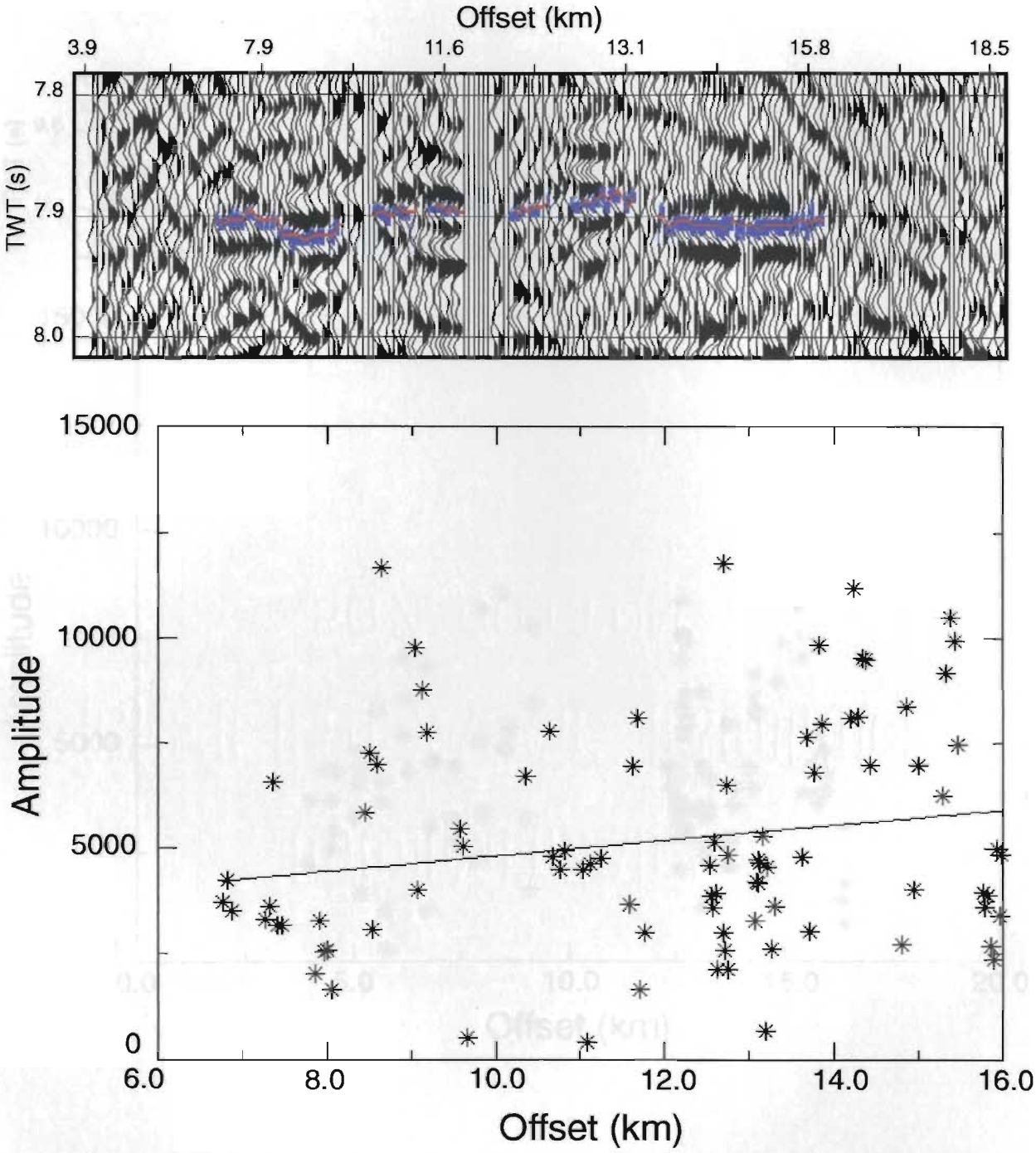

Figure 5.17 AVO results (method 2) for an event centred at 7.89 s on CDP 46.

The vertical axis on the plot is amplitude and the horizontal axis is shot-receiver offset. The section across the top of the AVO plot shows a blow-up of CDP 46 near 7.9 s with the selected horizon coloured blue. The line through the data points on the AVO plot is a linear regression (correlation coefficient of 0.19).

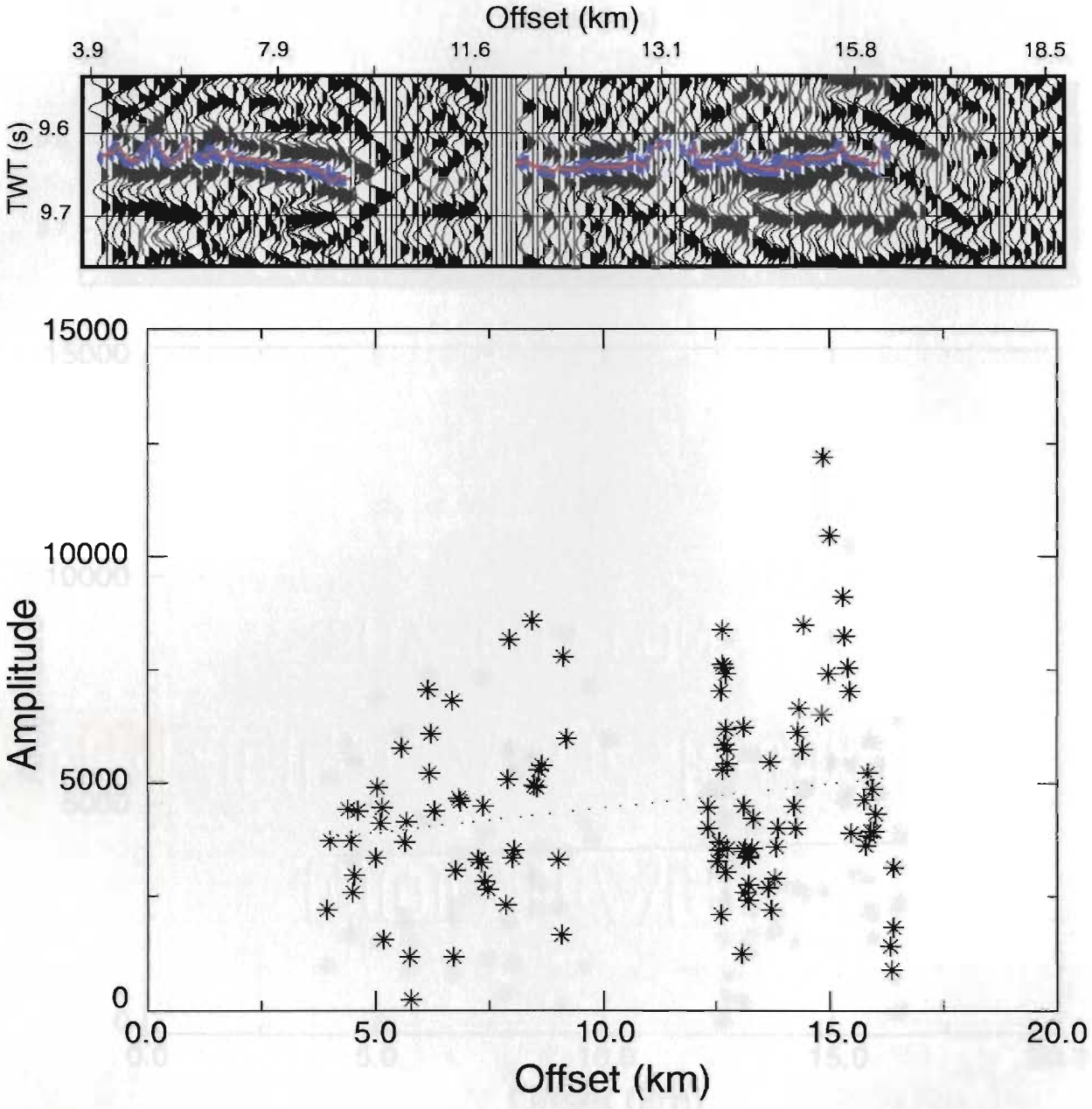

Figure 5.18 AVO results (method 2) for an event centred at 9.64 s on CDP 46.

The vertical axis on the plots is amplitude and the horizontal axis is shot-receiver offset (km). The section across the top of the AVO plot shows a blow-up of CDP 46 at approximately 9.6 s with the selected horizon coloured blue. The data has been coherency filtered (see description of MAKEUP in main text), as has the data in figures 5.17 and 5.20, and can be compared to figure 5.19, in which the data has not been coherency filtered.

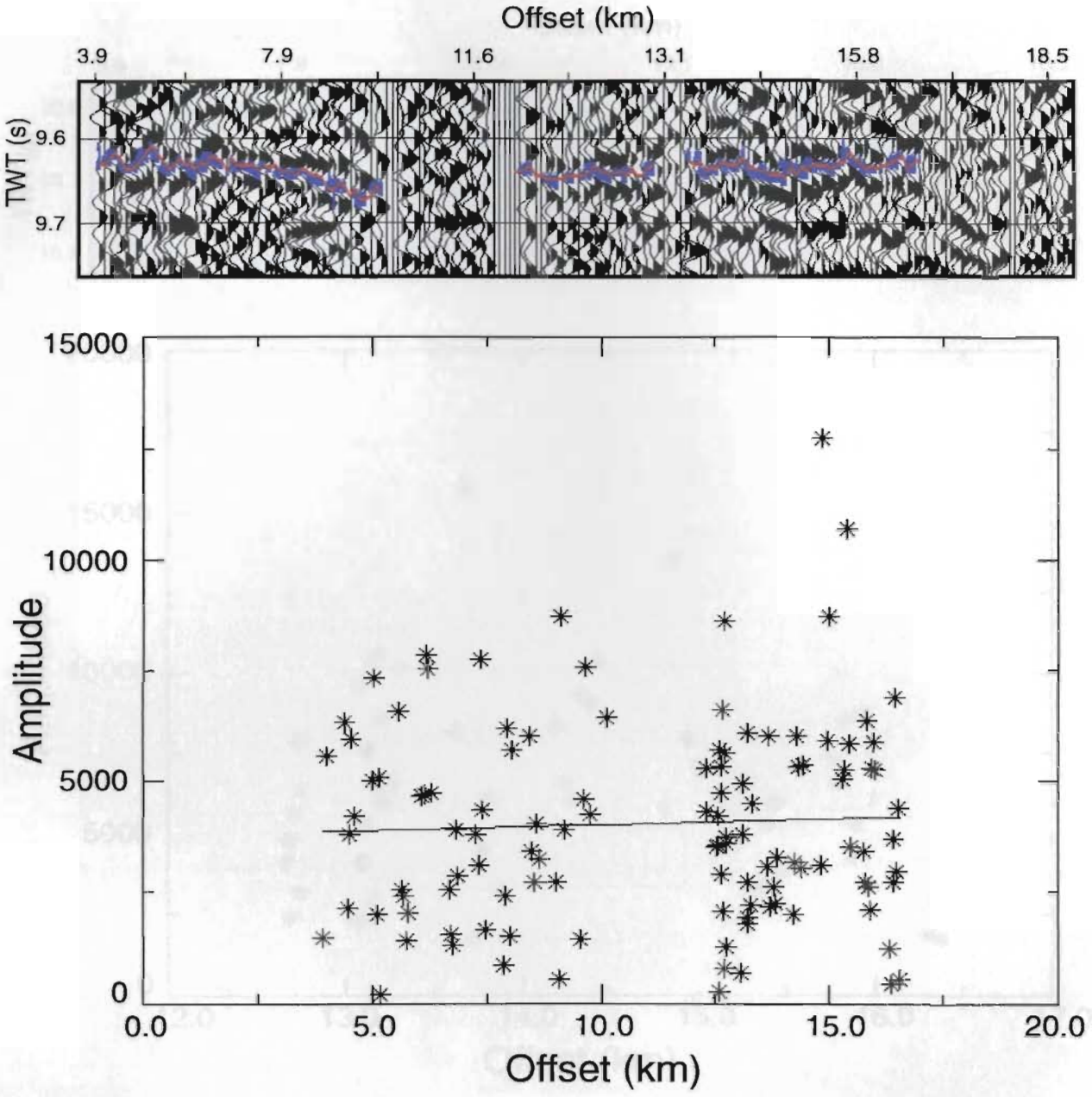

Figure 5.19 AVO results (method 2) for an event centred at 9.64 s on CDP 46.

The vertical axis on the plots is amplitude and the horizontal axis is shot-receiver offset (km). The section across the top of the AVO plot shows a blow-up of CDP 46 at approximately 9.6 s with the selected horizon coloured blue. This data has not been coherency filtered for comparison with figure 5.18.

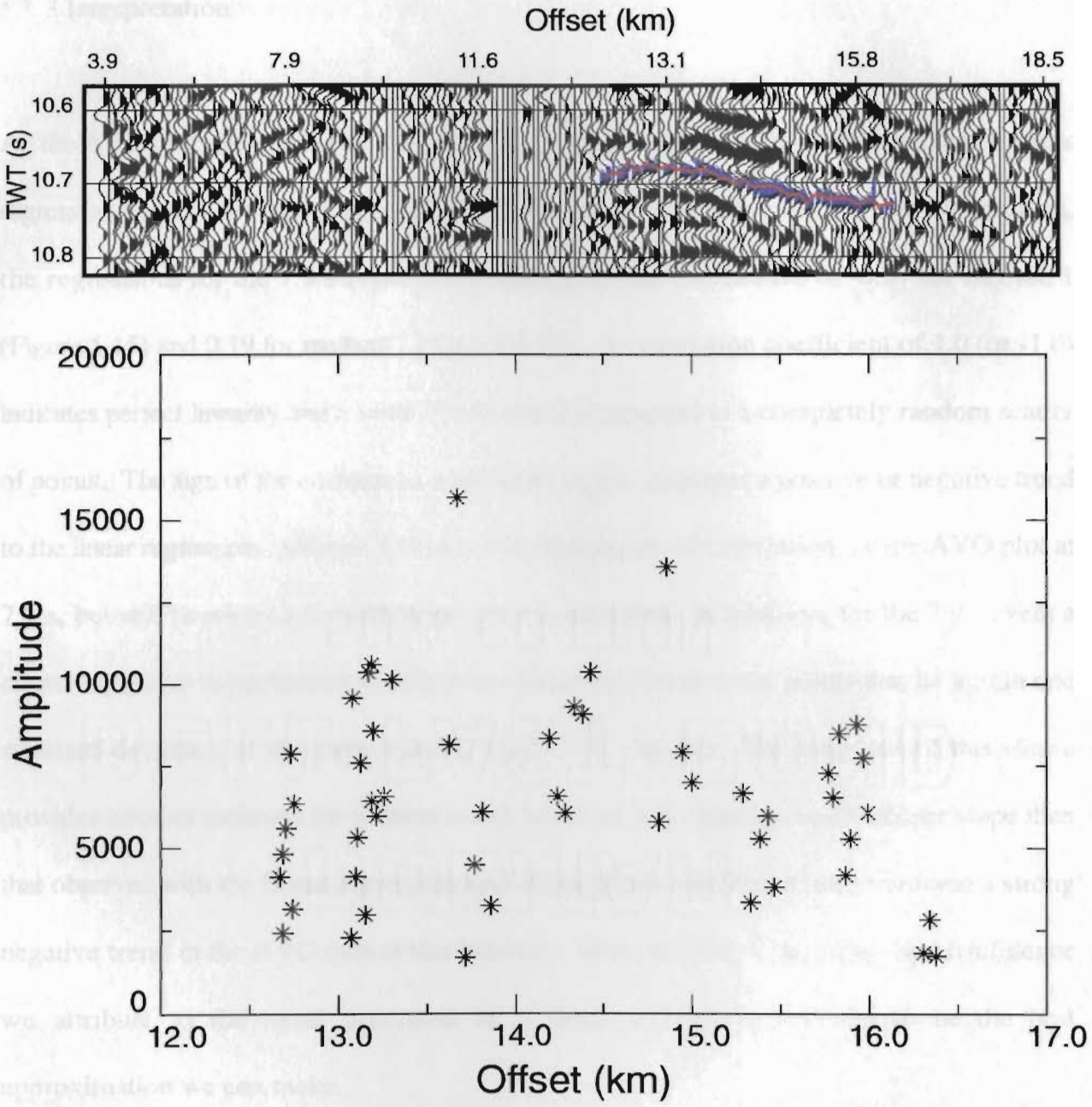

Figure 5.20 AVO results (method 2) for an event centred at 10.7 s on CDP 46.

The vertical axis on the plots is amplitude and the horizontal axis is shot-receiver offset (km). The section across the top of the AVO plot shows a blow-up of CDP 46 at approximately 10.7 s with the selected horizon coloured blue.

5.3.3 Interpretation

All the AVO plots (Figure 5.13 - 5.20) display a substantial scatter of data points, but a linear regression through the points on some of the plots indicate possible trends. For comparison, the regressions for the 7.9 s event produced correlation coefficients of -0.37 for method 1 (Figure 5.15) and 0.19 for method 2 (Figure 5.17). A correlation coefficient of 1.0 (or -1.0) indicates perfect linearity and a value of 0.0 would correspond to a completely random scatter of points. The sign of the correlation coefficient simply indicates a positive or negative trend to the linear regression. Method 1 shows a higher degree of correlation for the AVO plot at 7.9 s, but still provides low confidence for a linear trend. In addition, for the 7.9 s event a cluster analysis was performed in which an ellipse was fitted to the points that lie within one standard deviation of the mean value (Figure 5.15 - insert). The long axis of this ellipse provides another estimate for a linear trend, however it is clearly a much steeper slope than that observed with the linear regression and although not realistic, it does reinforce a strong negative trend in the AVO data at this horizon. Thus, in spite of the rather low confidence we attribute to the trend generated by a linear regression, it seems to be the best approximation we can make.

It is difficult to assess if the results from method 1 are meaningful. An amplitude is picked from each trace where an incidence angle is calculated whether the reflection signal is identifiable over the noise or not. Looking at the picked horizons from CDP 46 in Figures 5.17 to 5.20 it is evident that there are numerous traces which show no coherent signal at one

or more of the horizons. These may just be noisy traces, or may result from real discontinuities in the reflecting horizon. Either way, such traces could account for over 50% of the CDP gather and be more concentrated at the farther offsets. Thus it would appear that the main reason for the differences in the AVO plots for method 1 and method 2 is likely that the method 1 results include amplitude values for all the traces in the CDP gather. The AVO results for method 1 are biased towards the low amplitudes by the contribution of low signal traces, and contaminated by spurious data from the contribution of the noise traces. The method 2 results should be more representative of the true AVO response of a reflecting horizon since the event is picked with a certain degree of confidence. It was expected that method 2 would produce the most convincing results since the picked reflections are clearly identified and very few bad traces have been picked. However, the plots made using method 2 (Figures 5.17 to 5.20) show no clear positive or negative AVO trends and just as much scatter as the method 1 results (Figures 5.14 to 5.16).

Calculations made by Hughes et al. (1994) have provided an approximate σ of 0.25 for the upper crust in central Newfoundland (top 10 km), but a bulk σ of 0.23 to 0.24 for the entire crust. This suggests that a reduction in Poisson's ratio may be occurring at one or more interfaces within the crust. If we assume for now that the trends from the method 1 AVO analysis are valid, then results from this study indicate that the best candidates for reflections associated with a decrease in Poisson's ratio would be at approximately 5 and 8 s (15 and 24 km depth) (Figures 5.14 and 5.15). These horizons display the most convincing trends, both

generating significant negative slopes. At 5 s there is a strong sub-horizontal reflector observed in the regional reflection data, which has been modelled as a discrete "floating" reflector in the refraction modelling (Figure 5.12). To this point, no specific lithological significance has been attributed to this horizon; it is within the middle crust. The strong reflectivity at 8 s corresponds to the top of the lower crust, which Hughes et al. (1994) have interpreted as a 3-4 km thick gradational velocity zone (Figure 5.12). For this study, the reflector at 5 s does not lend itself to a quantitative analysis since we have no independent suggestion of a velocity or density contrast at this depth. However, the reflective zone at 8 s is better constrained and we can use the interpreted velocity contrast and lithological change to see whether or not a change (decrease) in σ is possible at that depth and estimate the magnitude of change.

Using the method 1 AVO response at 7.9 s (Figure 5.15) we estimate that $R(\theta)/R_0$ is 0.43 for $\sin^2(\theta) = 0.12$. We have already estimated A_0 to be -1.6 for a reasonable value of B (2), and using the velocities and approximate densities for a granodiorite-diorite middle crust and Granulite lower crust (V_p = 6.3 and 6.7 km/s; ρ = 2.7 and 2.9 Mgm^{-3} respectively) (Hughes et al., 1994), an estimation of $R_0 = 0.07$ can be made. Substituting all these values into (4) gives us a value of -0.2 for $\Delta\sigma$. This is an unreasonably large decrease in Poisson's ratio, but it would seem to indicate that $\Delta\sigma$ is likely negative. In order to see what the AVO trends look like at this horizon for varying values of $\Delta\sigma$ we have used the previously defined equation (4) and the physical parameters from Hughes et al (1994) detailed above, to generate

plots of $R(\theta)$ vs. $\sin^2(\theta)$ (Figure 5.21). We observe from this plot that it will be very difficult to confidently place a value on $\Delta\sigma$ given our scatter of points and, for example, it would likely be impossible to differentiate between $\Delta\sigma = +0.05$ and $\Delta\sigma = -0.05$ even though these are very different and significant changes in Poisson's ratio. Therefore, with the various uncertainties in this calculation and the scatter of points in the data, the best that can be said is that a decrease in Poisson's ratio at the top of the lower crust in central Newfoundland is not inconsistent with the method 1 AVO analysis, but we cannot confidently place a value on $\Delta\sigma$.

There are at least two reasonable causes for a decrease in Poisson's ratio at this deep crustal horizon: 1) P-wave velocities are higher in water saturated rocks than in dry rocks, whereas S-wave velocities remain relatively constant (Nur and Simmons, 1969). Hence, V_p/V_s and Poisson's ratio are higher in wet rocks and thus, a reduction in fluids can cause a decrease in Poisson's ratio. This correlation remains true even at pressures of up to 300 Mpa (Popp and Kern, 1994). Dehydration at the top of the lower crust could be caused by a decrease in effective pore space due to compositional variation or to a decrease in crack density at the higher pressures (Popp and Kern, 1994). 2) An increase in the quartz content at the top of the lower crust could cause a drop in Poisson's ratio since quartz has a very low Poisson's ratio ($\sigma = 0.08$) (Birch, 1961). This seems unlikely in central Newfoundland since V_p increases as we move into the lower crust (Hughes et al., 1994), suggesting that any corresponding lithological change would be to more mafic assemblages, with less quartz.

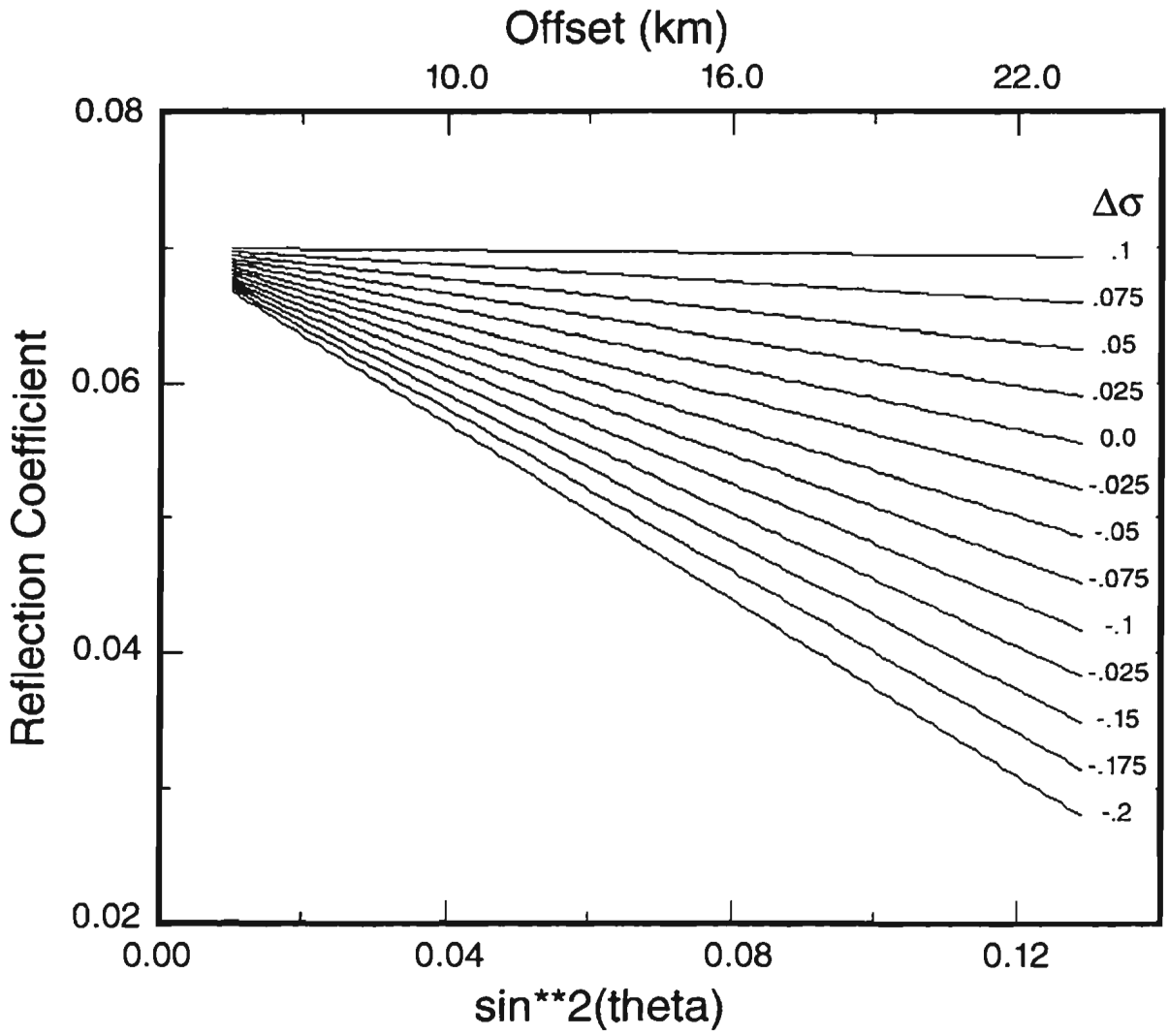

Figure 5.21 Predicted AVO trends for 7.89 s event and varying $\Delta\sigma$.

The vertical axis on the plots is reflection coefficient and the horizontal axis is sin**2(theta), where (theta) is the incidence angle of the reflecting waves. Sin**2(theta) approximately relates to offset as indicated by the scale shown across the top of the plot. The lines represent the AVO response for varying values of the change in Poisson's ratio ($\Delta\sigma$) at this interface while keeping all other physical values constant (i.e. density, velocity, bulk Poisson's ratio).

It would appear that no clear AVO trends can be convincingly demonstrated for CDP 46 and, more generally, the deep crustal reflections in this area of central Newfoundland. The reflection energy that we see in the data from the broadside experiment is likely not produced by "simple" lithological changes and perhaps no clear AVO trend can be predicted or expected for the deep reflections. The wide scatter of points for both AVO analyses methods is most likely due to a combination of a low signal to noise ratio and the lateral inhomogeneity of individual features, causing a significant amount of scattered energy that is constructively and destructively interfering. The following section summarizes some of the current thinking on what may be generating reflectivity in the lower crust.

5.4 Origins of Deep Crustal Reflections

During the analysis of the deep crustal data from the broadside and end-on experiment certain characteristics of the reflected wavefield have prompted questions as to what causes the reflections in the first place and what the observed data actually represent. It seems clear that signal strength and penetration are not a problem, with strong reflectivity in the lower crust, and the ambient noise level is low enough that the signal to noise ratio should be adequate. On the shot gathers we observe strong bands of reflectivity, but overall trace to trace coherency is poor leading to a "patchy" appearance (Figure 3.1). The 3D interpretation emphasizes the difficulty in tracing singular events across the grid area (36 km^2) and although it was possible to come up with a satisfactory interpretation of some events, it is not as detailed, nor as sure as one would like. The amplitude versus offset analysis has shown that no clear AVO trends can be confidently identified for the picked horizons. However, the observed horizons are probably not indicative of reflections generated by impedance contrasts between layered, stratigraphic units (e.g. in a sedimentary basin environment) and, although compositional variation is one factor in the reflected wavefield, it may or may not be the most important one.

In spite of the fact that many of the possible impedance contrasts generated by compositional variation in the crystalline crust are small, it has been demonstrated that a significant percentage (up to 17%) of the reflection coefficients arising from the layering of typical lithologies would lie between 0.1 and 0.2 (Hurich and Smithson, 1987). Hurich and Smithson

(1987) also note that the interference caused by relatively fine scale layering (layering in the order of 10 - 150m), whether it be constructive or destructive, has the potential to be more important than compositional variation in determining whether or not reflections are observed. This may be one reason why a horizon like the one we observe at approximately 8.0 s, which appears to be part of a wider band of reflectivity correlating with the top of the lower crust that is interpreted to be a complex layered and gradational velocity zone (Hughes et al., 1994), is strong for 1 to 2 km stretches, but virtually disappears between the strong segments (e.g. Figure 5.16). Other sources for deep crustal reflections in the crystalline crust may also be important. In addition to compositional variation these include fault or shear zones, water-filled pore spaces, and seismic anisotropy.

If a suitable compositional variation or other source exists for the generation of reflections the next question is what effect lateral heterogeneity plays in the observed wavefield. It is known from mapping areas in which cross-sections of crustal rocks are exposed at surface that lateral heterogeneity exists at many scales in crystalline terrains (e.g. Hollinger and Levander, 1994). This is typically a result of a complex tectonic and metamorphic history. One important factor is the relationship of the lateral heterogeneity to the Fresnel zone. The diameter of the Fresnel zone defines the minimum size for an isolated feature in order that it be unambiguously resolved in a CMP section. Features smaller than the Fresnel zone may produce a laterally similar response, but are not individually resolvable (Levander et al., 1994). For the top of the lower crust at roughly 25 km depth using a frequency of 20 Hz and an average crustal velocity of 6.4 km/s the Fresnel zone diameter would be about 4 km, and

for the Moho (~ 35 km) this increases to 4.7 km. It is easy to conceive that there could be significant lateral heterogeneity over distances in the order of 5 km. Thus we may be observing the effect of interfering scattering responses from numerous individual features that are smaller than the Fresnel zone. Where major lithological changes occur, the combined scattering energy may produce the bands of strong reflectivity that we observe in central Newfoundland. In this context it appears unlikely that individual horizons would have any kind of predictable AVO response and that we may see both constructive and destructive interference occurring at the same horizon. This may be another reason some of the events analysed during the AVO interpretation display relatively strong, coherent reflections which fade in and out as we move across the CDP gather (e.g. Figures 5.16 and 5.17).

Some authors have produced tectonic models which produce a strain regime that can be roughly matched to the observed crustal reflectivity patterns in compressional orogens (e.g. Beaumont et al., 1994; Quinlan et al., 1993). Possibly the strain field that develops as a result of orogenic events serves to focus the scattered and reflected energy such that well defined fabrics are developed and on a large scale correspond with crustal scale reflection patterns across orogenic belts. In such a scenario, individual events are perhaps less meaningful: sometimes, the closer you look the less you see.

6.0 CONCLUSIONS

During the data processing of the different data sets assembled from the broadside and end-on experiment some conclusions were arrived at regarding the optimal way to preserve coherent energy. The raw data contained undesirable "reverse sweep" noise and a method had to be devised to extract that noise without seriously affecting the data. This processing step was made possible because the uncorrelated shot gathers had been output to tape in the field. The effective removal of the reverse sweeps and the corresponding improvement to the shot gathers (Figure 4.2) emphasizes the need for careful quality control in the shot gather domain as a preliminary step to any processing sequence. The frequency spectrum of the raw data (8 to 40 Hz) was found to be limiting and, in retrospect, we would have preferred higher frequency data. However, the low frequency sweep did appear to be effective for lower crustal events (see discussion below). In the end it was decided that a relatively narrow bandpass filter (18 - 36 Hz) be applied to the data in order to best accentuate the signal. The data was found to be relatively insensitive to stacking velocity variations and velocity functions based on analyses performed for the nearby regional lines were used. Coherency filtering was fundamental in order that coherent seismic energy stand out above the background seismic "noise" and it is a trial and error method that must be fine-tuned for individual data sets. It was determined that the MAKEUP processor from the StarPak processing package could improve the coherency of events while retaining relative amplitude information (Figures 5.18 and 5.19) and thus, it was used to prepare the large-fold CDP gathers for amplitude versus offset analysis.

Add-on experiments have standard seismic reflection lines nearby which were recorded at or near the same time. These profiles can be used to calibrate the data from the special experiments. With the broadside and end-on survey there were two intersecting regional lines (LE89 line 6 and 7) with which collinear 2D lines generated from the broadside and end-on-south data could be compared. Processing lines were defined that closely followed the regional lines and comparisons indicate that the major features on LE89 line 7 can be identified on broadside line 13 (Figures 5.2 and 5.3) and, with somewhat less clarity, the structures on LE89 line 6 and end-on-south line 1 are also very similar (Figures 5.4 and 5.5). In the case of line 7 and broadside line 13 this is important because it demonstrates that, had line 7 not been acquired, a line produced by simply vibrating along a perpendicular line to the main regional transect (line 6) could provide significant information on the true dip of the key horizons provided there is no major change in geology along the perpendicular shooting line, which would alter the nmo velocity function. If cross-line data is to be acquired, this technique has the potential to save time during data acquisition and hence, reduce costs while enabling the final interpretation to be more complete.

The midpoint coverage generated by the broadside shots had enough areal extent that a 3D grid could be defined (Figure 4.10). Using basically the same data processing flow that was used for producing the 2D sections, a 3D reflection volume was created and certain horizons were selected for mapping in 3D space. For a mid-crustal event centred at approximately 4.5 s it was determined that the structure is slightly antiformal and is dipping at 27° to the northeast (N50°W strike) (Figure 5.6) and by looking at the data from LE89 line 7 (Figure

5.2) it appears that this is representative of a series of reflections between 4 and 6 s which display similar dips. These reflections are dipping in the same approximate direction as the regional strike of the tectonostratigraphic zones in central Newfoundland (~N40°E) possibly indicating a significant degree of obliquity in the collision within the Dunnage Zone (assuming that the reflection fabrics indicate shearing), although the attitude of this reflection package may also represent pre-existing northwest-southeast trending folds or thrusts which have been preserved during the northwest directed orogenic activity. An event which correlates with the top of the lower crust (8.2 s or ~25 km) was mapped and found to be dipping at 21° to the north (Figure 5.8). The small areal extent of good quality data for the 8.2 s reflection prohibits making any concrete statements on the dip direction of this horizon other than saying it appears to approximately strike north. The interpretation of the horizon at 8.2 s is consistent with Quinlan's (1992) cartoon model and the reflection data from LE89 line 6, which predicts north dipping fabrics in the middle to lower crust (Figure 2.1A and B), indicating that these fabrics are being imaged in their true dip direction along line 6. The final horizon mapped from the 3D volume correlates with the Moho and is at approximately 11.0 s (~35 km). The Moho reflection is one of the strongest and most coherent events from the broadside data and it is demonstrated that the Moho displays noticeable topography through the 3D grid area with a well-defined ridge striking southwest-northeast (N40°E). The flanks of the ridge display dips of 33° to the northwest and southeast with a total topographical relief of approximately 1.1 km. This ridge in the Moho topography roughly parallels the regional strike direction of the major surface structures in the Appalachian belt suggesting that compressional forces have acted in a roughly perpendicular direction to the regional strike for

the lower crust/upper mantle during continent-continent collision.

By creating some large-fold CDP gathers from the end-on-south data, it was possible to undertake an amplitude versus offset (AVO) analysis of some deep crustal events. AVO results obtained by using two different methods of tracking horizons have proved inconclusive. The scatter of points on AVO plots, likely due to the combined effects of varying signal to noise ratio and lateral heterogeneity within the crust over scales of 2 to 5 km, fails to indicate a clear AVO trend (Figures 5.14 to 5.20). One method provided a statistically significant negative trend for a reflection at 7.89 s (Figure 5.15) and, although method 2 puts this conclusion in doubt (Figure 5.17), a calculation was performed that attempts to determine the gross change in Poisson's ratio that such a trend would imply. It was shown that the data was consistent with a downward decrease in Poisson's ratio on the order of 5 to 10% at the top of the lower crust. If real, this might indicate a dehydration front since hydrated rocks tend to show higher Poisson's ratios than their dehydrated equivalents (Popp and Kern, 1994). An alternative explanation of a higher quartz content in the lower crust is less likely since Vp increases downwards (Hughes et al., 1994). The discussion on what causes reflections in the crystalline crust in Chapter 5 leads to the conclusion that lateral heterogeneity is probably responsible for the lack of coherency that we observe in specific reflecting horizons, and that horizons likely consist of the combined effects of scattered energy from a collection of individual features, all smaller than the Fresnel zone. It appears unlikely that an AVO trend could effectively be identified for such events and the results of this study seem to confirm this conclusion.

Special experiments, like the one presented herein, have varying potential for what they can add to the existing knowledge base and how they can complement the primary data set being acquired. The usefulness in many ways is linked to logistical factors controlled by geography. The road network and the roughness of the terrain serve to define the survey geometry and extents. Also important to the success of such experiments are the geological targets that are available for imaging. Experiments that are well laid out due to favourable logistics may not be particularly successful because they happen to be in an area where the crust is somewhat transparent with few strong reflecting horizons (e.g. Kanasewich et al., 1995). The broadside and end-on survey was positioned in an area where the crust is quite reflective throughout and thus, was able to achieve some modest goals despite a less than optimal geometry. Given the relatively minor extra costs, special add-on experiments are highly recommended if a suitable location is defined both logistically and scientifically.

The LITHOPROBE East 1989 broadside and end-on seismic experiment, while not making any direct links to the surface geology in central Newfoundland, has made important connections to interpretations from both the regional LE89 reflection and LE91 refraction surveys, and has therefore proved to be a useful research tool in further defining the structure of the northern Appalachian orogen.

REFERENCES

Beaudoin, B.C. 1994. Lower-crustal deformation during terrane dispersion along strike-slip faults. Tectonophysics, **232**: 257-266.

Beaumont, C., Fullsack, P., and Hamilton, J. 1994. Styles of crustal deformation in compressional orogens caused by subduction of the underlying lithosphere. Tectonophysics, **232**: 119-132.

Beck, M.E., Jr. 1986. Model for late Mesozoic-early Tertiary of coastal California and western Mexico. Tectonics, **5**: 49-64.

Birch, F. 1961. The velocities of compressional waves in rocks to 10kb, part 2. Journal of Geophysical Research, **66**: 2199-2224.

Blackwood, R.F. 1982. Geology of the Gander Lake (2 D/15) and Gander River (2 E/2) area. Newfoundland Department of Mines and Energy, Mineral Development Division, Report 82-4, 56 pp.

Bradley, D.C. 1982. Subsidence in late Paleozoic basins in the northern Appalachians. Tectonics, **1**: 107-123.

Brown, P.A. and Colman-Sadd, S.P. 1976. Hermitage Flexure; figment or fact? Geology, **4**: 561-564.

Colman-Sadd, S.P. and Swinden, H.S. 1984. A tectonic window in central Newfoundland? Geological evidence that the Appalachian Dunnage Zone may be allochthonous. Canadian Journal of Earth Sciences, **21**: 1349-1367.

Colman-Sadd, S.P. 1987. Geology of the Snowshoe Pond (12A/7) map area. *In* Current research Newfoundland Department of Mines, Mineral Development Division, Report 87-1, pp. 297-310.

Colman-Sadd, S.P. 1988. Geology of the Snowshoe Pond (12A/7) map area. *In* Current research Newfoundland Department of Mines, Mineral Development Division, Report 88-1, pp. 127-134.

Colman-Sadd, S.P., Hayes, J.P., and Knight, I. 1990. Geology of the Island of Newfoundland. Map 90-01, Geol. Surv. Branch of Newfoundland and Labrador, Dep. of Mines and Energy, St. John's, Canada.

Colman-Sadd, S.P., Dunning, G.R., and Dec, T. 1992. Dunnage-Gander relationships and Ordovician orogeny in central Newfoundland: a sediment provenance and U/Pb study.

American Journal of Science, **292**: 317-355.

Cook, F.A. and Coflin, K.C. 1990. Experimental three-dimensional imaging of crustal structure in the northwestern Canadian Arctic. *In* Leven, J.H., Finlayson, D.M., Wright, C., Dooley, J.C., and Kennett, B.L.N., (*Editors*)., Seismic probing of the continents and their margins. Tectonophysics, **173**: 43-52.

Dunning, G.R., O'Brien, S.J., Colman-Sadd, S.P., Blackwood, R.F., Dickson, W.L., O'Neill, P.P., and Krogh, T.E. 1990. Silurian orogeny in the Newfoundland Appalachians. Journal of Geology, **98**: 895-913.

Hughes, S., Hall, J., and Luetgert, J.H. 1994. The seismic velocity structure of the Newfoundland Appalachian orogen. Journal of Geophysical Research, **99**: 13,633-13653.

Hollinger, K. and Levander, A. 1994. Seismic structure of gneissic/granitic upper crust: geological and petrophysical evidence from the Strona-Ceneri Zone (northern Italy) and implications for crustal seismic exploration. Geophysical Journal International, **119**: 497-510.

Hurich, C.A. and Smithson, S.B. 1987. Compositional variations and the origin of deep crustal reflections. Earth and Planetary Science Letters, **85**: 416-426.

Kanasewich, E.R., Burianyk, M.J.A., Dubuc, G.P., Lemieux, J.F., and Kalantzis, F. 1995. Three-dimensional seismic reflection studies of the Alberta basement. Canadian Journal of Exploration Geophysics, **31**: 1-10.

Kean, B.F., Jayasinghe, N.R. 1980. Geology of the Lake Ambrose (12A/10) - Noel Paul's Brook (12A/9) map areas, central Newfoundland. *In* Current research Newfoundland Department of Mines, Mineral Development Division, Report 80-2, pp. 2-29.

Kean, B.F., Evans, D.T.W. 1988. Regional metallogeny of the Victoria Lake Group. *In* Current research Newfoundland Department of Mines, Mineral Development Division, Report 88-1, pp. 319-327.

Keen, C.E., Keen, M.J., Nichols, B., Reid, I., Stockmal, G.S., Colman-Sadd, S.P., O'Brien, S.J., Miller, H., Quinlan, G., Williams, H., and Wright, J. 1986. Deep seismic reflection profile across the Northern Appalachians. Geology, **14**: 141-145.

Kennedy, M.J. 1976. Southeastern margin of the Northeastern Appalachians: Late Precambrian orogeny on a continental margin. Geological Society of America Bulletin, **87**: 1317-1325.

Kennedy, M.J., Blackwood, R.F., Colman-Sadd, S.P., O'Driscoll, C.F., and Dickson, W.L. 1982. The Dover-Hermitage Bay Fault: Boundary between the Gander and Avalon Zones,

eastern Newfoundland. *In* Major structural zones and faults of the northern Appalachians, *Edited by* P. St. Julien and J. Belard, Geological Association of Canada Special Paper 24: 280 pp.

Koefoed, O. 1955. On the effect of Poisson's ratios of rock strata on the reflection coefficients of plane waves. Geophys. Prosp., **3**: 381-387.

Levander, A., Hobbs, R.W., Smith, S.K., England, R.W., Snyder, D.B., and Hollinger, K. 1994. The crust as a heterogeneous "optical" medium, or "crocodiles in the mist". Tectonophysics, **232**: 281-297.

Louie, J.N. 1990. Physical properties of deep crustal reflectors in southern California from multioffset amplitude analysis. Geophysics, **50**: 609-614.

Marillier, F., Keen, C.A., Stockmal, G.S., Quinlan, G., Williams, H., Colman-Sadd, S.P., and O'Brien, S.J. 1988. Crustal structure and surface zonation of the Canadian Appalachians: implications of deep seismic reflection data. Canadian Journal of Earth Sciences, **26**: 305-321.

Marillier, F., Dentith, M., Michel, K., Reid, I., Roberts, B., Hall, J., Wright, J., Louden, K., Morel-a-l'Huissier, P., and Spencer, C. 1990. Coincident seismic-wave velocity and reflectivity properties of the lower crust beneath the Appalachian Front, west of Newfoundland. Canadian Journal of Earth Sciences, **28**: 94-101.

Marillier, F., Hall, J., Hughes, S., Louden, K., Reid, I., Roberts, B., Clowes, R., Cote, T., Fowler, J., Guest, S., Lu, H., Luetgert, J., Quinlan, G., Spencer, C., and Wright, J. 1994. Lithoprobe East onshore-offshore seismic refraction survey - constraints on interpretations of reflection data in the Newfoundland Appalachians. Tectonophysics, **232**: 43-58.

Michel, H.K., Louden, K.E., Marillier, F., and Reid, I. 1991. The seismic velocity structure of northern Appalachian crust around western Newfoundland. Canadian Journal of Earth Sciences, **29**: 462-478.

Milkereit, B., Bittner, R., and Meissner, R. 1986. Off-line acquisition of crustal reflection and refraction data. Geophysical Research Letters, **13**: 1161-1164.

Milkereit, B. and Eaton, D. 1997. Imaging and interpreting the shallow crystalline crust. Tectonophysics, *in press*.

Miller, H.G. 1990. A synthesis of the geophysical characteristics of terranes in eastern Canada. *In* Ph. Matte (*Editor*), Terranes in the Variscan Belt of Europe and Circum-Atlantic Paleozoic Orogens. Tectonophysics, **177**: 171-191.

Nur, A. and Simmon, G. 1969. The effect of saturation on velocity in low porosity rocks.

Earth and Planetary Science Letters, **7**: 183.

Ostrander, W.J. 1984. Plane-wave reflection coefficients for gas sands at nonnormal angles of incidence. Geophysics, **49**: 1637-1648.

Popp, T. and Kern, H. 1994. The influence of dry and water saturated cracks on seismic velocities of crustal rocks - a comparison of experimental data with theoretical model. Surveys in Geophysics, **15**: 443-465.

Piasecki, M.A.J., Williams, H., Colman-Sadd, S.P., and Swinden, H.S. 1990. Tectonic relationships along the Meelpaeg, Burgeo and Burlington Lithoprobe transects in Newfoundland. *In* Current research Newfoundland Department of Mines, Geological Survey Branch, Report 90-1, pp. 327-339.

Quinlan, G.M., Hall, J., Williams, H., Wright, J.A., Colman-Sadd, S.P., O'Brien, S.J., Stockmal, G.S.,and Marillier, F. 1992. Lithoprobe onshore seismic reflection transects across the Newfoundland Appalachians. Canadian Journal of Earth Sciences, **29**: 1865-1877.

Quinlan, G., Beaumont, C., and Hall, J. 1993. Tectonic model for crustal seismic reflectivity patterns in compressional orogens. Geology, **21**: 663-666.

Resnick, J.R., Ng, P., and Larner, K. 1987. Amlitude versus offset analysis in the presence of dip. SEG Expanded Abstracts, pp. 617-619.

Roberts, B. 1990. Broadside and wide angle seismic experiment Lake Ambrose, Newfoundland. *In* Report of Lithoprobe East Transect Meeting, Oct. 24-25, Memorial University of Newfoundland, St. John's, pp. 159-164.

Seriff, A.J. and Kim, W.H. 1970. The effect of harmonic distortion in the use of vibratory surface sources. Geophysics, **35**: 234-246.

Shuey, R.T. 1985. A simplification of the Zoeppritz equations. Geophysics, **50**: 609-614.

Stockmal, G.S., Colman-Sadd, S.P., Keen, C.E., Marillier, F., O'Brien, S.J., and Quinlan, G. 1987. Collision along an irregular margin: a regional plate tectonic interpretation of the Canadian Appalachians. Canadian Journal of Earth Sciences, **24**: 1098-1107.

Stockmal, G.S., Colman-Sadd, S.P., Keen, C.E., Marillier, F., O'Brien, S.J., and Quinlan, G. 1990. Deep seismic structure and plate tectonic evolution of the Canadian Appalachians. Tectonics, **9**: 45-62.

Vasudevan, K. and Maier, R. 1994. SUN/INSIGHT 3D processing course guide. Lithoprobe Seismic Processing Facility, University of Calgary, Calgary, Alberta: 72 pp.

Vasudevan, K., Cook, F.A., and Maier, R. 1995. Three dimensional seismic crustal structure of the Monashee hinterland core complex on the Lithoprobe Southern Canadian Cordillera transect. Canadian Journal of Earth Sciences, **32**: 1531-1540.

Williams, H. and Stevens, R.K. 1974. The ancient continental margin of eastern North America. *In* The geology of continental margins. *Edited by* C.A. Burk and C.L. Drake. Springer-Verlag, New York, NY, pp. 781-796.

Williams, H. 1979. Appalachian orogen in Canada. Canadian Journal of Earth Sciences, **16**: 792-807.

Williams, H. and Hatcher, R.D. 1982. Suspect terranes and accretionary history of the Appalachian orogen. Geology, **10**: 530-536.

Williams, H., Colman-Sadd, S.P., and Swinden, H.S. 1988. Tectonic-stratigraphic subdivisions of central Newfoundland. *In* Current research, part B. Geological Survey of Canada, Paper 88-1B, pp. 91-98.

Williams, H., Colman-Sadd, S.P., and Swinden, H.S. 1989. Tectonic relationships along the proposed central Newfoundland Lithoprobe transect and regional correlations. *In* Current research, part B. Geological Survey of Canada, Paper 89-1B, pp. 55-66.

Williams, H., Hoffman, P.F., Lewry, J.F., Monger, J.W.H., and Rivers, T. 1991. Anatomy of North America: thematic geologic portrayals of the continent. *In* T.W.C. Hilde and R.L. Carlson (*Editors*), Silver Anniversary of Plate Tectonics. Tectonophysics, **187**: 117-134.

Wilson, J.T. 1966. Did the Atlantic close and then re-open? Nature, **211**: 676-681.

Yilmaz, O. 1987. Seismic data processing. Investigations in Geophysics, Volume 2, Neitzel, E.B. (*Editor*), Society of Exploration Geophysics, Tulsa, OK: 526 pp.